ACR No. L4I18

NATIONAL ADVISORY COMMITTEE FOR AERONAUTICS

WARTIME REPORT

ORIGINALLY ISSUED

September 1944 as
Advance Confidential Report L4I18

HIGH-SPEED INVESTIGATION OF LOW-DRAG WING INLETS

By Norman F. Smith

Langley Memorial Aeronautical Laboratory
Langley Field, Va.

NACA

WASHINGTON

NACA ACR No. L4I18

IONAL ADVISORY COMMITTEE FOR AERONAUTICS

ADVANCE CONFIDENTIAL REPORT

HIGH-SPEED INVESTIGATION OF LOW-DRAG WING INLETS

By Norman F. Smith

SUMMARY

Tests of a low-drag wing-inlet section, which had been developed in a previous low-speed investigation at LMAL, were conducted at high speeds in the NACA 8-foot high-speed tunnel. Near the design angle of attack, the inlet section was found to have minimum profile drag comparable to that of a similar low-drag plain airfoil section and to have negligible inlet losses. These results corroborate those obtained in the low-speed development program. The inlet section was found to have a higher critical Mach number than a comparable airfoil section, as predicted in the previous low-speed tests of this inlet section. A gain in critical Mach number of about 0.02 was measured, which is approximately one-half the gain indicated by the previous low-speed data and the data obtained at low Mach numbers in the present investigation. No inordinate changes in section characteristics with Mach number were found. In general, the variations were quite similar to those variations found for the comparable plain airfoil section tested simultaneously.

Satisfactory section characteristics could be obtained only for a small range of angle of attack and inlet-velocity ratio, as a result of internal separation and external pressure peaks. The maximum lift found for the inlet section was considerably lower than that found for the similar low-drag plain airfoil section. Tests of the inlet section with two amounts of camber showed that the introduction of a moderate amount of camber improves the section characteristics and the useful angle-of-attack range. Further development is shown to be necessary to produce inlet shapes having satisfactory characteristics through the desired ranges of angle of attack and air-flow quantity.

INTRODUCTION

A program was initiated by the NACA that included tests at low speeds in the NACA two-dimensional

low-turbulence tunnel to develop air-inlet shapes for low-drag airfoils and subsequent tests at high speeds in the NACA 8-foot high-speed tunnel to determine compressibility effects on the characteristics of the most promising shapes. A development program in the NACA two-dimensional low-turbulence tunnel produced wing-inlet sections having a minimum section profile drag comparable to that of similar low-drag plain airfoil sections (reference 1). The low-speed pressure data also indicated that the critical compressibility speed might be higher for an airfoil of a given thickness ratio with air flowing into an efficient air-inlet opening than for a similar section of the same thickness ratio with no inlet opening.

The present investigation was made in the NACA 8-foot high-speed tunnel with three models designed from one of the best inlet sections (shape 9) presented in reference 1. As a part of the general program, shape 9 was tested in its original symmetrical form; in order to study the general application of the inlet shape to cambered sections, two additional cambered models were designed and tested.

Section characteristics of the wing-inlet models were determined from pressure distributions, internal-flow measurements, and wake-survey measurements. For purposes of comparison, the corresponding characteristics of a comparable low-drag plain airfoil section were similarly determined.

SYMBOLS

a_o speed of sound in free-stream air, feet per second

M_o free-stream Mach number (V_o/a_o)

M_{cr} critical Mach number

α_o section angle of attack, degrees

ρ_o free-stream density, slugs per cubic foot

q_o free-stream dynamic pressure, pounds per square foot $\left(\frac{1}{2}\rho_o V_o^2\right)$

ΔH total-pressure loss from free stream to internal survey rake shown in figure 1, pounds per square foot

$\Delta H/q_o$ total-pressure-loss coefficient

p local static pressure, pounds per square foot

p_o free-stream static pressure, pounds per square foot

P pressure coefficient $\left(\frac{p - p_o}{q_o}\right)$

P_{cr} critical pressure coefficient, corresponding to a Mach number of 1.0 at that point

c wing chord, feet

d_o section profile drag, pounds per foot of span

c_{d_o} section profile-drag coefficient $\left(\frac{d_o}{q_o c}\right)$

d_{int} internal drag, pounds per foot of span

$c_{d_{int}}$ internal drag coefficient $\left(\frac{d_{int}}{q_o c}\right)$

n section normal force, pounds per foot of span

c_n section normal-force coefficient $\left(\frac{n}{q_o c}\right)$

m section pitching moment about quarter-chord point, foot-pounds per foot of span

$c_{m_{c/4}}$ section pitching-moment coefficient $\left(\frac{m}{q_o c^2}\right)$

R Reynolds number

V_o free-stream velocity, feet per second

V_1 velocity at air inlet, feet per second

V_1/V_o inlet-velocity ratio

A_1 area of air inlet, square feet per foot of span

A_4 area of air outlet, square feet per foot of span (station number designations follow those used in reference 2)

x distance along chord from leading edge of airfoil (see fig. 1)

y, y_d distance perpendicular to chord for respective surfaces (see fig. 1)

c_l section lift coefficient

APPARATUS AND TESTS

Apparatus

The NACA 8-foot high-speed tunnel, in which this investigation was conducted, is a closed-throat, circular-section, single-return tunnel with airspeed continuously controllable from about 75 to 600 miles per hour. The turbulence of the airstream is low but is somewhat higher than the turbulence of free air.

Models

The three models tested were of 2-foot chord and were constructed of wood. The general layout of the models and a scale drawing of each section tested are presented in figure 1. The inlet section of each model extended over one-fourth of the span and was faired, in an "end-closure" length approximately 2.75 times the inlet height, into a low-drag "basic airfoil section" that made up the rest of the span (figs. 1 and 2). General and detail views of one of the wing-inlet models are presented in figures 2 and 3, respectively. It should be noted that the basic airfoil section matches the inlet section only in maximum thickness, maximum-thickness location, and camber, and is representative of many sections that might be used in conjunction with the particular inlet section. The model ordinates are given in percent chord in table I.

The inlet section of the symmetrical wing is externally an exact reproduction of shape 9 of reference 1 (reduced to 2-foot chord). The inlet height is approximately 32.5 percent of the maximum thickness of the section. The basic airfoil section is the NACA 66(218)-018.9 airfoil section (reference 3).

For the medium-camber wing, shape 9 of reference 1 was fitted to an NACA 65,3-018 airfoil section and cambered. The procedure was as follows:

(a) The length of the original inlet section ahead of the maximum-thickness station (0.45c) was reduced by the ratio of 40/45 to make the location of maximum thickness coincide with that of the basic airfoil section (0.40c).

(b) The thickness was reduced to that of the basic airfoil section by subtracting 0.44 percent chord from the inlet-section ordinates.

(c) An arbitrary fairing to the exit was begun at the 65-percent-chord station of the airfoil.

(d) The fairness of the resulting inlet section was checked by computing the slope of the surface between consecutive ordinates and modifying the ordinates where necessary to make the variation of slope along the chord smooth.

(e) The final ordinates were combined with a camber line of design $c_l = 0.30$, mean line $a = 0.6$ (reference 3).

The inlet height is approximately 29.5 percent of the maximum thickness of the section. The basic airfoil section is the NACA 65,3-318 airfoil section.

In the high-camber wing, the inlet and the basic airfoil sections have the same thickness distribution as the symmetrical wing but are cambered to $c_l = 0.50$, mean line $a = 0.6$.

The three inlet sections very closely represent a family of cambered sections, and the test data can be analyzed to establish the general effects of camber on the inlet section. The duct for the three models had the same "thickness distribution" and was designed to give a low value of internal loss. The camber line of each inlet section was applied to the duct for that model. (See fig. 1.) No simulated internal resistance was employed, because resistance serves merely to reduce the inlet-velocity ratio that can be obtained with a given exit area and does not appreciably affect the external conditions over the section or the internal

conditions at the entrance. Removable exit plates were modified as shown in figure 1 to give the desired exit areas and inlet-velocity ratios. Streamline steel spacers were installed both in entrances and exits to provide additional strength. During the tests no modifications to the sections were made except for several small changes in the internal-lip shape, which was designed to reduce entrance losses. (See fig. 4.)

Measurements

Each inlet section was equipped with surface static-pressure orifices to measure external pressure distributions and with an internal survey rake to determine internal-flow conditions. (See fig. 1.) The basic airfoil section of each wing was also provided with surface static-pressure orifices at approximately the same distance from the tunnel center line. The pressure tubing passed from the model through a passage in the wing and was connected to a multiple-tube manometer in the test chamber.

Section normal-force and pitching-moment coefficients were obtained by integration of pressure-distribution plots. Total-pressure loss and inlet-velocity ratio were computed from measurements obtained with the internal survey rake. Section profile drag was measured by the wake-survey method behind sections not influenced by the surface pressure-distribution orifices or the inlet end-closure.

For several tests, wool tufts were installed at appropriate points on the symmetrical inlet section to permit observation of flow conditions. The models were tested through the complete angle-of-attack range from approximately -4° to an angle higher than the angle for maximum lift at low speeds. The angle-of-attack range at higher speeds was reduced because of structural limitations of the wing. The inlet-velocity ratio of each inlet section was varied from approximately 0.25 to 0.85. The tests were run through a range of Mach number from 0.20 to approximately 0.70 corresponding to a range of Reynolds number from 3,000,000 to 7,700,000 (fig. 5).

RESULTS AND DISCUSSION

External-Flow Conditions

Pressure distributions.- Pressure distributions are shown in figures 6 to 8 for the inlet section of the three wings at $\alpha_o = 0^o$ and $V_1/V_o = 0.5$; for comparison, the pressure distributions over the basic airfoil sections are also presented.

In figures 9 to 14 the pressures over the inlet sections are shown to be very sensitive to changes in α_o and V_1/V_o. The upper surfaces of the cambered inlet sections are less sensitive than the symmetrical inlet section, because the introduction of camber results in a favorable increase in curvature of the upper lip. The decrease in curvature of the lower lip results in a pressure peak on this surface at the design angle of attack. External-flow conditions improve with increase in inlet-velocity ratio.

The results show that only a small range of angle of attack and inlet-velocity ratio exists wherein a favorable pressure distribution can be maintained over the inlet sections. When well established, the pressure peaks produced outside this small range will result in preclusion of laminar flow on one surface and in reduction of critical speed.

Critical Mach number.- Critical Mach number M_{cr} is defined as the free-stream Mach number at which a local Mach number of 1.0 is attained at some point on the section. Figure 15 shows the variation of peak pressures with Mach number for the symmetrical wing at various angles of attack. It is apparent that the variations for the inlet section do not follow the normally assumed variation. Prediction of critical speeds by the usual methods from low-speed data of this kind would be greatly in error, because of the high peak pressures involved. Previous experience indicates that a very steep pressure gradient can cause the formation of a local separation bubble which effectively changes the shape of the body and lowers the pressure peak as M_o is increased. A separation bubble of this kind is evidently produced on the upper lip of the symmetrical inlet section at moderate angles of attack. Because the bubble is quite small, no large

increase in drag results. At the higher angles of attack, however, serious separation takes place over the lips.

Figures 16 and 17 show the critical speeds at various angles of attack and inlet-velocity ratios for the inlet and basic airfoil sections of the symmetrical wing. The critical speed of the inlet section is slightly higher than that of the basic airfoil section near the design angle of attack because of the effective reduction in thickness caused by the passage of air through the section. Gains in critical Mach numbers of approximately 0.02 over those obtained for the basic airfoil sections were found for the symmetrical inlet section. These gains are somewhat less than the values of 0.035 to 0.040 obtained from extrapolating the results of the low-speed tests of reference 1 and the low-speed data from the present investigation. When the angle of attack is reached beyond which the critical speed is governed by the pressure peaks on the inlet lips, the critical speed of the inlet section is reduced below that of the basic airfoil section. The extent of the angle-of-attack range for high critical speed is a function of inlet-velocity ratio.

A similar gain in critical Mach number was found for the medium-camber inlet section. A comparison of figures 18 and 19 with figures 16 and 17 indicates that a moderate amount of camber improves the critical-speed characteristics in the range beyond the design angle of attack without appreciably affecting conditions at the design angle. Figures 20 and 21 show, however, that a large amount of camber changes the shape of the lower inlet lip to such an extent that the critical speed near the design angle of attack is seriously reduced.

Internal-Flow Conditions

The variation of V_1/V_o with angle of attack for the three inlet sections with various exit areas are shown in figures 22 to 24. The inlet-velocity ratio, in most cases, decreased slightly as the angle of attack was changed from the design angle of attack, mainly because of internal-flow separation at the entrance.

Total-pressure-loss-coefficient data for the inlet section of the symmetrical wing is presented in figure 25 as a function of angle of attack. The angle-of-attack

range for low total-pressure loss was small, particularly for high inlet-velocity ratios. Tuft tests showed that separation occurred on the inside of the inlet lower lip at $\alpha_o = 2^\circ$, $V_1/V_o = 0.53$; this separation led to an immediate sharp rise in $\Delta H/q_o$ as the angle of attack was increased further. Because of increased entrance losses, $\Delta H/q_o$ rises with increase in inlet-velocity ratio. Similar internal-flow characteristics were found for the two cambered inlet sections (figs. 26 and 27).

Changes in inlet-velocity ratio and total-pressure-loss coefficient with Mach number were small. The angle of attack at which internal separation began did not change appreciably with Mach number.

A tuft test was made to investigate the flow in the vicinity of the inlet end-closure of the symmetrical wing. The test showed that, as the angle of attack was increased, both internal and external separation occurred first in the end-closure section of the inlet. Further development of inlet end-closure shapes is shown to be necessary.

Section Characteristics

Profile drag.- The results of the profile-drag measurements for the three wings are given in figures 28 to 30. The values of the profile-drag coefficients presented for the inlet sections include both internal and external drag, and the internal drag for each configuration is also shown. Inasmuch as the change in internal drag with Mach number was small, data for only one Mach number are presented.

The minimum values of c_{d_o} for the inlet and the basic airfoil sections of the symmetrical wing are approximately equal at medium inlet-velocity ratios. At the highest V_1/V_o tested, no low-drag range exists (fig. 28(e)). Because the internal drag for this condition is very low, the high drag is believed due primarily to the flared exit that was required to produce this high inlet-velocity ratio. (See exit details, fig. 1.) Inasmuch as flaps are usually used in connection with trailing-edge air exits to obtain high flow rates, high drag for this condition is usually encountered. Some reduction

in this drag may be obtained through improvements in design. At the lowest test value of V_1/V_o no low-drag range exists (fig. 28(a)). Because of the high local angle of attack of both inlet lips, pressure peaks occur and preclude the existence of laminar flow over both external surfaces. The drag coefficient at $\alpha_o = 1^\circ$ is less than at $\alpha_o = 0^\circ$ because the pressure peak on the lower surface has disappeared and some laminar flow exists on that surface.

The low-drag range is smaller for the inlet section than for the basic airfoil section. The extent of the low-drag range decreases as V_1/V_o decreases because external-flow conditions become more critical at low values of V_1/V_o. The drag of the inlet section beyond the low-drag range (above approximately 4°) increases at a much greater rate with angle of attack at low inlet-velocity ratios than does the drag of the basic airfoil section. Examination of the internal-drag data shows that this steeper slope is due principally to unfavorable external-flow conditions.

The medium-camber wing shows the same general drag characteristics found for the symmetrical wing, except that the low-drag range is somewhat greater and the center of the range is shifted in the positive angle-of-attack direction. The shape of the upper lip has been improved by cambering and the lower lip has been impaired only slightly.

For the high-camber wing, the minimum profile-drag coefficient of the inlet section at all values of V_1/V_o is higher than that of the basic airfoil section. The drag rise is rapid at angles of attack below the angle for minimum drag, largely because of separation over the lower lip of the inlet. At positive angles of attack, separation over the upper surface causes a rapid rise in drag. From observations of the wake profile and pressure distributions, this separation was found to occur back of the maximum-thickness station. The profile drag could not be accurately measured because of the extreme width and rapid fluctuations of the wing wake. At high Mach numbers, the separation became severe over both the inlet and the basic airfoil sections at all angles of attack. The camber for $c_l = 0.50$, used with a thickness ratio of 18.9 percent, apparently results in sections with serious flow-separation tendencies.

The minimum values of c_{d_o} and the width of the low-drag range for the basic airfoil sections of the three wings tested are in agreement with values obtained from two-dimensional tests of similar sections (reference 3).

Pitching moment.- The variations of section pitching-moment coefficient with Mach number are of the same order for the inlet and the basic airfoil sections of the symmetrical wing (fig. 31). At the low inlet-velocity ratio a larger variation of pitching moment with angle of attack occurs, because of alteration of the chordwise lift loading by pressure peaks on the inlet lips.

The same general trends are indicated for the medium- and high-camber wings (figs. 32 and 33). Larger changes in pitching-moment coefficient with angle of attack and Mach number took place with the high-camber wing, probably because of the separation effects previously noted.

Although not conclusive, these tests indicate that the addition of a properly designed air inlet to a low-drag airfoil section need not appreciably change the pitching-moment characteristics of the original section.

Lift.- Section normal-force coefficients are presented instead of section lift coefficients. Analysis shows that the two are approximately equal; the difference is less than 5 percent at maximum lift.

Normal-force-coefficient curves for the inlet and the basic airfoil sections of the symmetrical wing are shown in figure 34. A considerable deficiency in maximum lift for the inlet section is evident. Maximum lift increases with increase in inlet-velocity ratio because of the improvement of external-flow conditions. Tuft tests indicated that early separation over the upper inlet lip is responsible for the low value of maximum lift.

The inlet section of the medium-camber wing, when compared with the basic airfoil section (fig. 35), shows only a small loss in maximum lift because the inlet upper lip has been improved by cambering. Both the inlet and the basic airfoil sections of the high-camber wing show a decrease in lift-curve slope at angles of

attack greater than approximately 4° as a result of separation over the rear portion of the section (fig. 36). The angle of maximum lift was not reached in the tests of this wing.

The angle of zero lift for the two cambered inlet sections shifts somewhat with inlet-velocity ratio (figs. 35 and 36). This effect is due largely to changes in exit fairing. The symmetrical inlet section exhibits very little shift in angle of zero lift because accurately symmetrical exit fairings are easily produced.

The variations of normal-force coefficient with Mach number are of the same order for the inlet section and the corresponding basic airfoil section of each wing (figs. 37 to 39). Data for only one inlet-velocity ratio are presented because the effect of inlet-velocity ratio was very small for moderate values of lift.

Modifications

Two internal inlet-lip modifications, which were designed to improve entrance conditions, were tested on the inlet section of the symmetrical wing. Modification A was an arbitrary fairing involving no change in lip radius; modification B was the same as modification A with a 50-percent increase in lip radius (fig. 4).

The results show (fig. 40) that an addition to the lower lip of a simple fairing such as modification A increases the angle-of-attack range for low total-pressure loss in the inlet from 4° to 8°. Tuft tests showed that the fairing increased the angle-of-attack range by delaying internal-flow separation off the inlet lower lip. The results obtained with modification B show little improvement over results obtained with the original inlet. The larger lip radius apparently nullifies the effect of the fairing and produces, in addition, an unfavorable effect on the external flow.

Design Considerations

The angle-of-attack range through which low inlet losses and low section drag are desired is approximately 7°, or from high-speed attitude to climb attitude. The data indicate that the original inlet shape (shape 9 of reference 1) does not have the desired range.

Tests of the inlet section of the symmetrical wing with modifications A and B indicate that the angle-of-attack range for low inlet losses can be easily increased to a satisfactory extent. No tests of external modifications, as such, were included in the present investigation. Tests of the cambered wings indicate, however, that increasing the curvature of the inlet upper lip results in an improvement over the original section. Unpublished data from wind-tunnel programs in which wing inlets were developed for specific airplanes corroborate this finding and show that an appreciable gain in maximum lift can be realized by improving the flow over the inlet upper lip. These development programs indicate also that judicious use of lip stagger beyond the amount produced by camber can improve both internal-flow conditions and maximum lift.

The tests indicate that cambering a symmetrical inlet section by normal methods (reference 3) is unsatisfactory in the vicinity of the inlet lips. The inlet lower lip, because of decreased curvature due to camber, produced an adverse pressure distribution at the design angle of attack on the medium-and high-camber wings.

A method for fitting an inlet section to a given airfoil section has been described under the design of the medium-camber wing. The characteristics of the inlet section produced by this method depend, of course, upon the characteristics of the inlet section from which this section is designed. In addition, the procedure merely utilizes normal cambering methods and does not give needed special consideration to the inlet lips. The medium-camber inlet, therefore, evinces the same limitations found for the original inlet section except for the slight improvement due to camber. As a general method of application, the procedure is indicated by the tests to be satisfactory from considerations of pressure distribution, drag, and critical speed near the design angle of attack.

Further development is apparently needed to produce useful, efficient inlet shapes. Satisfactory section characteristics must be available for sufficiently wide ranges of inlet-velocity ratio and angle of attack.

CONCLUSIONS

1. Tests at high speed of three wing-inlet models designed from one of the best wing-inlet sections developed in a previous investigation at low speeds showed that the inlet section has minimum section drag comparable with that of a similar low-drag plain airfoil section and has negligible inlet losses near the design angle of attack. A properly designed air inlet can be installed in a low-drag wing at virtually no cost in external drag.

2. Critical Mach numbers approximately 0.02 higher than those of the basic airfoil sections were found for the symmetrical and medium-camber inlets. These values are approximately one-half the gains indicated by extrapolation of low-speed data from the previous development program or from the present investigation.

3. The inlet section is quite sensitive to changes in angle of attack. Adverse effects are produced on the inlet lips that result in small angle-of-attack ranges for low drag, high critical speed, and low entrance losses. A considerable deficiency in maximum lift, as compared to the maximum lift of the basic airfoil section, results from unfavorable flow conditions over the inlet upper lip for the symmetrical and low-camber inlet sections.

4. Introduction of a moderate amount of camber improves most of the section characteristics and the useful angle-of-attack range. The improvement is due primarily to the increased curvature of the upper lip, which reduces or delays the adverse effects incurred by the original shape. The decreased curvature of the lower lip, however, produces adverse effects, indicating that special methods must be devised for cambering inlet sections.

5. The variations in inlet section characteristics due to compressibility were, in general, quite similar to the variations found for the comparable plain airfoil section.

6. The method devised for fitting an inlet section to a basic airfoil section (used in the design of the

medium-camber wing) is shown by the data to be satisfactory, as compared with the original symmetrical section, with regard to pressure distribution, critical speed, and drag.

7. Further development is apparently needed to produce efficient inlet shapes from which satisfactory wing inlets for any desired ranges of inlet-velocity ratio and angle of attack can be designed and adapted to a wing section having any design camber.

Langley Memorial Aeronautical Laboratory
National Advisory Committee for Aeronautics
Langley Field, Va.

REFERENCES

1. von Doenhoff, Albert E., and Horton, Elmer A.: Preliminary Investigation in the NACA Low-Turbulence Tunnel of Low-Drag-Airfoil Sections Suitable for Admitting Air at the Leading Edge. NACA ACR, July 1942.

2. Becker, John V., and Baals, Donald D.: Analysis of Heat and Compressibility Effects in Internal Flow Systems and High-Speed Tests of a Ram-Jet System. NACA Rep. No. 773, 1943.

3. Abbott, Ira H., von Doenhoff, Albert E., and Stivers, Louis S., Jr.: Summary of Airfoil Data. NACA ACR No. L5C05, 1945.

TABLE I.- MODEL ORDINATES

Ordinates in percent chord

Symmetrical wing					Medium-camber wing											
Basic airfoil section		Inlet section			Basic airfoil section				Inlet section							
Upper and lower surfaces		Upper and lower surfaces			Upper surface		Lower surface		Upper surface				Lower surface			
x	y	x	y	y_d	x	y	x	y	x	y	x	y_d	x	y	x	y_d
0	0	0	3.343	3.083	0	0	0	0	-0.567	2.846	-------	-----	0.567	2.846	------	-----
.5	1.508	.5	3.835	↑	.283	1.404	.717	1.208	-.058	3.479	0.067	2.737	1.058	3.287	0.933	2.546
.75	1.812	.75	3.976		.508	1.717	.992	1.446	.208	3.687	.346	2.800	1.292	3.412	1.154	2.525
1.25	2.283	1.25	4.228		.979	2.196	1.521	1.779	.729	4.025	.883	2.892	1.771	3.608	1.617	2.475
2.50	3.079	2.50	4.745		2.187	3.075	2.812	2.346	1.998	4.737	2.179	3.142	3.004	4.004	2.821	2.408
5.00	4.175	5.00	5.532		4.642	4.437	5.358	3.192	4.508	5.862	4.725	3.554	5.492	4.612	5.275	2.304
7.50	5.037	7.50	6.137	Straight	7.121	5.529	7.879	3.846	7.025	6.729	7.250	3.942	7.975	5.046	7.750	2.258
10	5.750	10	6.652	line	9.617	6.442	10.387	4.379	9.542	7.442	9.767	4.300	10.458	5.383	10.233	2.242
15	6.858	15	7.467		14.629	7.904	15.371	5.208	14.587	8.617	14.796	4.946	15.412	5.917	15.204	2.246
20	7.696	20	8.098		19.662	9.029	20.342	5.825	19.637	9.504	19.821	5.500	20.362	6.296	20.179	2.292
25	8.342	25	8.593		24.704	9.900	25.296	6.279	24.696	10.204	24.846	6.029	25.304	6.583	25.154	2.404
30	8.825	30	8.965		29.762	10.537	30.237	6.596	29.754	10.696	29.875	6.500	30.246	6.754	30.125	2.558
35	9.162	35	9.224		34.825	10.954	35.175	6.775	34.821	11.017	34.904	6.937	35.179	6.842	35.096	2.762
40	9.367	40	9.379	5.208	39.892	11.158	40.108	6.821	39.892	11.158	39.937	7.279	40.108	6.821	40.062	2.937
45	9.433	45	9.435	5.208	44.962	11.125	45.037	6.704	44.962	11.125	44.979	7.412	45.037	6.704	45.021	2.987
50	9.367	50	9.391	5.208	50.037	10.804	49.962	6.383	50.037	10.804	50.021	7.412	49.962	6.383	49.979	2.987
55	9.142	55	9.240	5.208	55.112	10.208	54.887	5.879	55.112	10.208	55.075	7.367	54.887	5.879	54.925	3.033
60	8.717	60	8.966	5.208	60.208	9.379	59.792	5.250	60.208	9.379	60.142	7.004	59.792	5.250	59.858	2.879
65	7.996	65	8.510	5.208	65.271	8.325	64.729	4.562	65.271	8.325	65.183	6.208	64.729	4.562	64.817	2.442
70	6.979	70	7.804	5.208	70.275	7.129	69.729	3.829	70.275	7.171	70.183	5.367	69.724	3.871	69.817	2.067
75	5.792	75	6.878	4.583	75.246	5.837	74.758	3.058	75.254	6.000	75.171	4.483	74.745	3.225	74.829	1.708
80	4.504	80	5.816	3.583	80.196	4.492	79.804	2.275	80.217	4.896	80.146	3.633	79.783	2.675	79.854	1.437
85	3.175	85	4.679	3.042	85.137	3.137	84.862	1.504	85.179	3.842	85.137	3.154	84.821	2.208	84.862	1.521
90	1.875	90	3.522	3.042	90.075	1.850	89.925	.796	90.137	2.921	-------	-----	89.862	1.871	------	-----
95	.704	95	2.387	-----	95.025	.737	94.975	.246	95.100	2.162	-------	-----	94.896	1.671	------	-----
100	0	100	1.314	1.925	100	0	100	0	100.079	1.717	100.071	1.671	99.925	1.717	99.929	1.671
L.E. radius = 2.417		Fairing point x = 0.408, y = 3.067 L.E. radius center x = 0.250, y = 3.342 L.E. radius = 0.250			L.E. radius = 1.921				Fairing point x = -0.087, y = 2.671 L.E. radius center x = -0.296, y = 2.904 L.E. radius = 0.250				Fairing point x = 0.821, y = 2.554 L.E. radius center x = 0.800, y = 2.792 L.E. radius = 0.250			

TABLE I - MODEL ORDINATES - Continued

High-camber wing									
Basic airfoil section				Inlet section					
Upper surface		Lower surface		Upper surface			Lower surface		
x	y	x	y	x	y	y_d	x	y	y_d
0	0	0	0	-1.021	3.167	-----	1.021	3.167	-----
.100	1.617	.900	1.292	-.512	3.858	3.042	1.512	3.533	2.833
.304	1.779	1.196	1.529	-.229	4.083	3.125	1.729	3.625	2.750
.742	2.571	1.758	1.879	.308	4.471	3.250	2.192	3.779	2.625
1.917	3.633	3.083	2.417	1.600	5.267	3.667	3.400	4.050	2.417
4.354	5.167	5.646	3.083	4.146	6.508	4.292	5.858	4.425	2.167
6.829	6.396	8.175	3.587	6.679	7.487	4.833	8.321	4.679	1.917
9.321	7.425	10.679	3.992	9.217	8.321	5.292	10.783	4.887	1.750
14.354	9.075	15.646	4.583	14.296	9.679	6.083	15.704	5.187	1.583
19.417	10.346	20.583	5.004	19.383	10.746	6.750	20.617	5.404	1.458
24.496	11.342	25.504	5.308	24.479	11.592	7.417	25.521	5.558	1.375
29.592	12.100	30.417	5.533	29.583	12.242	8.000	30.417	5.675	1.333
34.695	12.642	35.304	5.675	34.692	12.704	8.458	35.308	5.737	1.333
39.808	12.983	40.192	5.750	39.808	12.996	8.750	40.192	5.762	1.375
44.933	13.117	45.067	5.750	44.933	13.117	8.875	45.067	5.750	1.437
50.067	13.050	49.933	5.683	50.067	13.075	8.917	49.933	5.708	1.458
55.217	12.746	54.787	5.529	55.217	12.846	8.833	54.783	5.629	1.542
60.412	12.150	59.587	5.267	60.425	12.400	8.625	59.575	5.517	1.667
65.558	11.112	64.442	4.837	64.471	11.625	8.333	64.404	5.350	2.000
70.583	9.708	69.417	4.200	70.654	10.533	7.833	69.346	5.025	2.375
75.525	8.083	74.475	3.450	75.646	9.167	6.833	74.354	4.533	2.292
80.429	6.329	79.571	2.637	80.588	7.637	5.333	79.442	3.946	1.583
85.308	4.517	84.672	1.800	85.454	6.017	4.292	84.546	3.300	1.625
90.179	2.746	89.821	.987	90.333	4.383	3.833	89.667	2.625	2.042
95.062	1.112	94.937	.287	95.212	3.000	-----	94.787	2.175	-----
100	0	100	0	100.096	1.979	1.925	99.904	1.979	1.925
L.E. radius = 1.808				Fairing point x = -0.717, y = 3.000 L.E. radius center x = -0.771, y = 3.237 L.E. radius = 0.250			Fairing point x = 1.237, y = 2.896 L.E. radius center x = 1.292, y = 3.125 L.E. radius = 0.250		

NATIONAL ADVISORY
COMMITTEE FOR AERONAUTICS

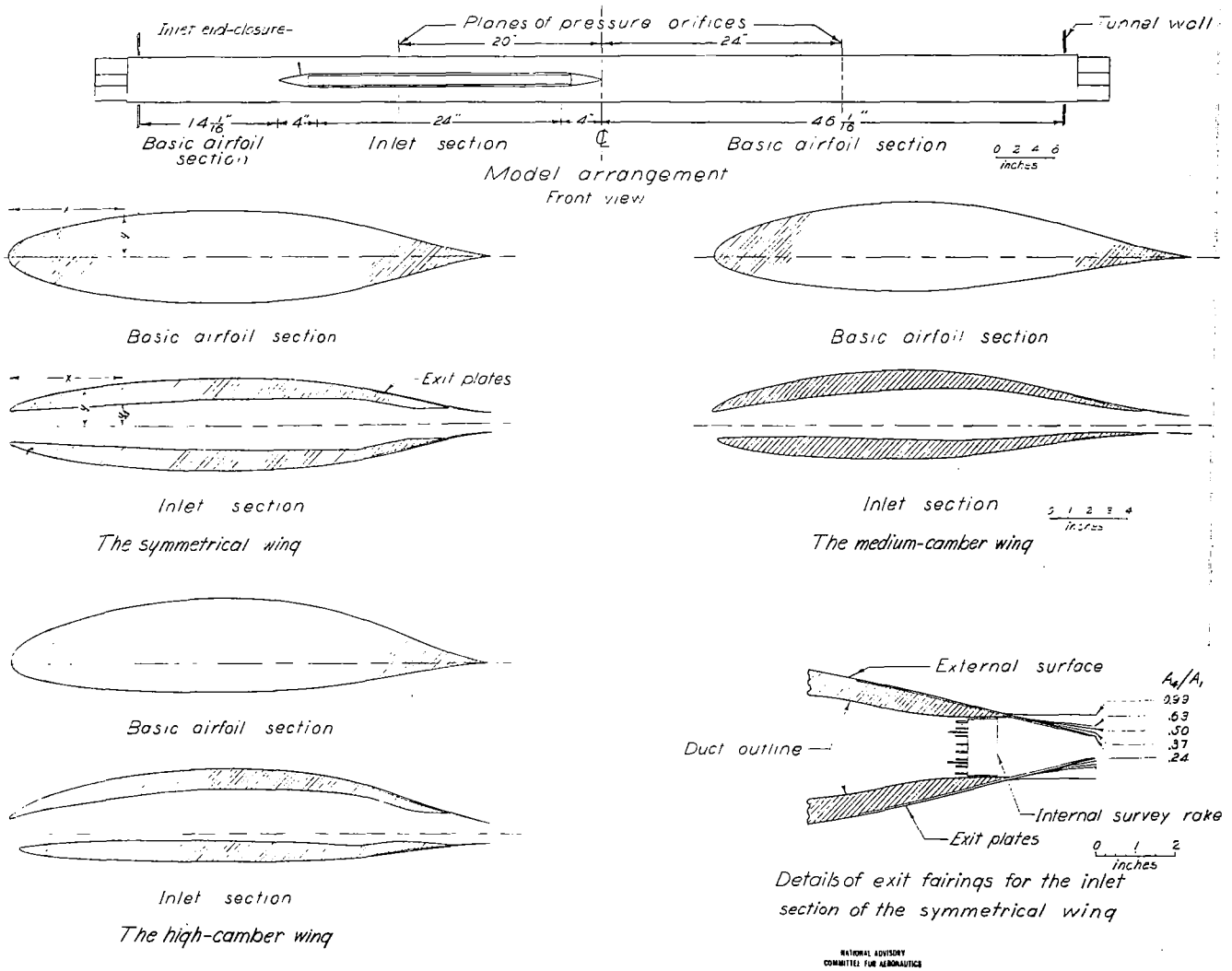

Figure 1.- Model arrangement and section details.

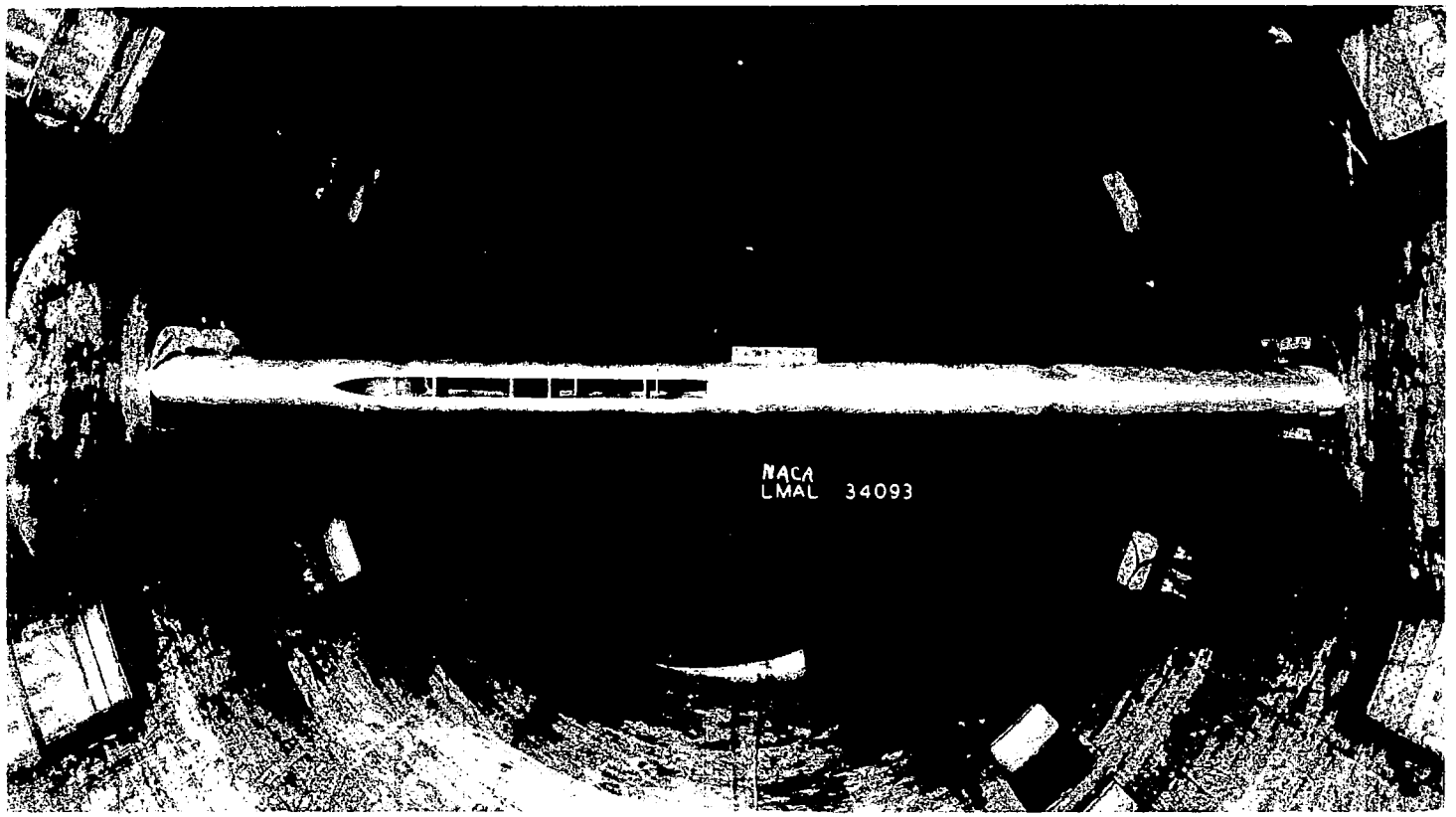

Figure 2.- Installation of wing-inlet model in NACA 8-foot high-speed tunnel.

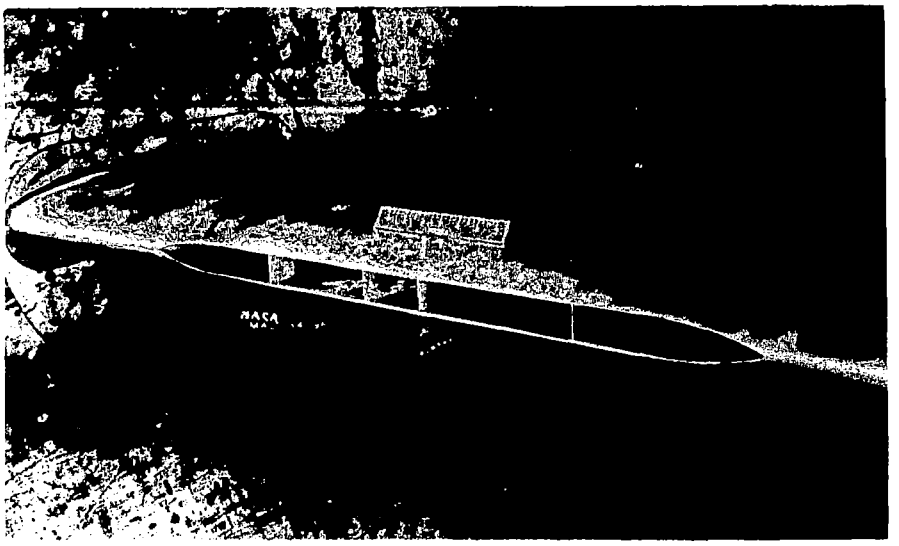

(a) Air inlet.

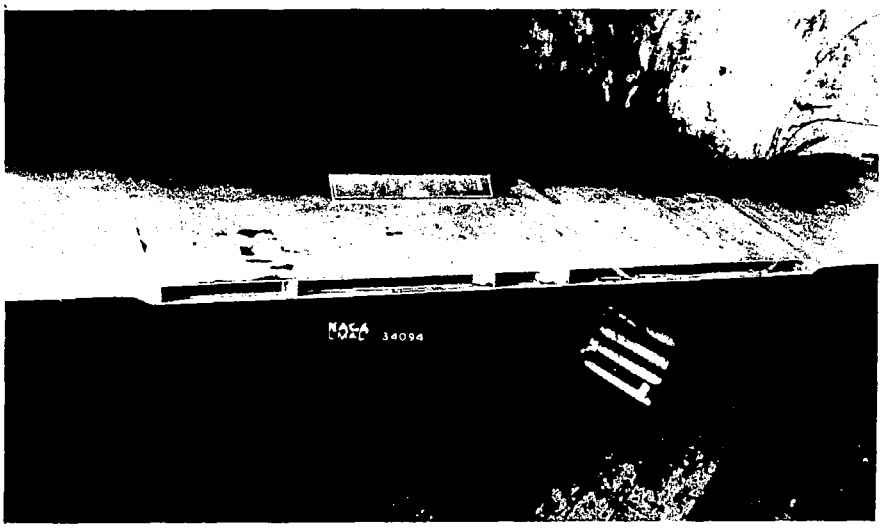

(b) Air outlet.

Figure 3.- Details of inlet section of symmetrical wing.

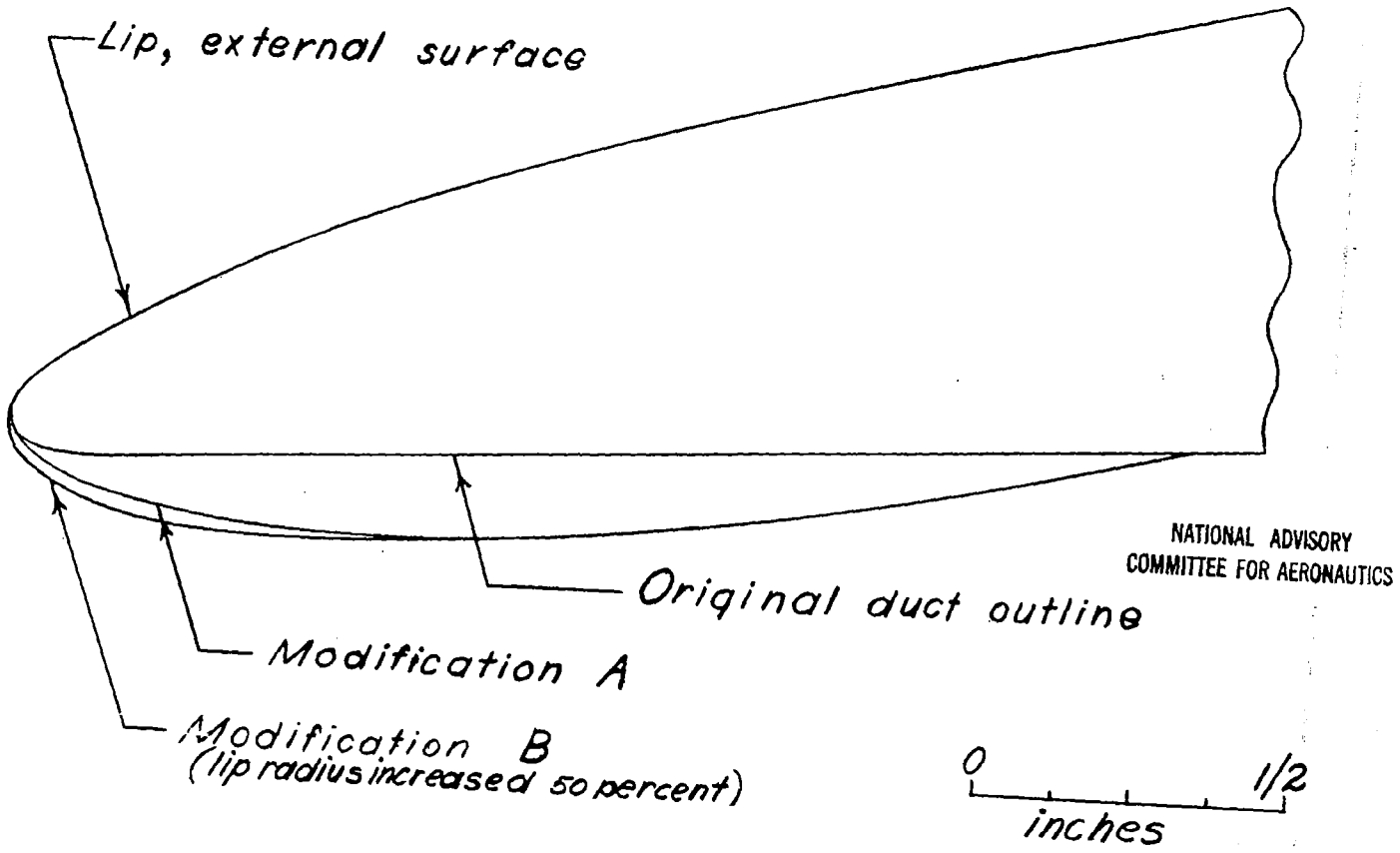

Figure 4.—Internal-lip modifications on the inlet section of the symmetrical wing.

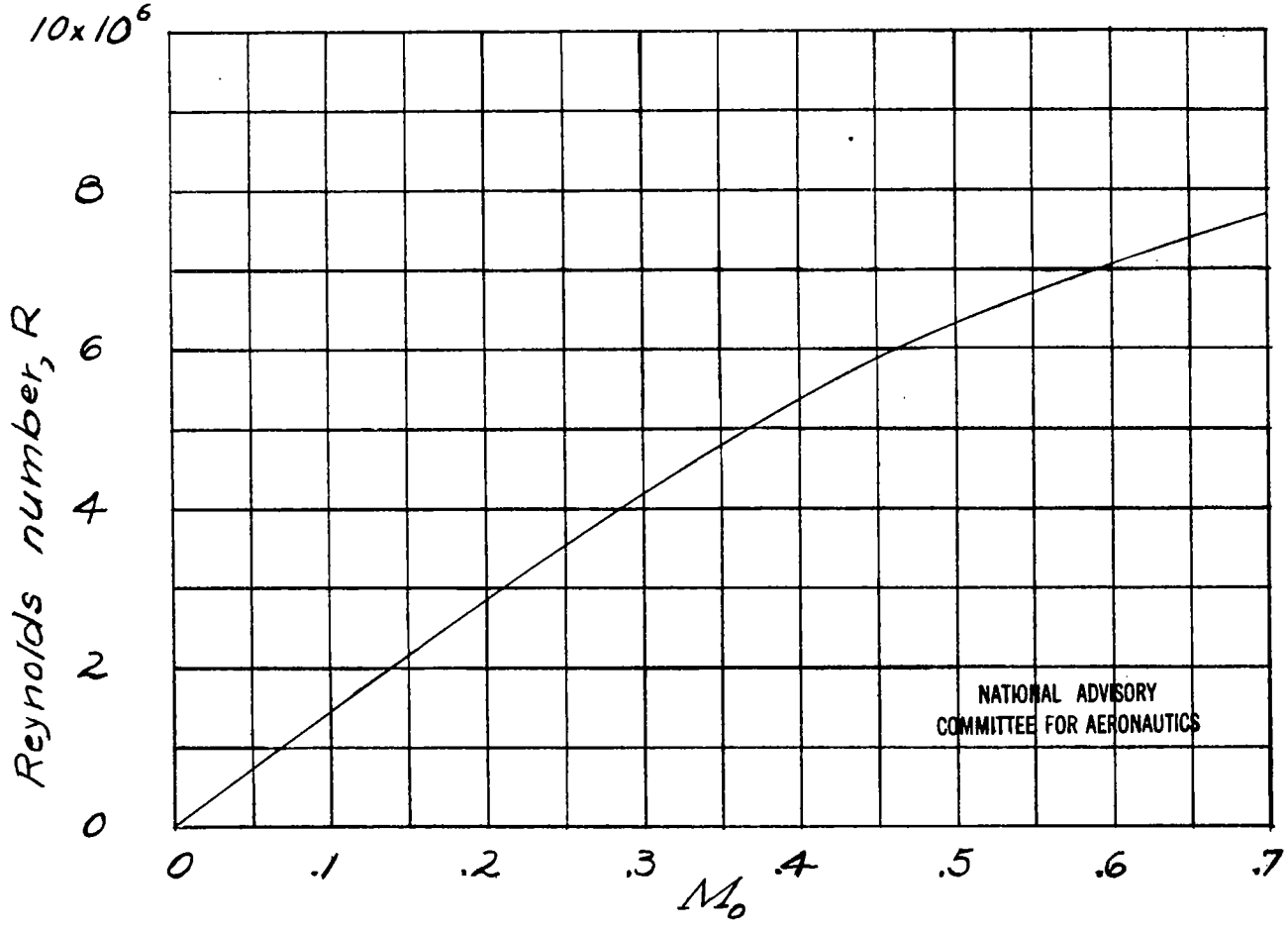

Figure 5.- Variation of Reynolds number with free-stream Mach number for 2-foot-chord airfoil in NACA 8-foot high-speed tunnel.

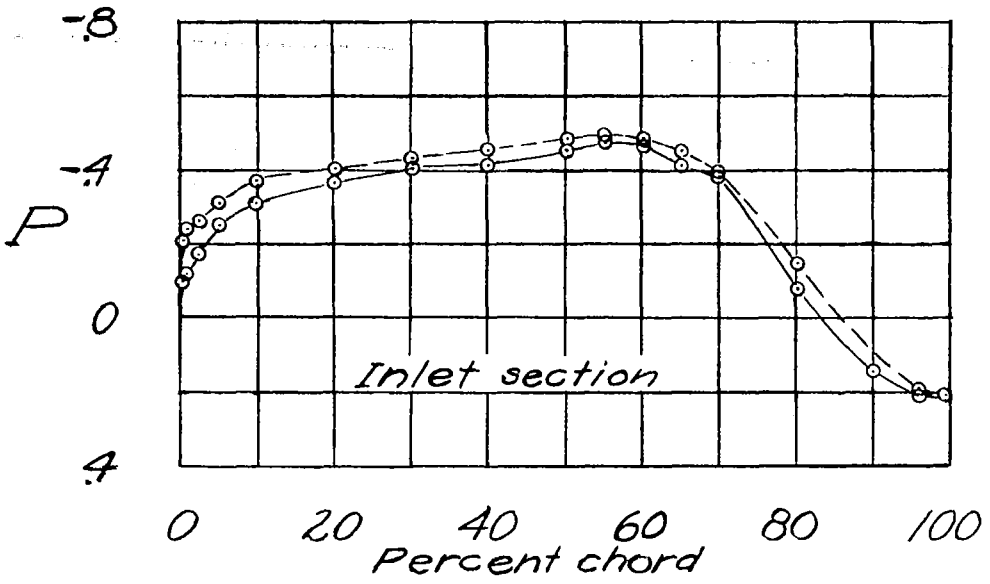

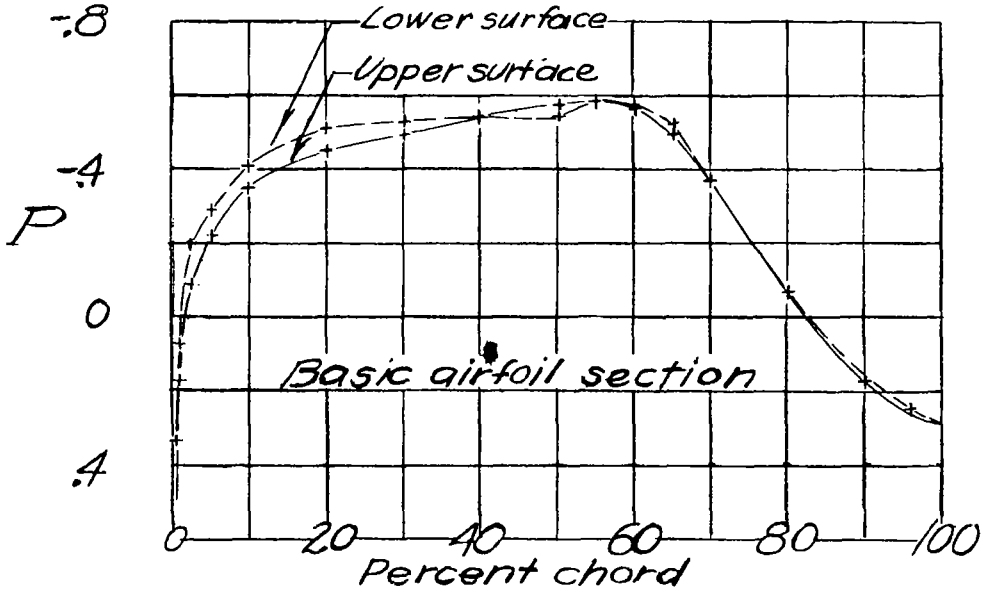

(a) $M_o = 0.20$.

Figure 6.- Pressure distributions over symmetrical wing. $\alpha_o = 0^o$; inlet section, $V_1/V_o = 0.53$.

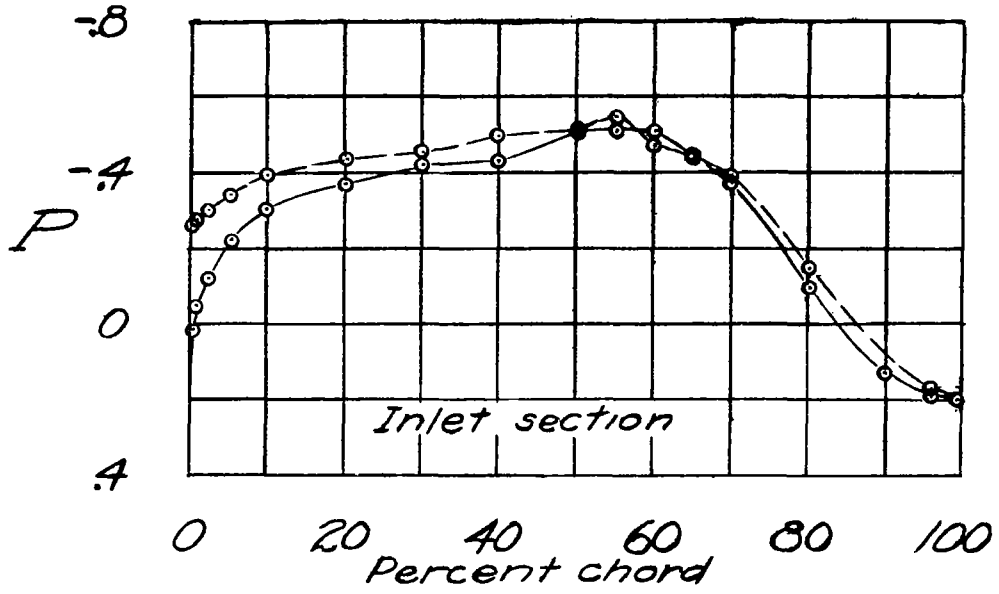

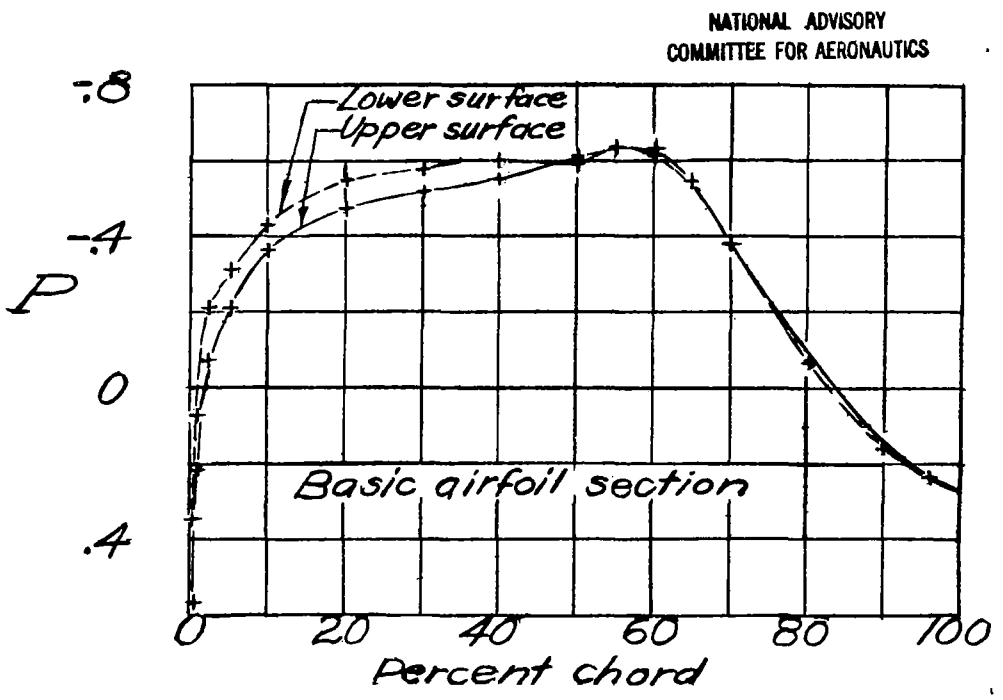

(b) $M_0 = 0.40$.

Figure 6.- Continued.

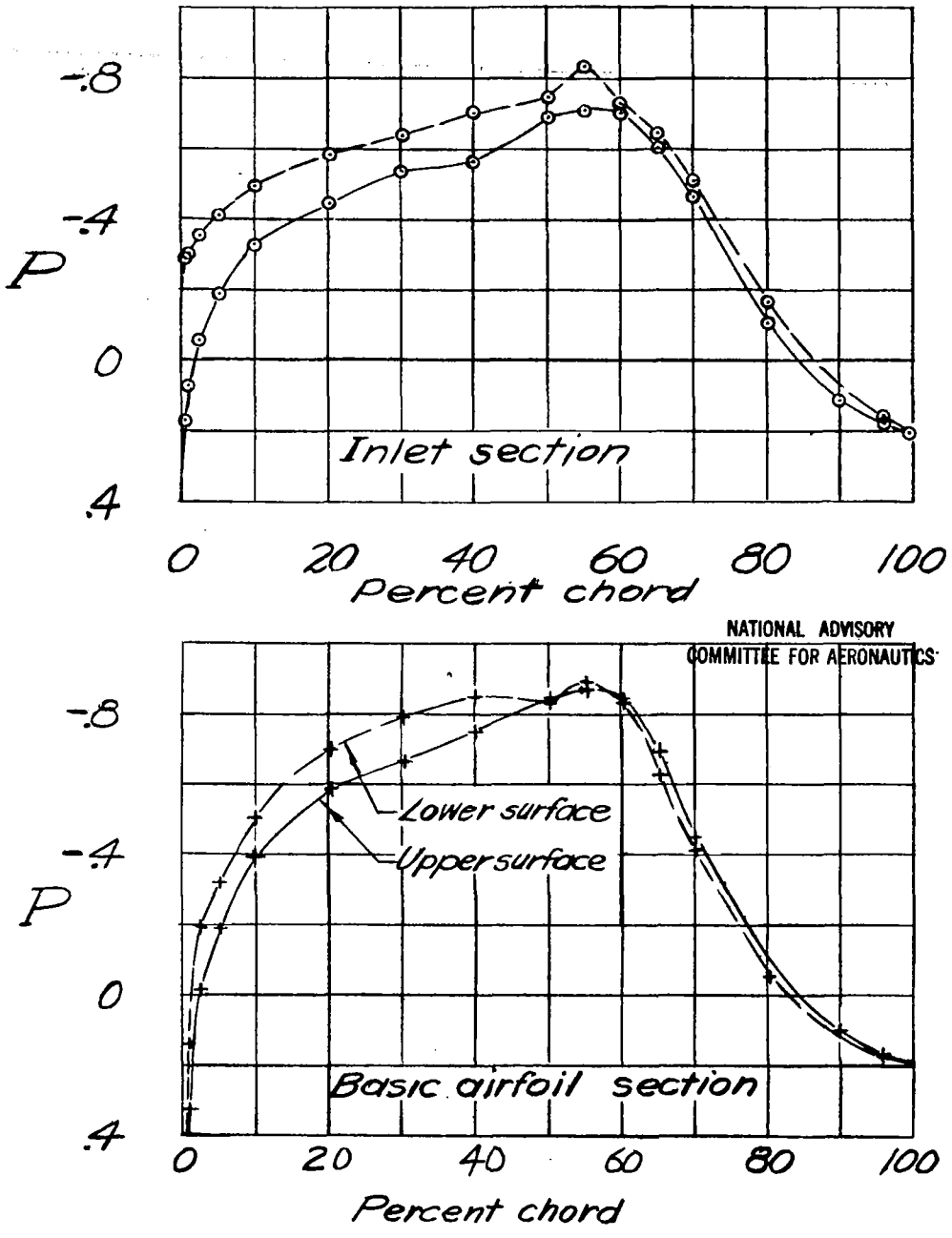

(c) $M_0 = 0.65$.

Figure 6.- Concluded.

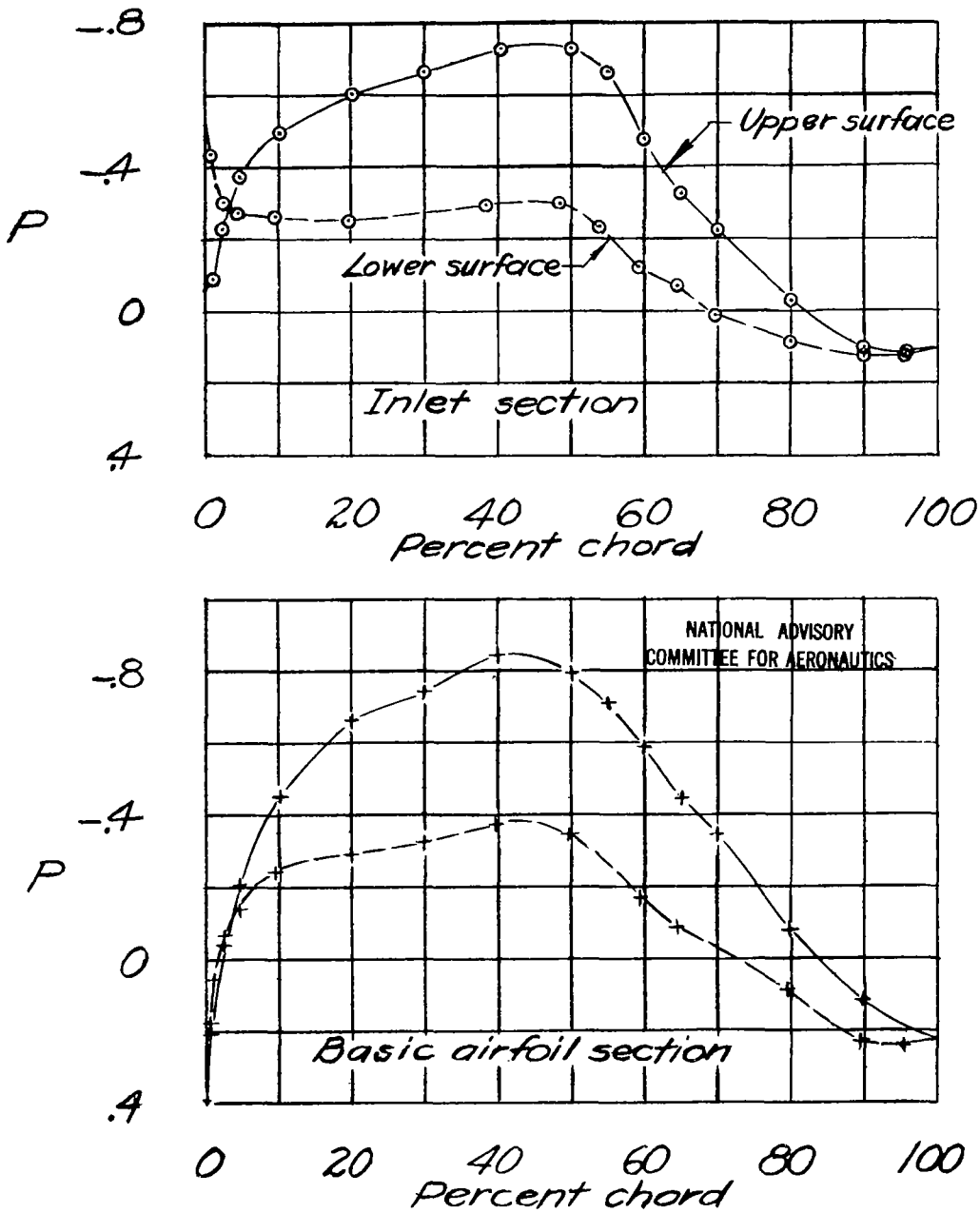

(a) $M_o = 0.20$.

Figure 7.- Pressure distributions over medium-camber wing. $\alpha_o = 0^o$; inlet section, $V_1/V_o = 0.53$.

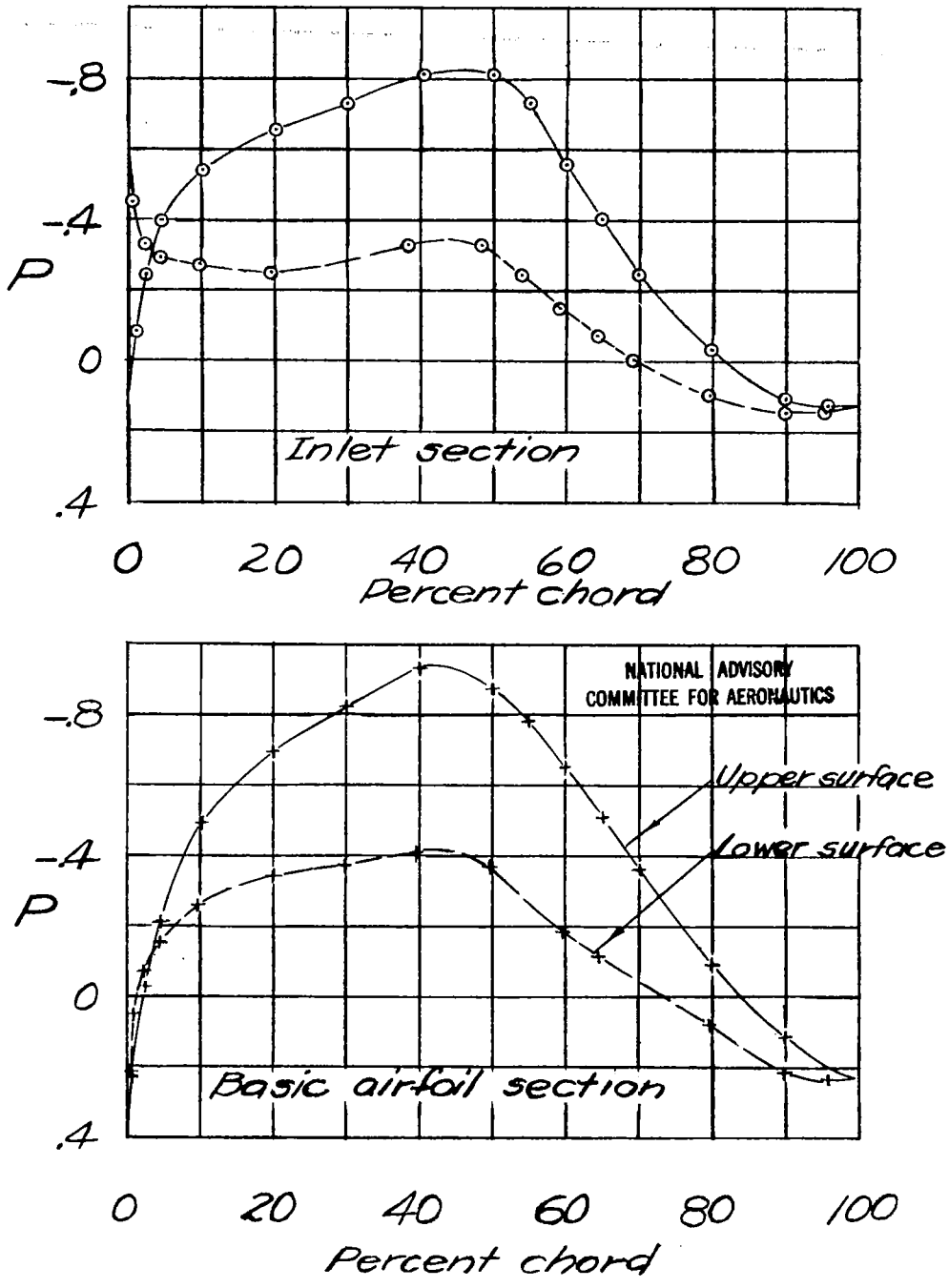

(b) $M_0 = 0.40$.

Figure 7.- Continued.

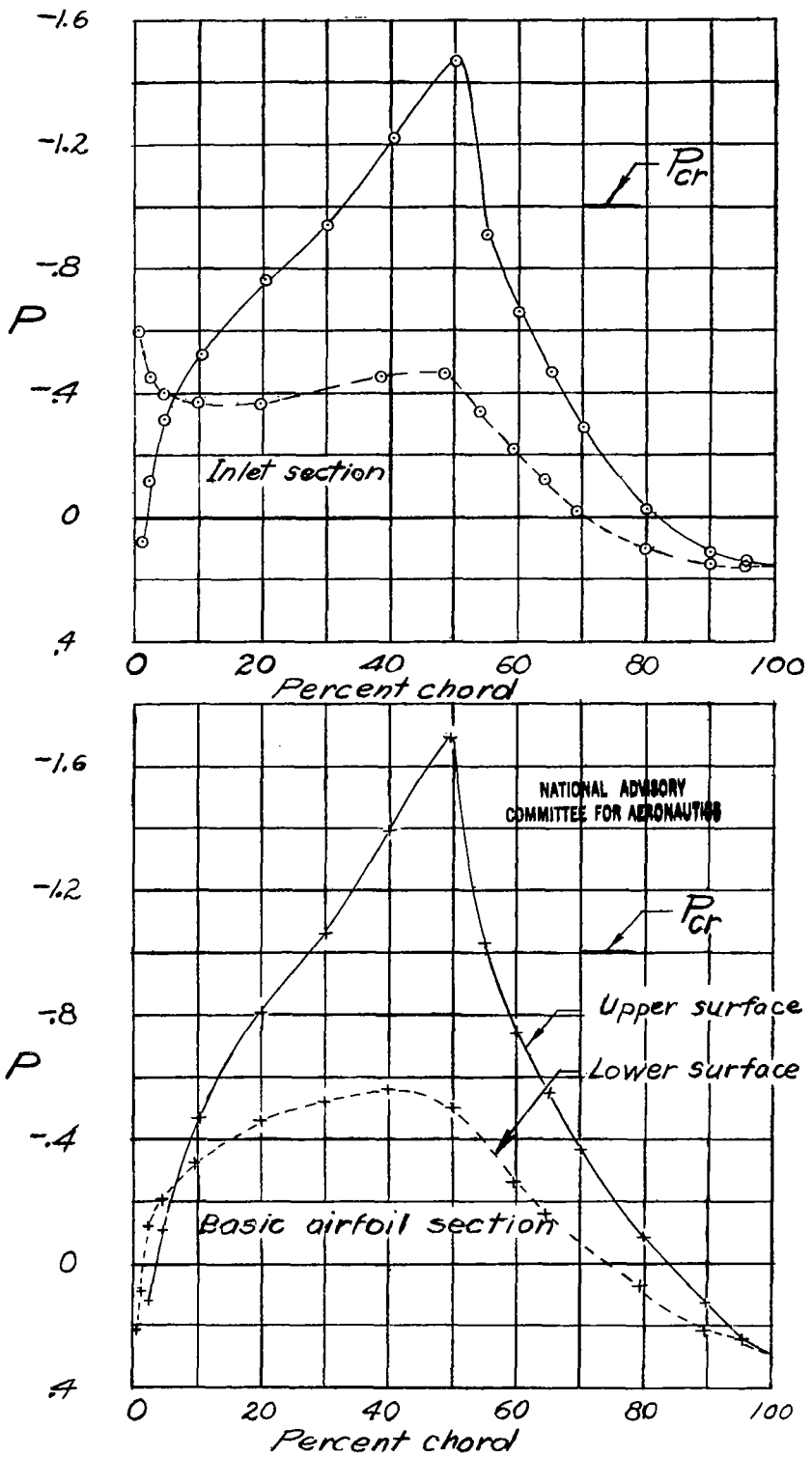

(c) $M_0 = 0.65$.

Figure 7.- Concluded.

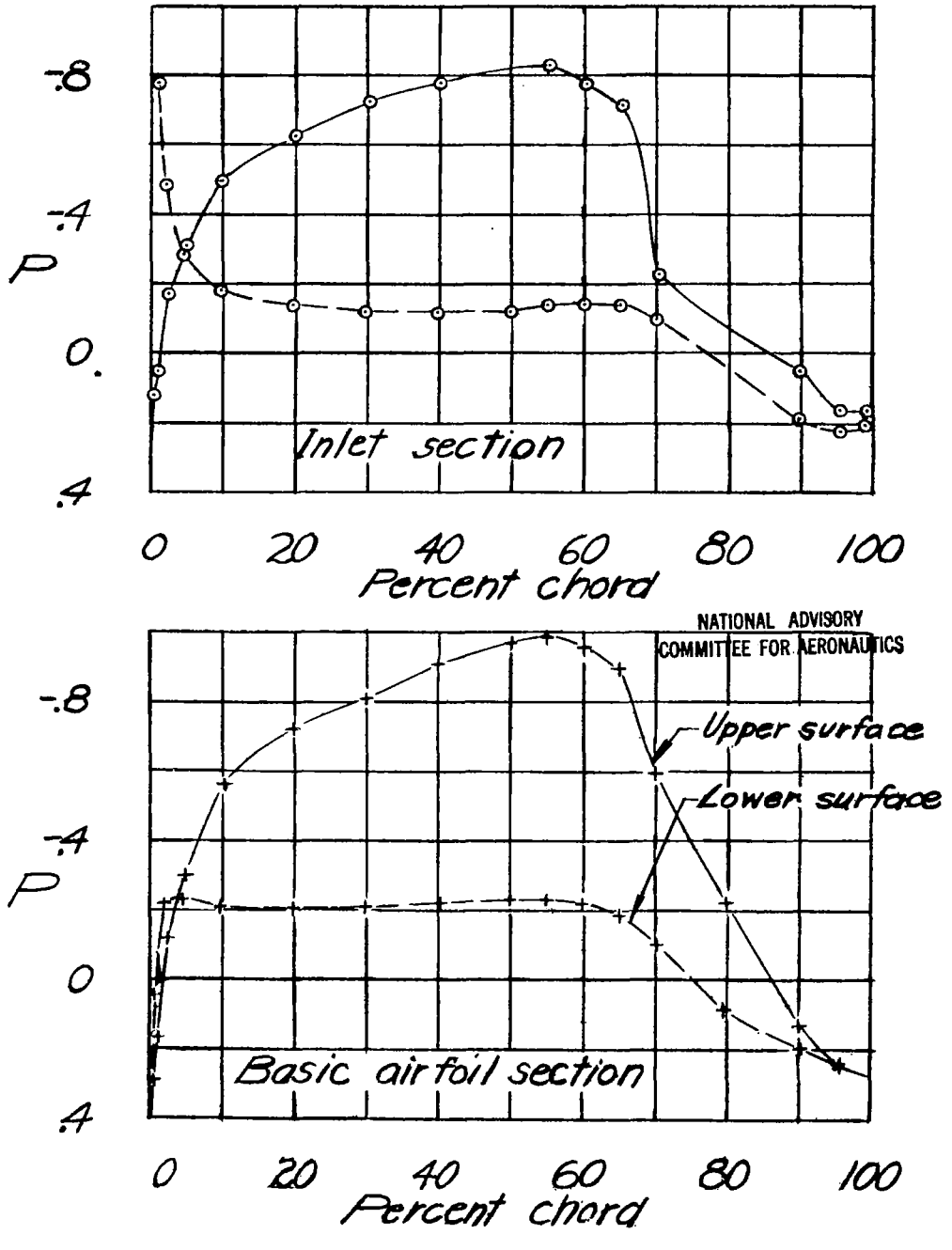

(a) $M_o = 0.20$.

Figure 8.- Pressure distributions over high-camber wing. $\alpha_o = 0^o$; inlet section, $V_1/V_o = 0.55$.

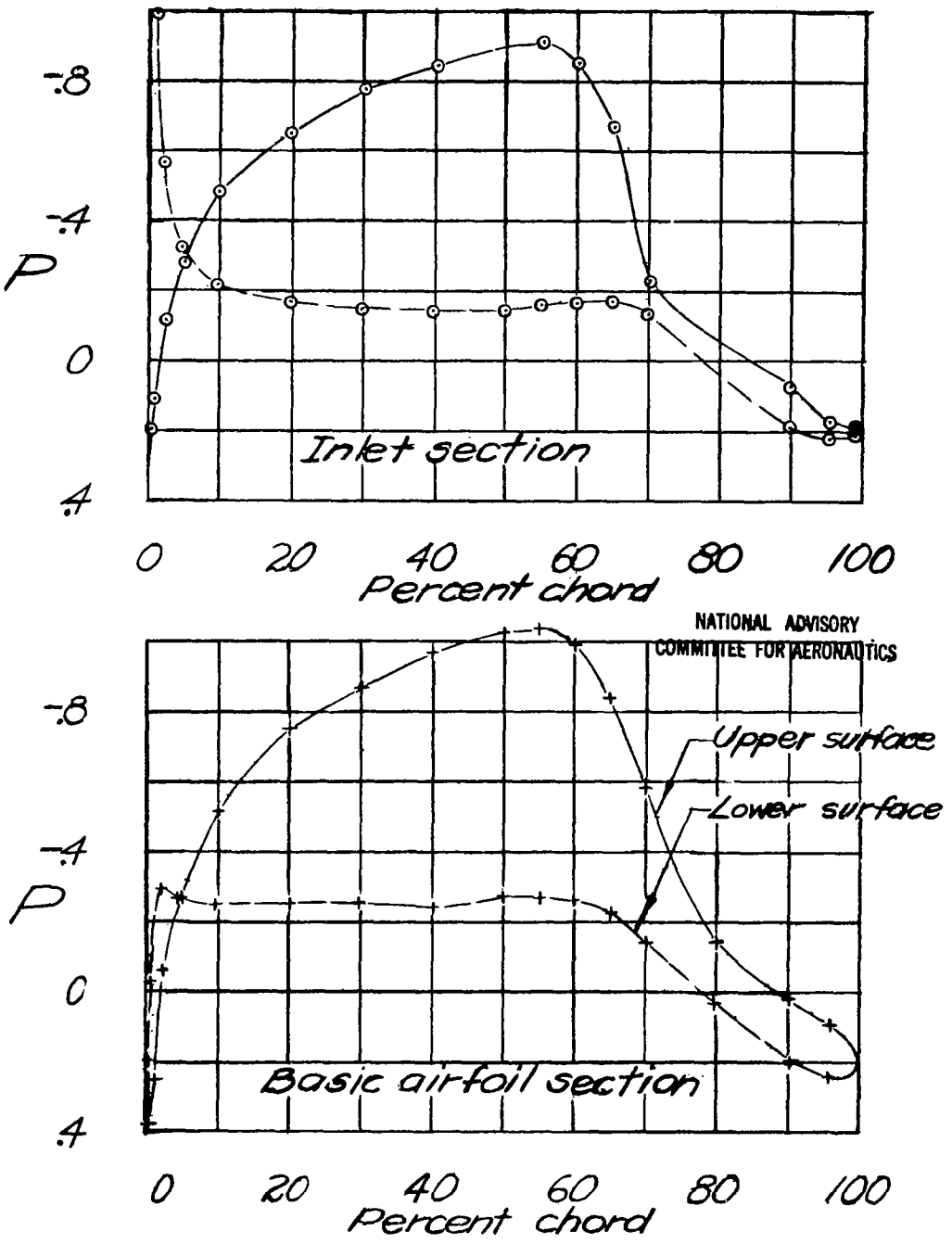

(b) $M_0 = 0.40$.

Figure 8.- Continued.

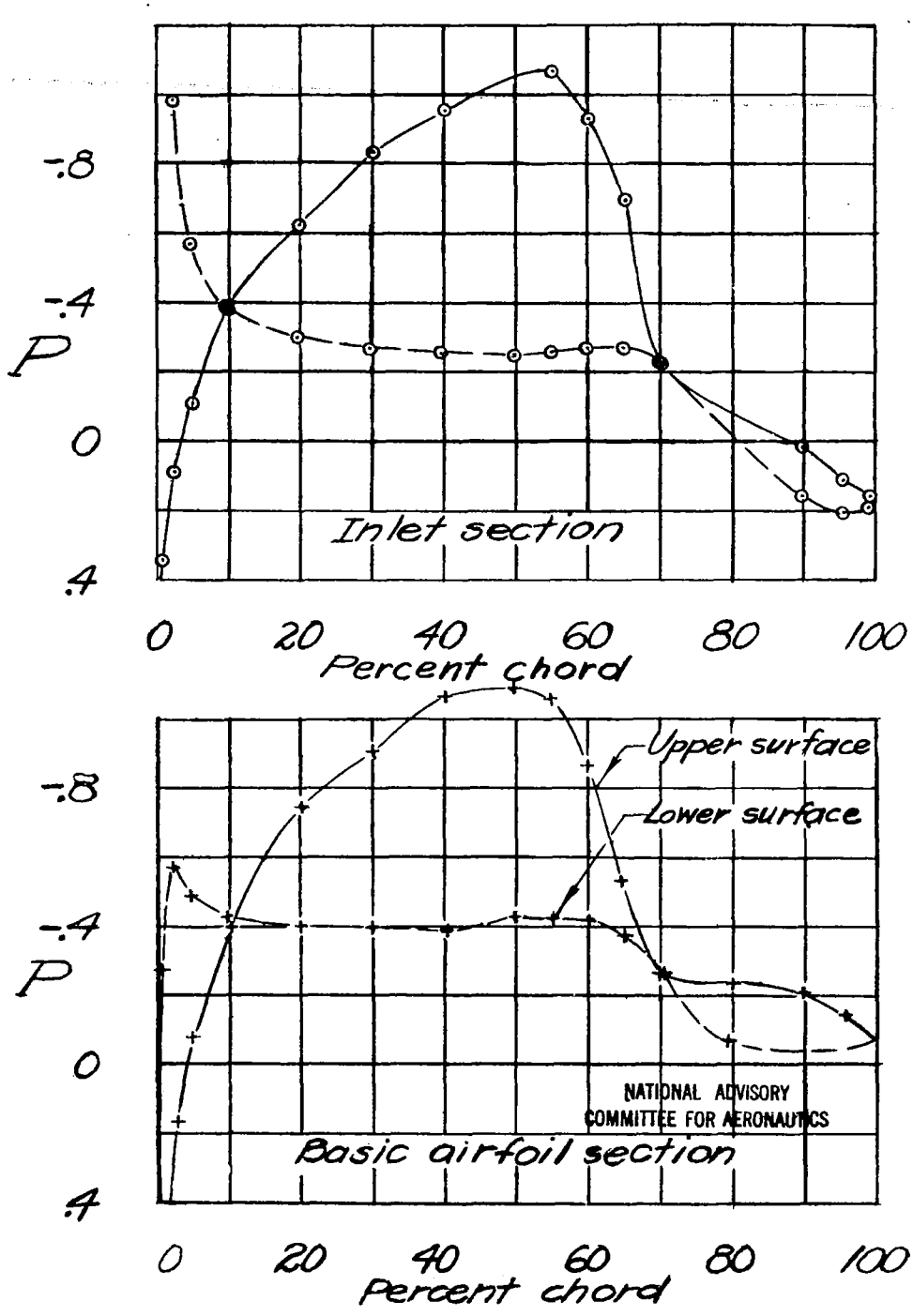

(c) M_o = 0.60.

Figure 8.- Concluded.

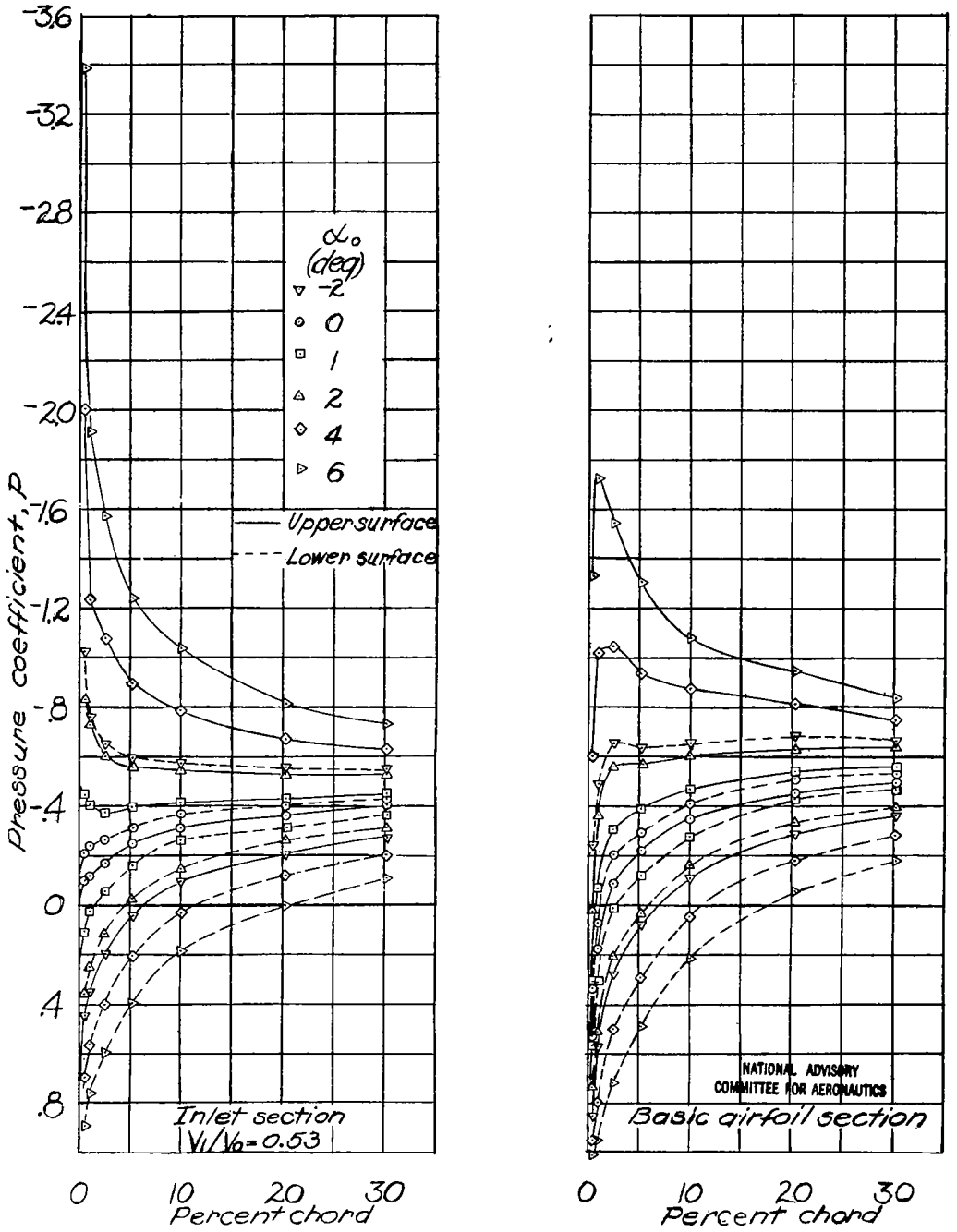

(a) $M_0 = 0.20$.

Figure 9.- Pressure distributions over forward portion of symmetrical wing for various angles of attack.

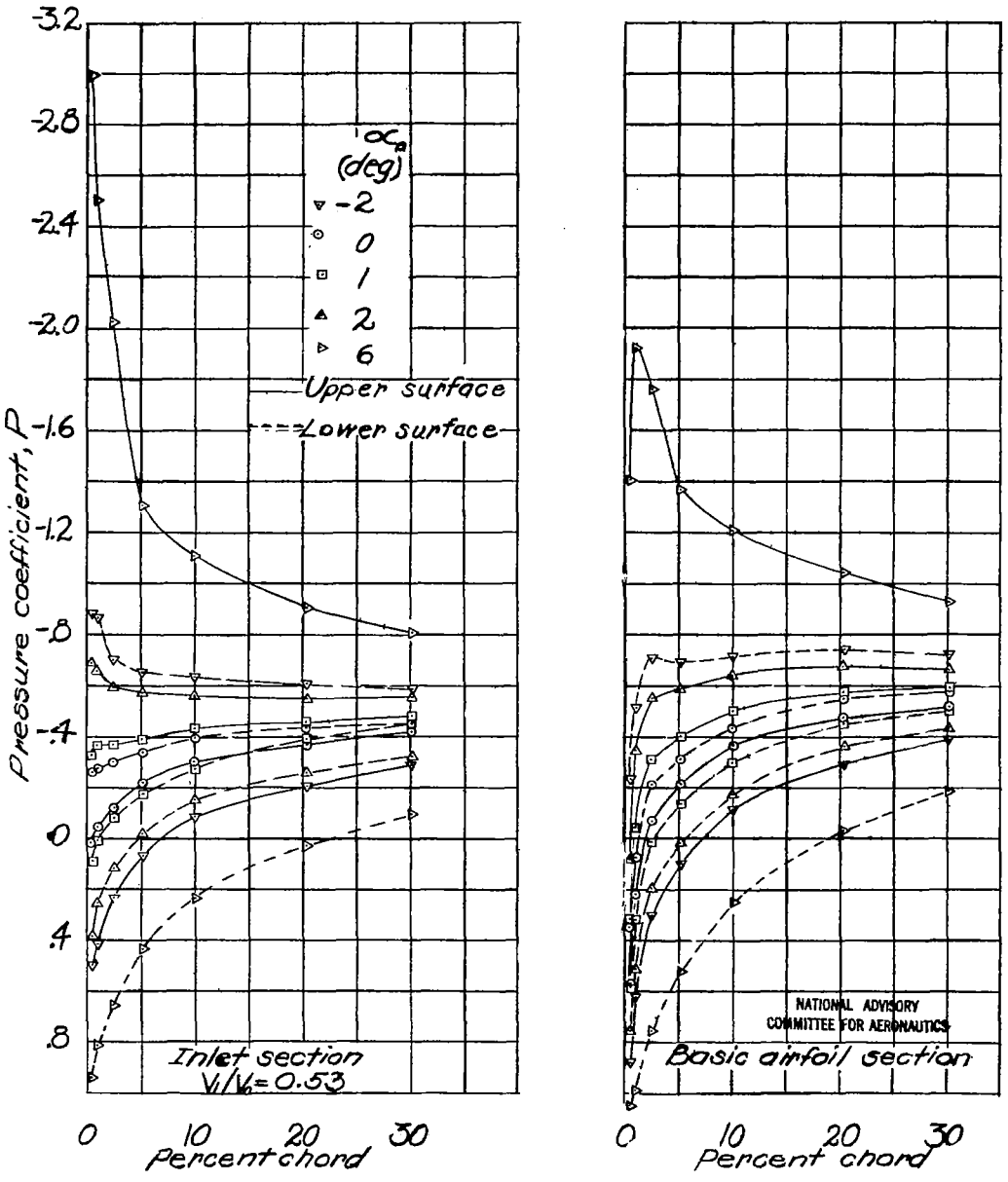

(b) M_0 = 0.40.

Figure 9.- Continued.

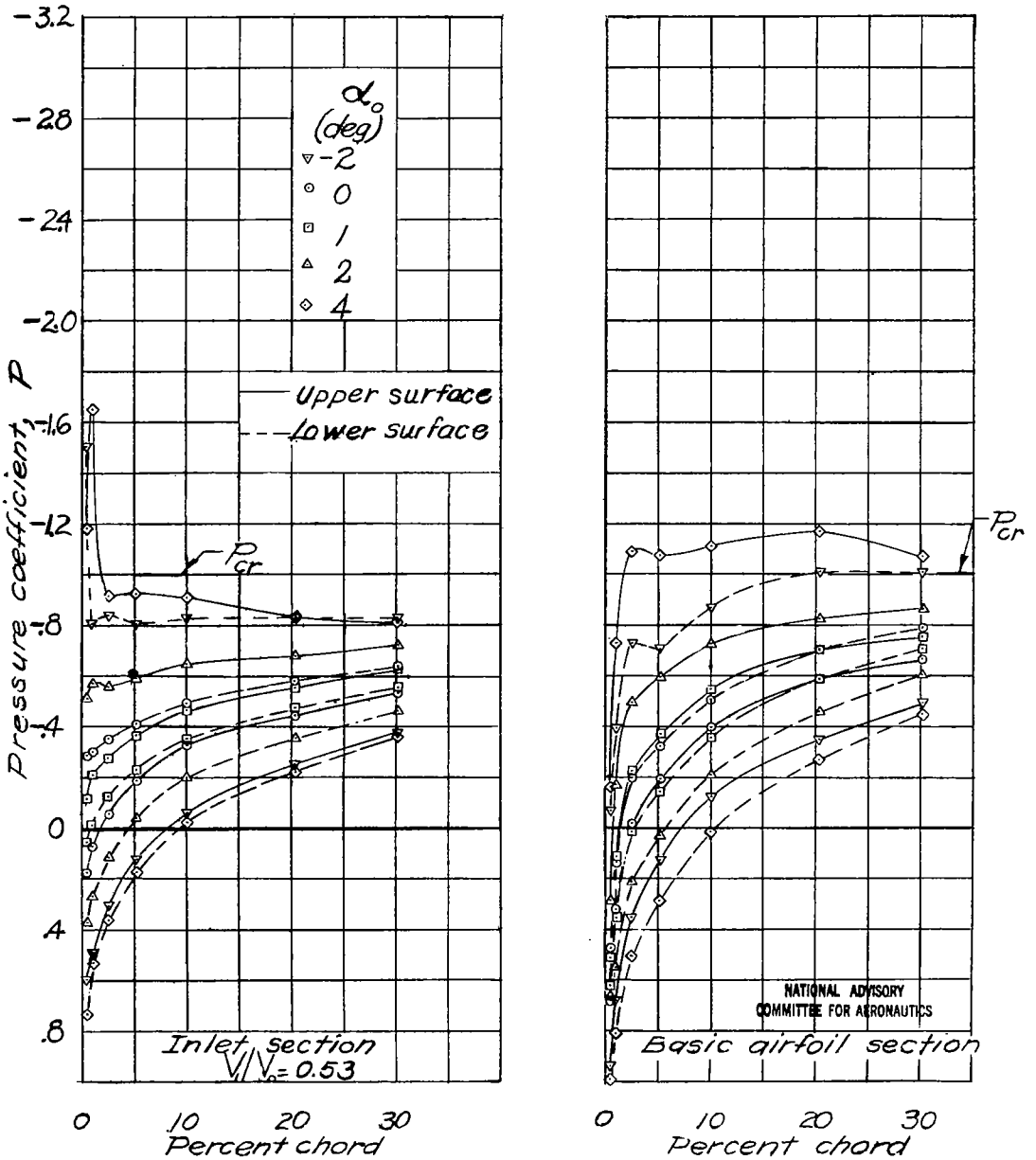

(c) M_o = 0.65.

Figure 9.- Concluded.

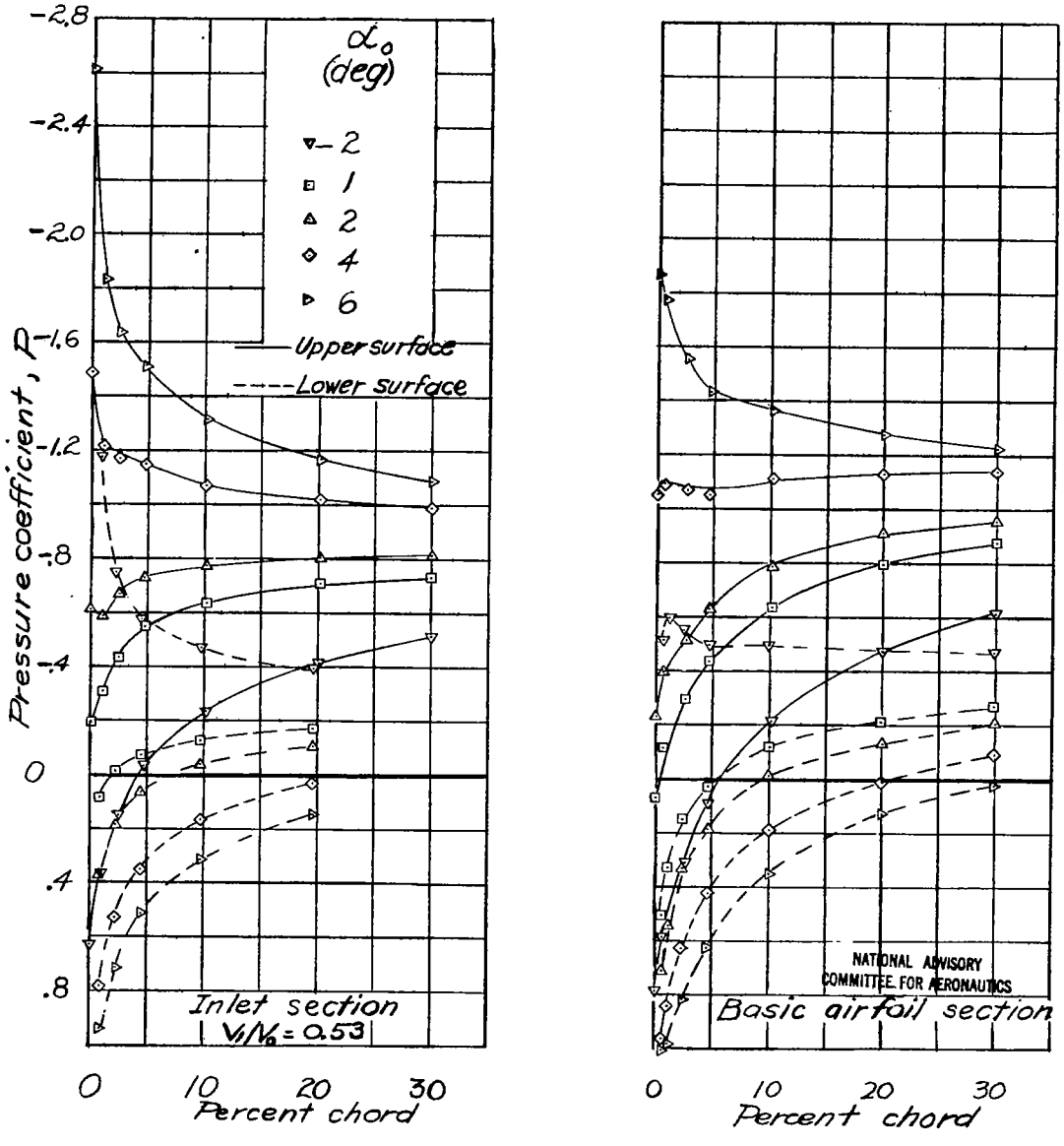

(a) M_o = 0.20.

Figure 10.- Pressure distributions over forward portion of medium-camber wing for various angles of attack.

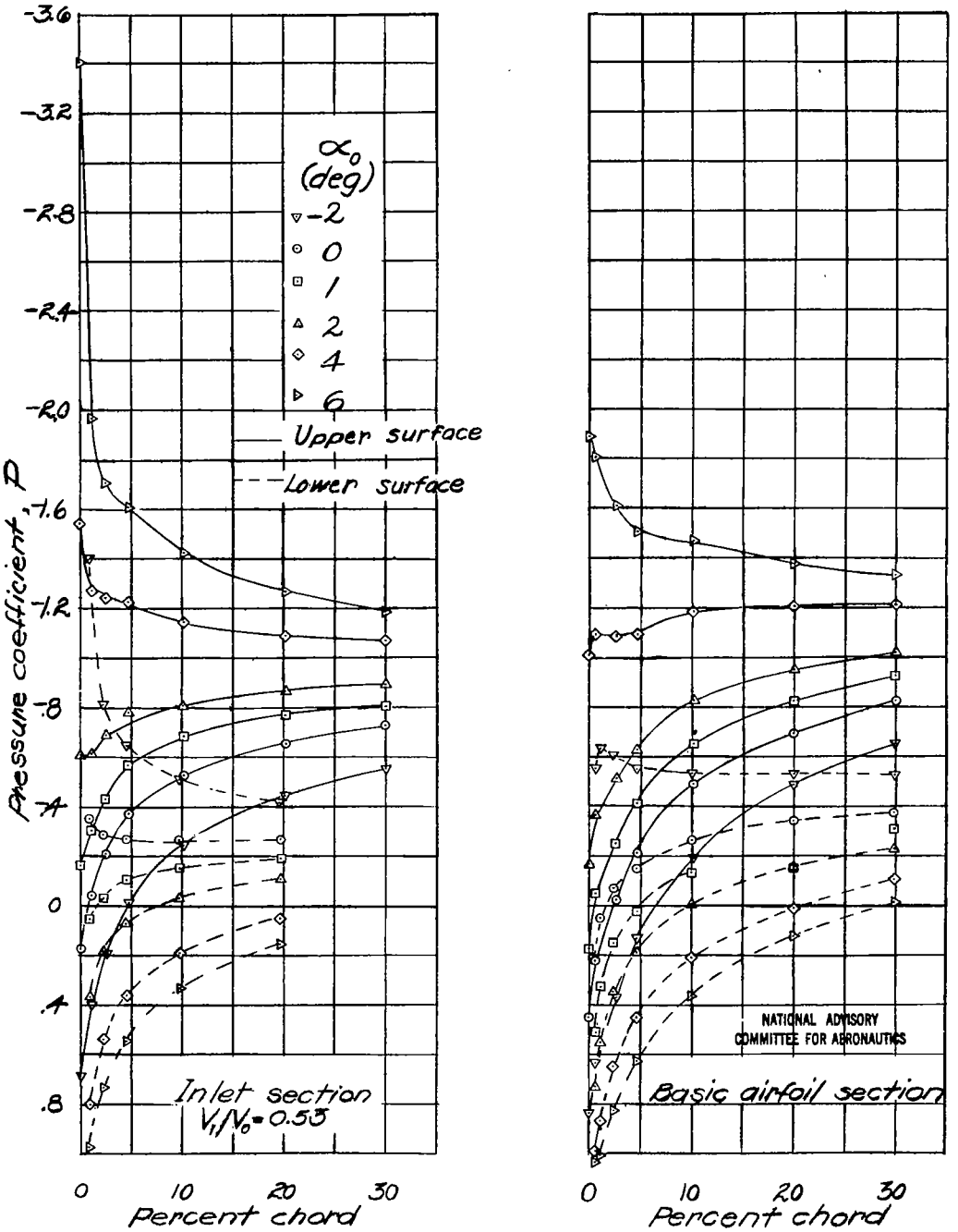

(b) M_o = 0.40.

Figure 10.- Continued.

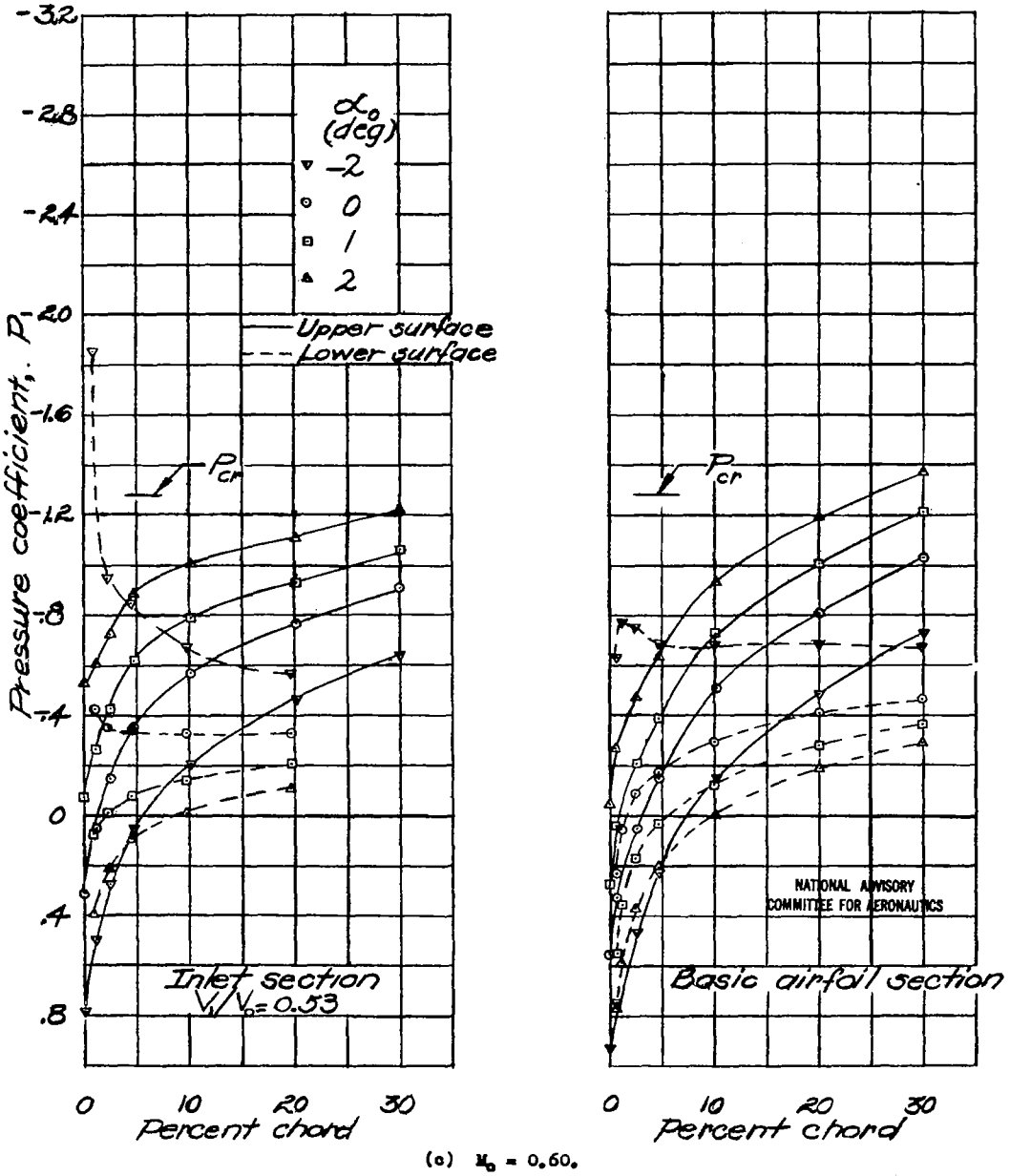

(c) $M_o = 0.60$.

Figure 10.- Concluded.

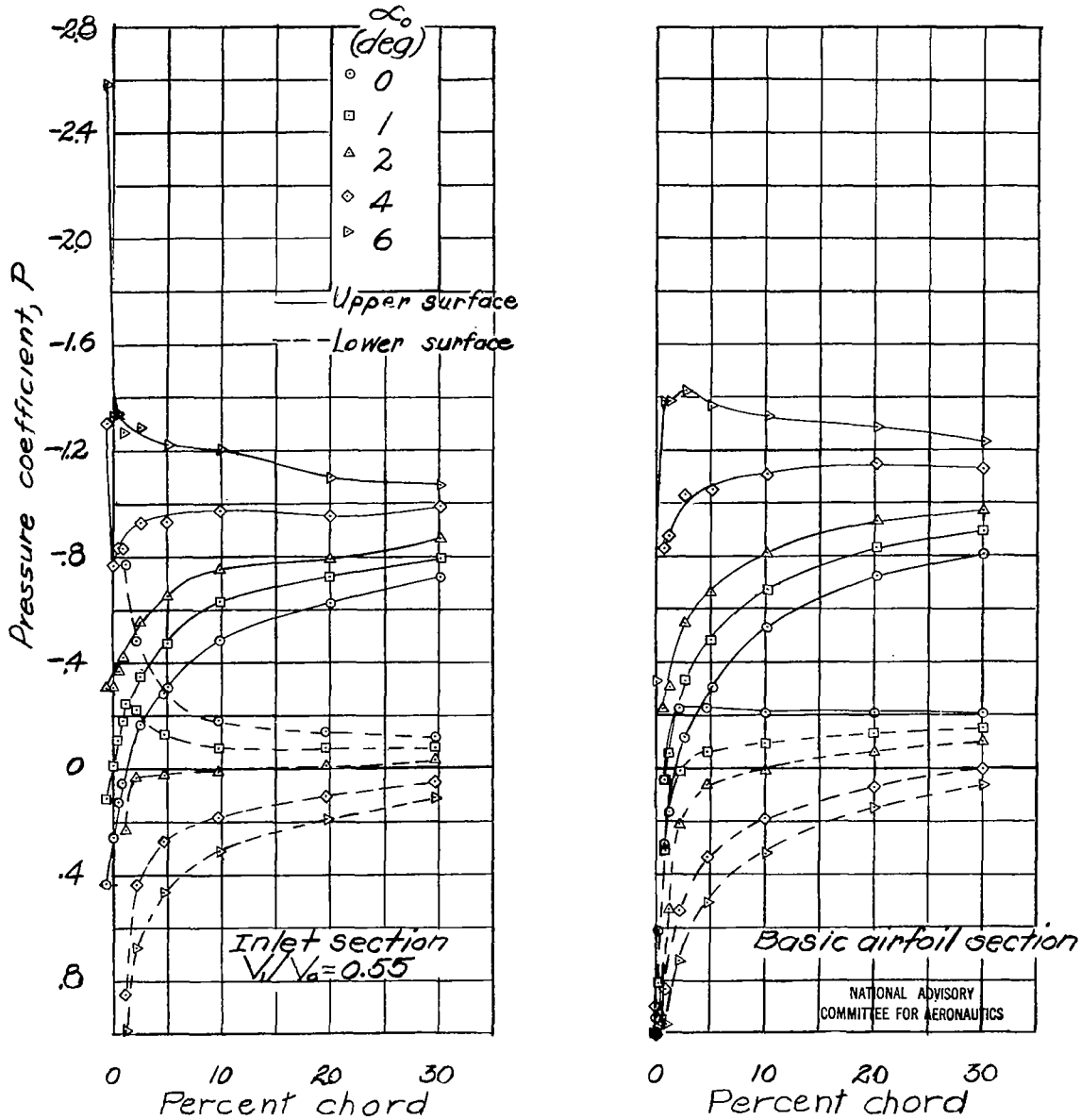

(a) M_o = 0.20.

Figure 11.- Pressure distributions over forward portion of high-camber wing for various angles of attack.

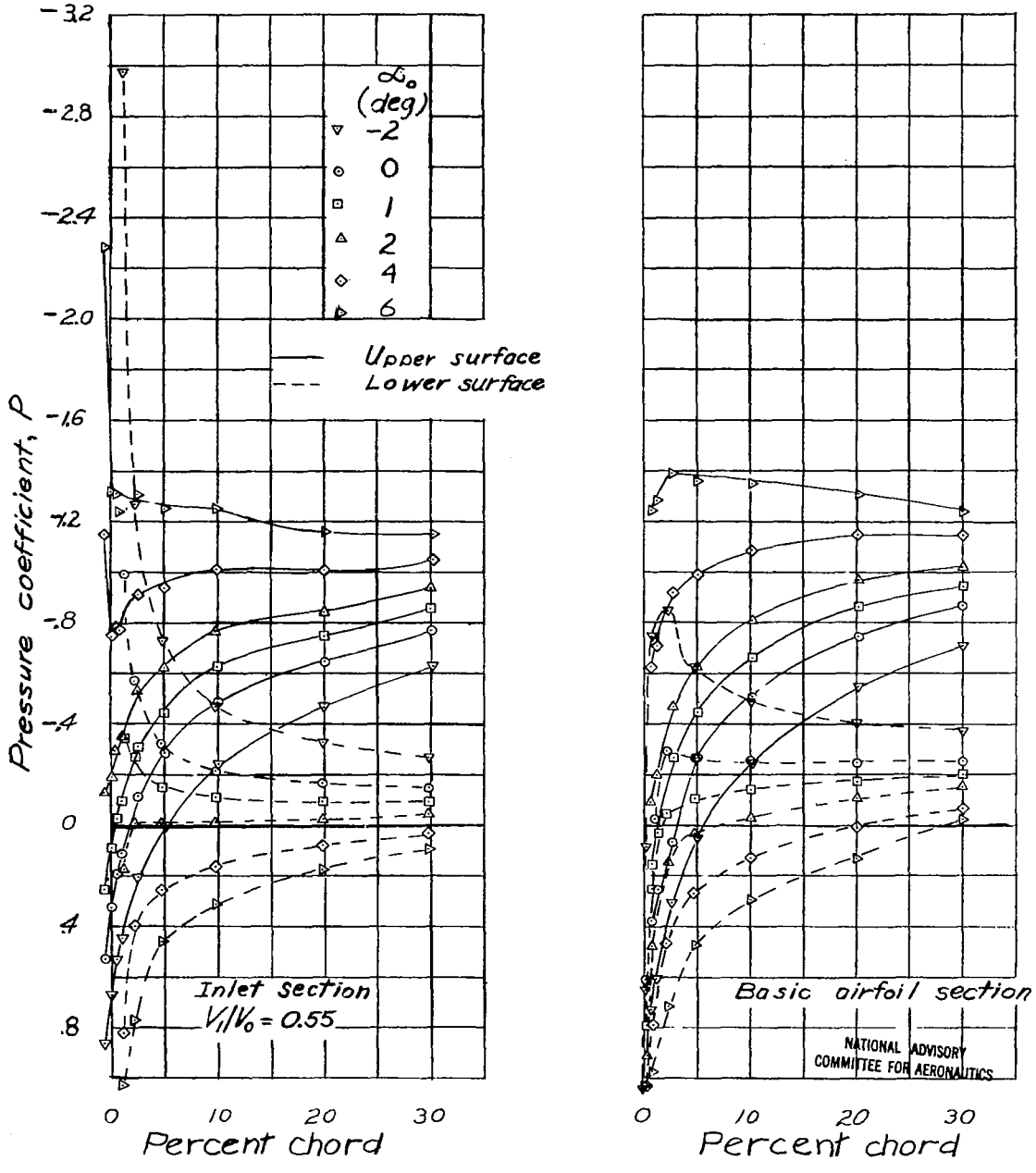

(b) $M_o = 0.40$.

Figure 11.- Continued.

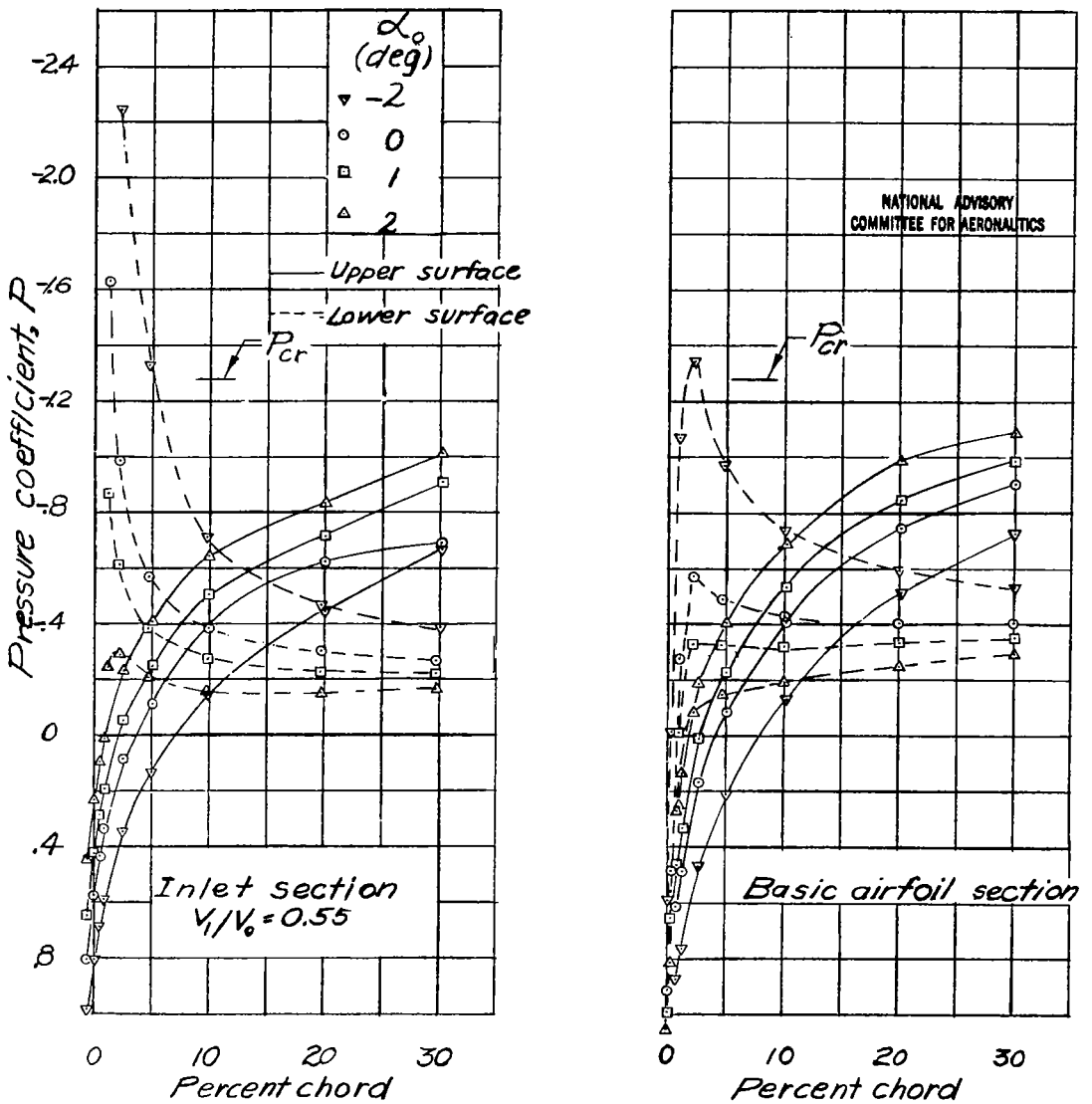

(c) $M_o = 0.60$.

Figure 11.- Concluded.

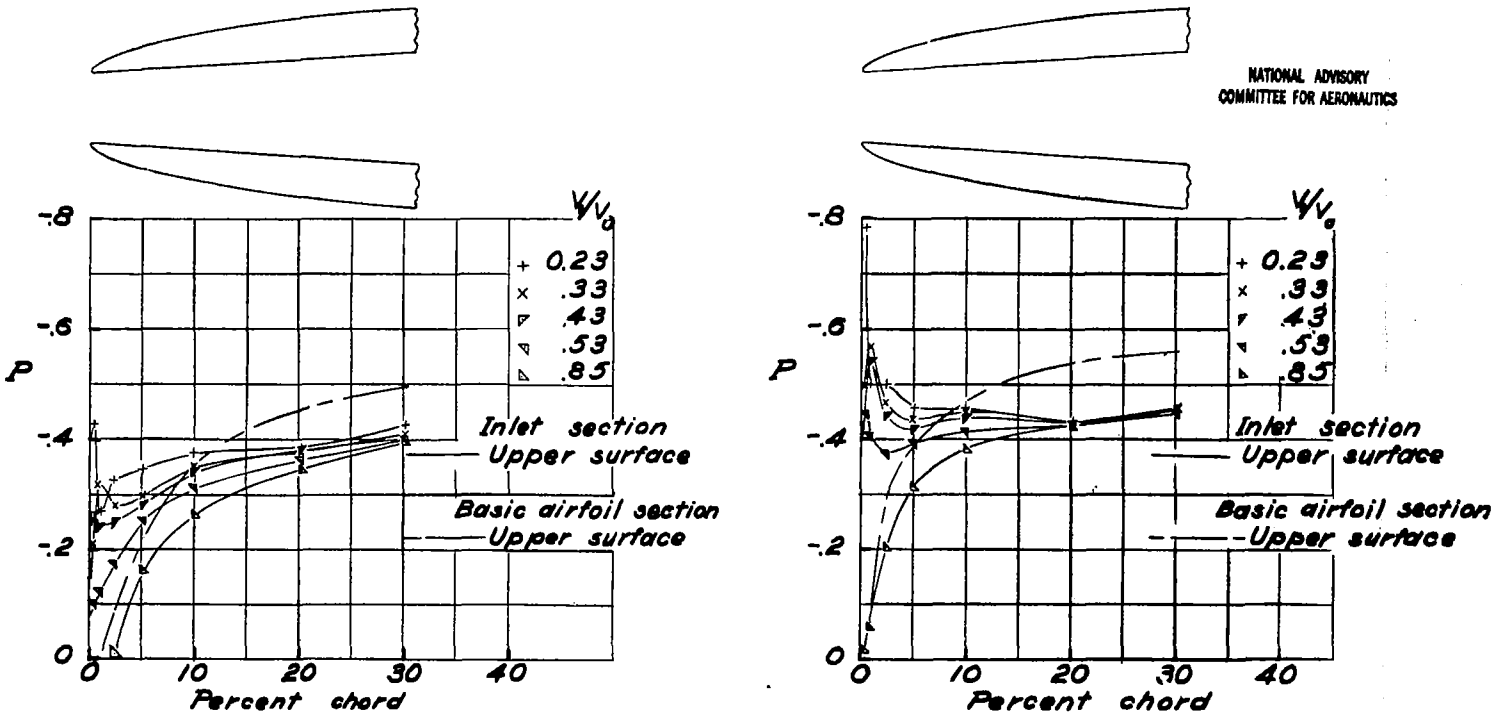

(a) $\alpha_0 = 0^\circ$.

(b) $\alpha_0 = 1^\circ$.

Figure 12.- Pressure distributions over forward portion of inlet section of symmetrical wing for various inlet-velocity ratios. $M_0 = 0.20$.

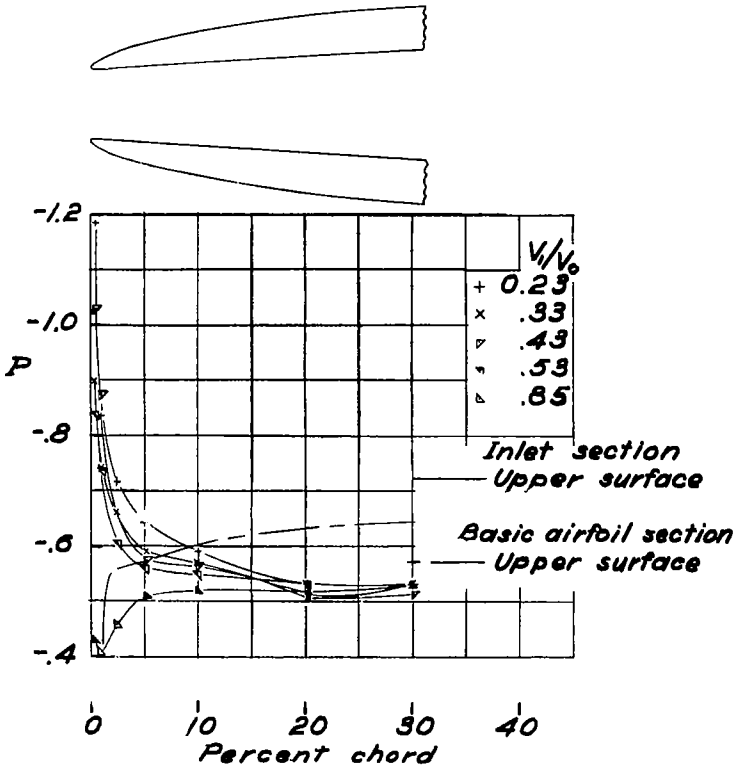

(c) $\alpha_o = 2^\circ$.

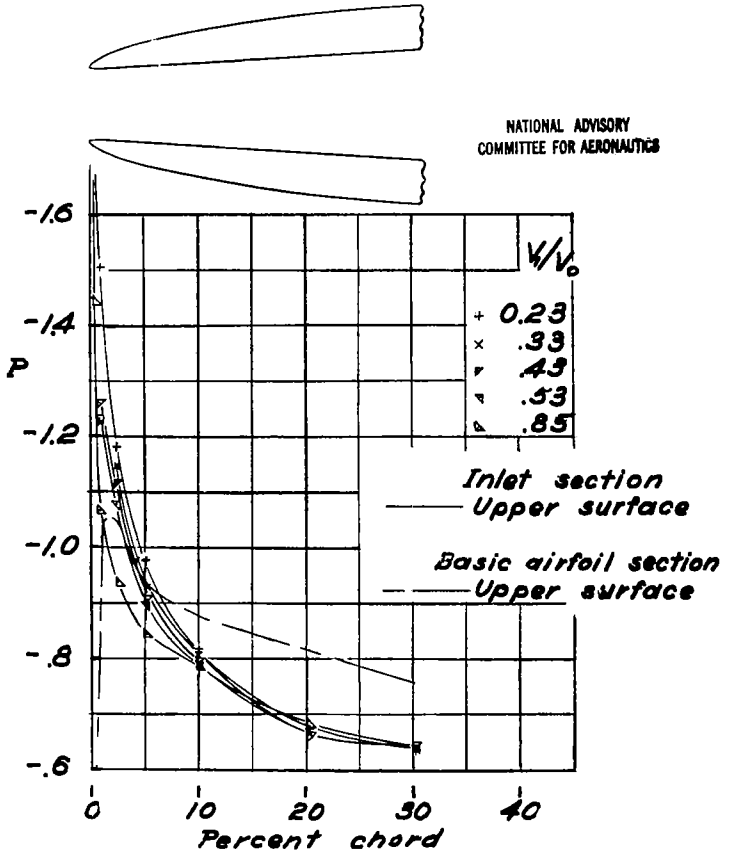

(d) $\alpha_o = 4^\circ$.

Figure 12.- Concluded.

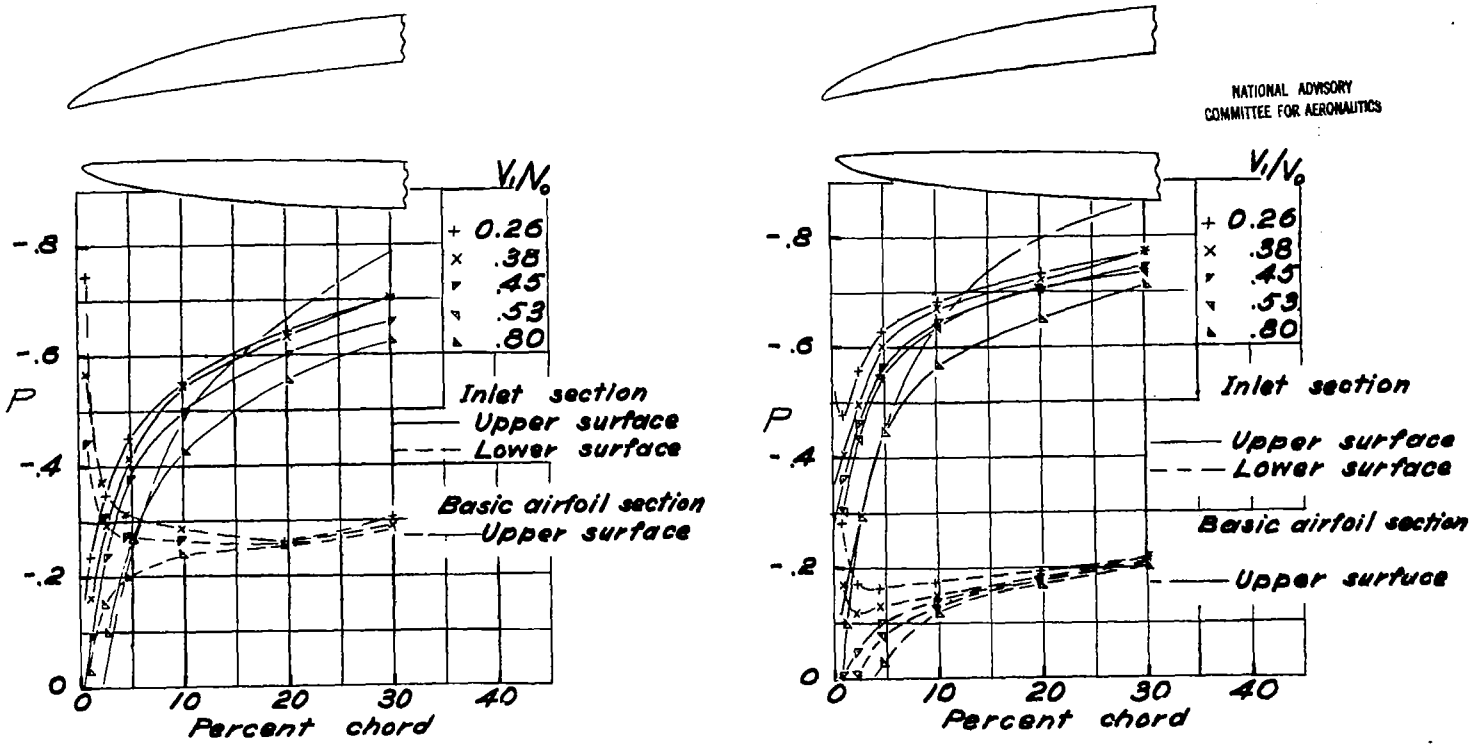

(a) $\alpha_0 = 0^\circ$.

(b) $\alpha_0 = 1^\circ$.

Figure 13.- Pressure distributions over forward portion of inlet section of medium-camber wing for various inlet-velocity ratios. $M_0 = 0.20$.

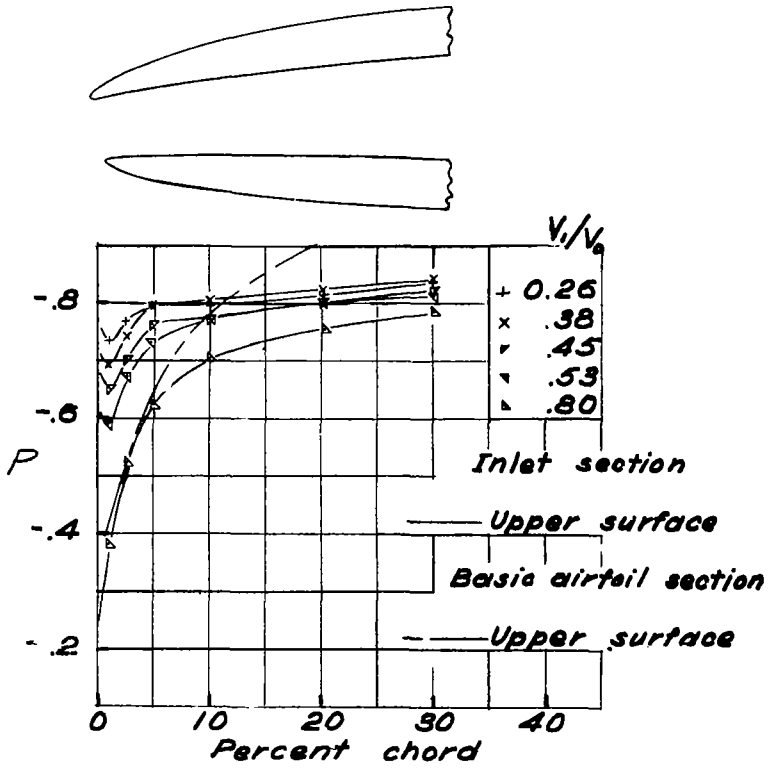

(c) $\alpha_0 = 2°$.

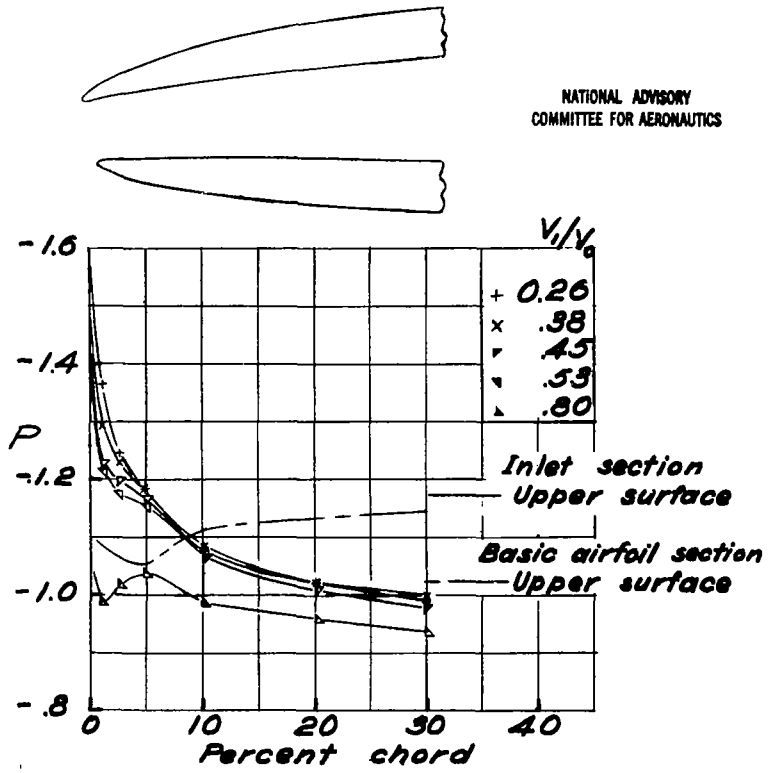

(d) $\alpha_0 = 4°$.

Figure 13.- Concluded.

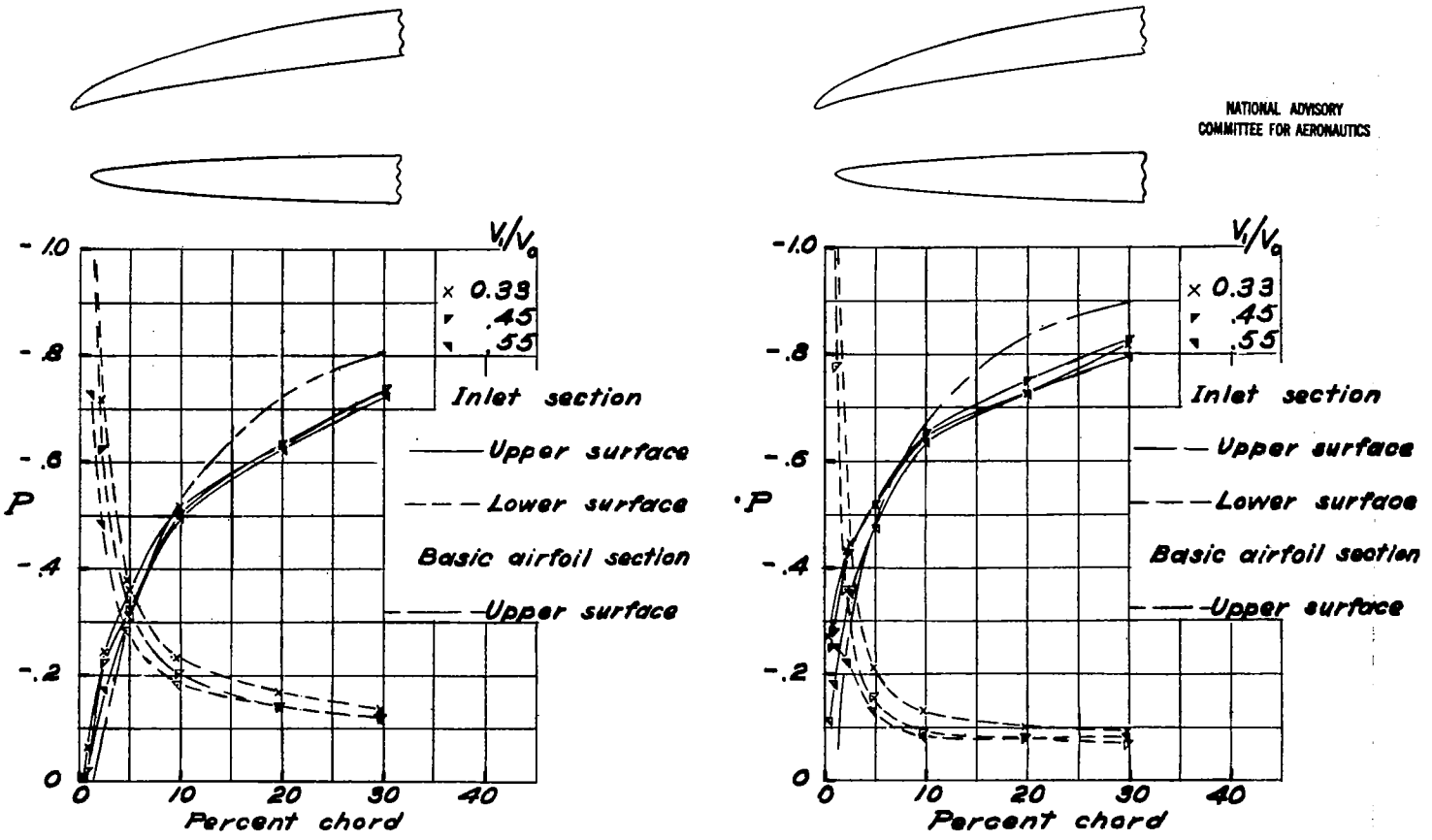

(a) $\alpha_0 = 0°$.

(b) $\alpha_0 = 1°$.

Figure 14.- Pressure distributions over forward portion of inlet section of high-camber wing for various inlet-velocity ratios. $M_0 = 0.20$.

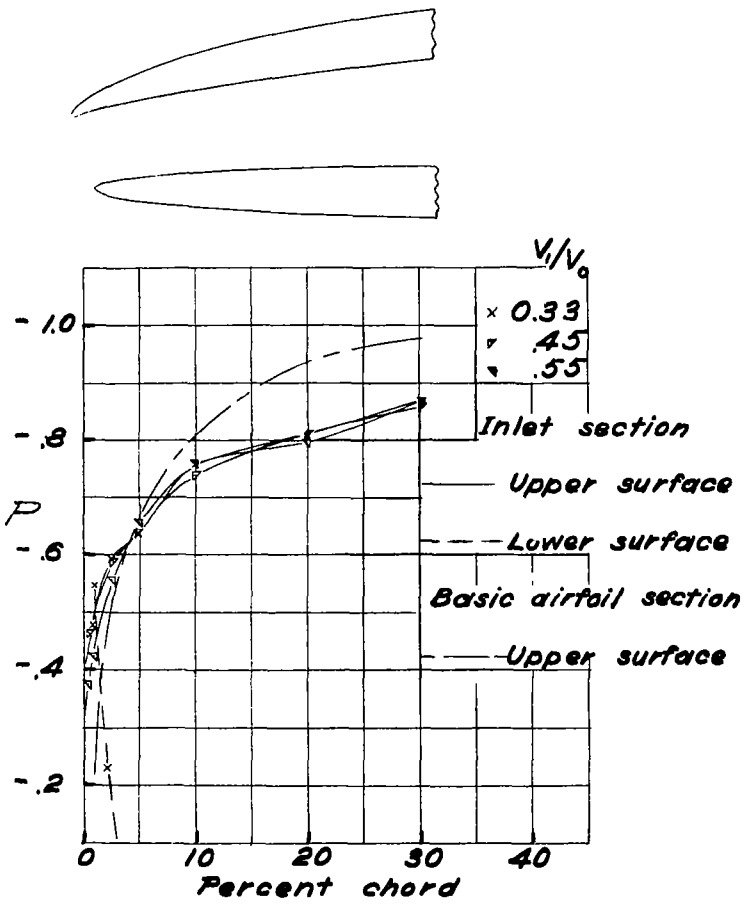

(a) $\alpha_0 = 2°$.

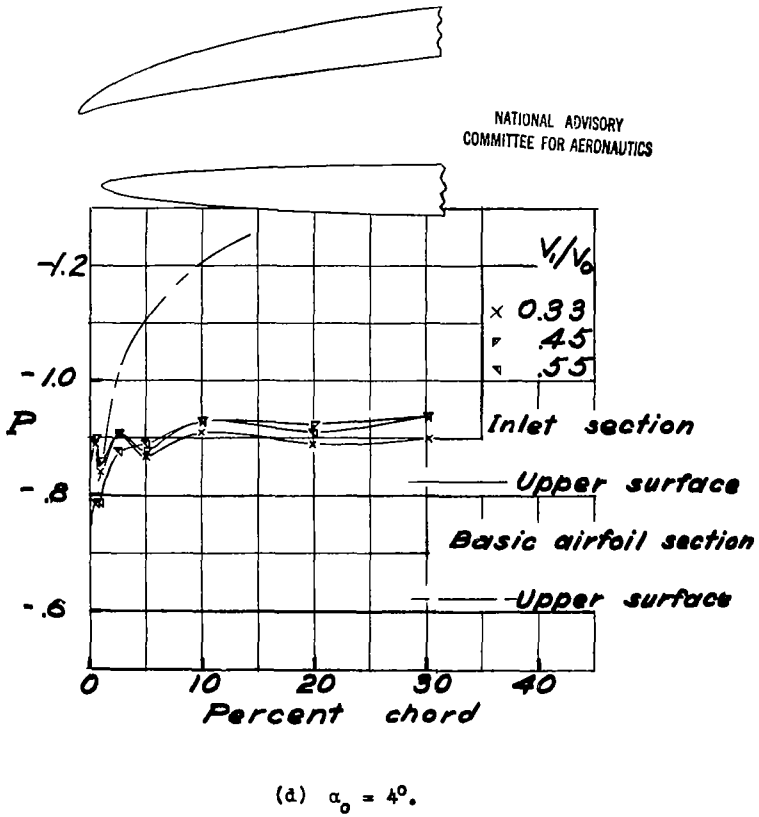

(d) $\alpha_0 = 4°$.

Figure 14.- Concluded.

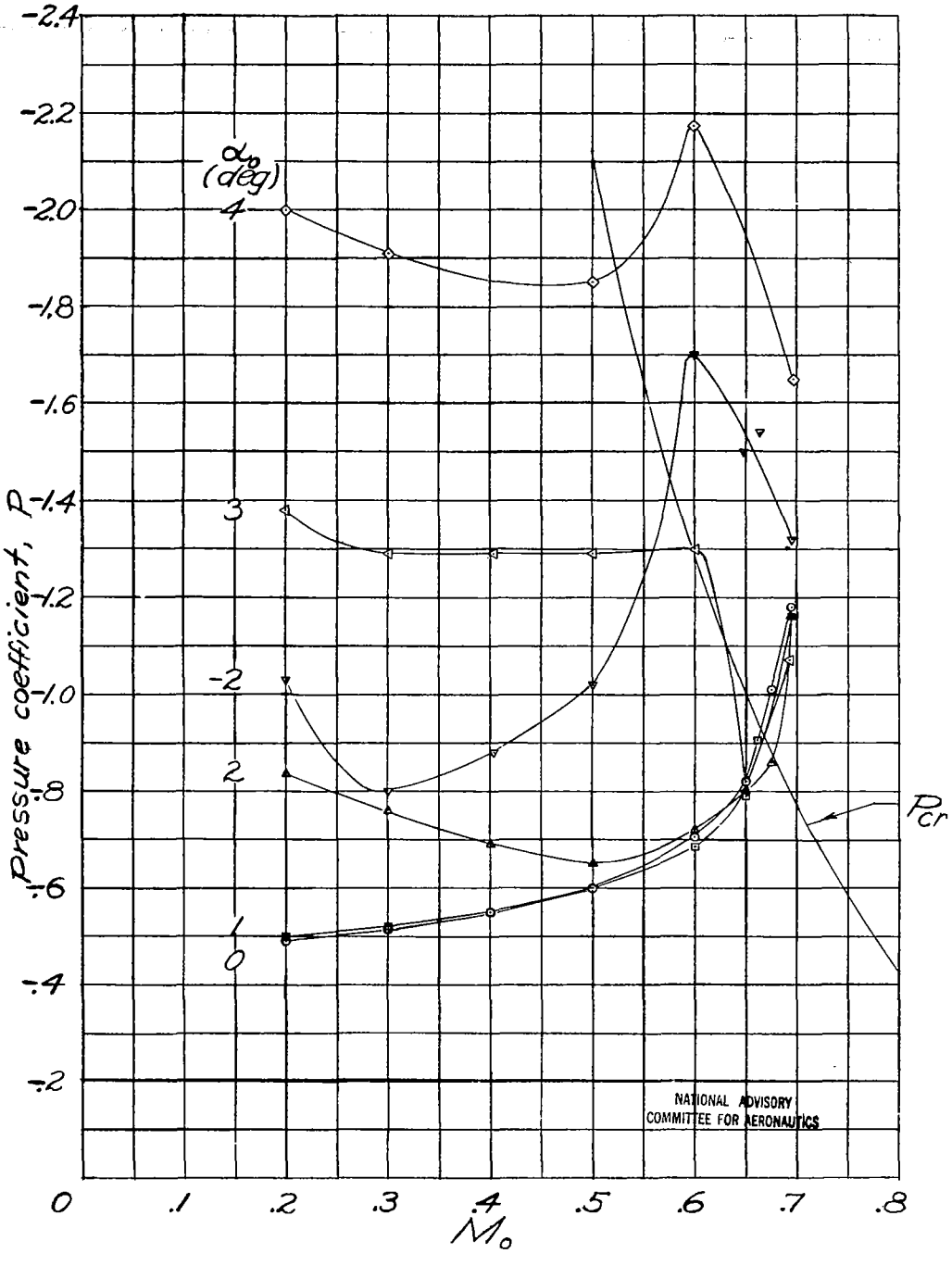

(a) Inlet section, $V_1/V_o = 0.53$.

Figure 15.- Variation with Mach number of peak negative pressure coefficients for symmetrical wing.

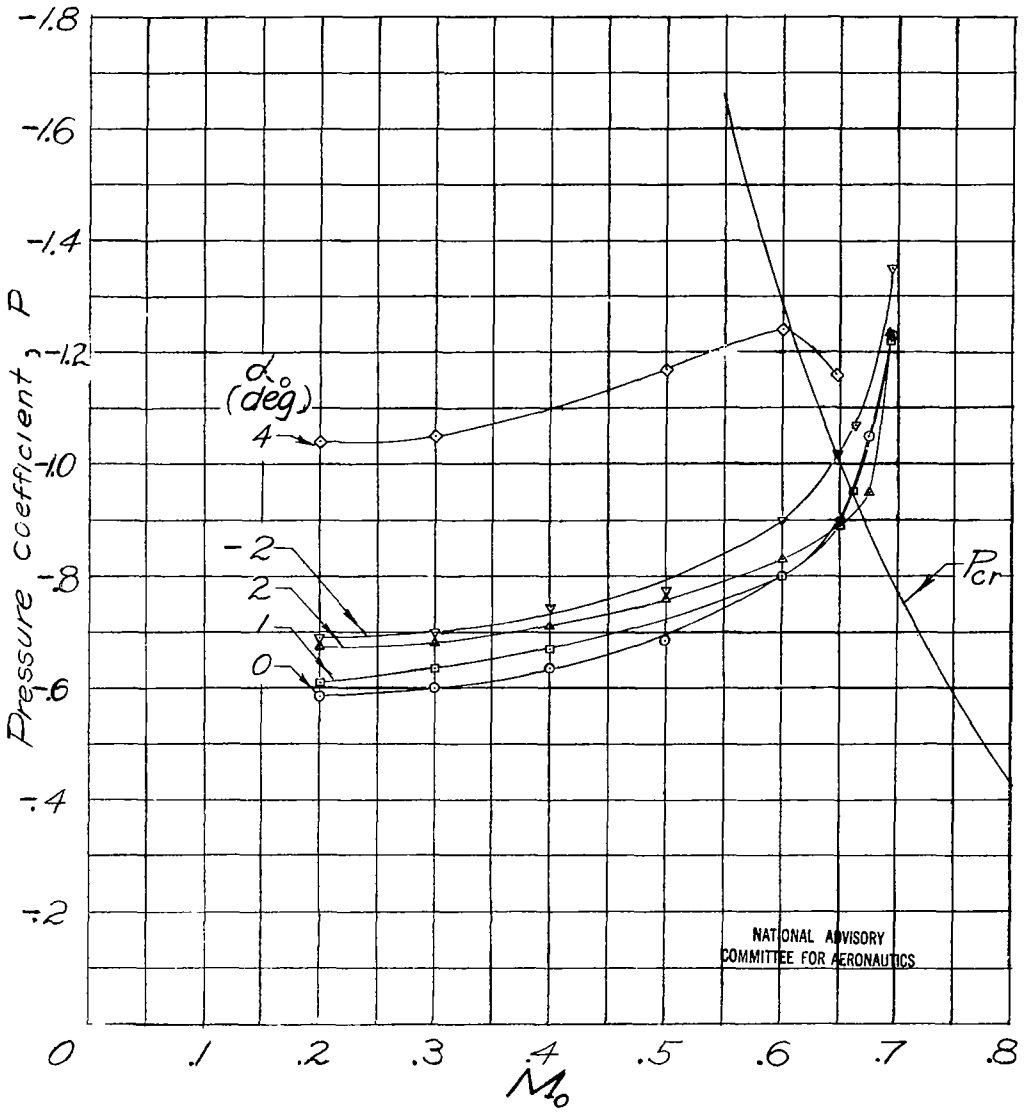

(b) Basic airfoil section.

Figure 15.- Concluded.

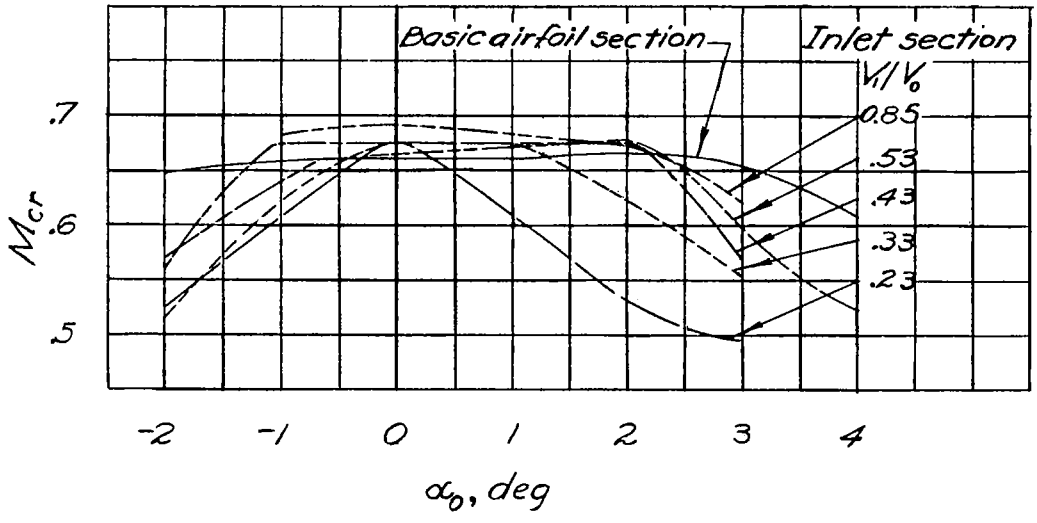

Figure 16.- Variation of critical Mach number with angle of attack for symmetrical wing.

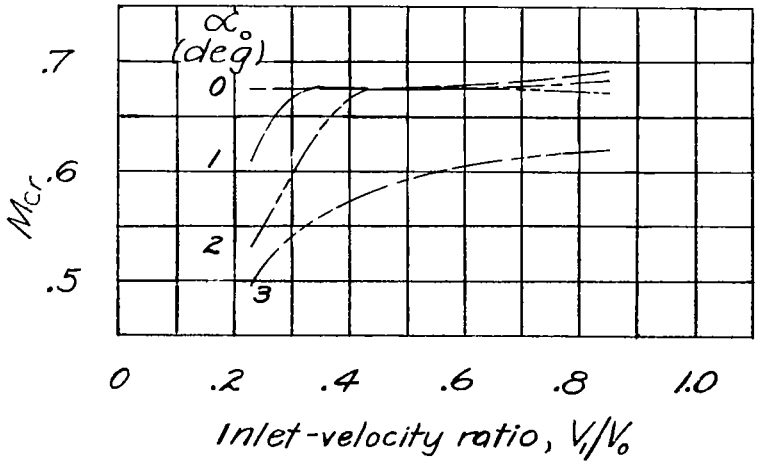

Figure 17.- Variation of critical Mach number with inlet-velocity ratio for inlet section of symmetrical wing.

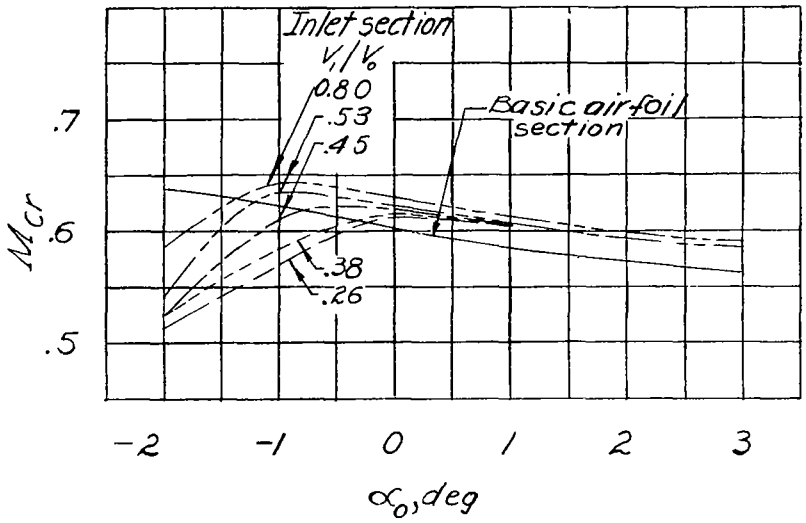

Figure 18.- Variation of critical Mach number with angle of attack for medium-camber wing.

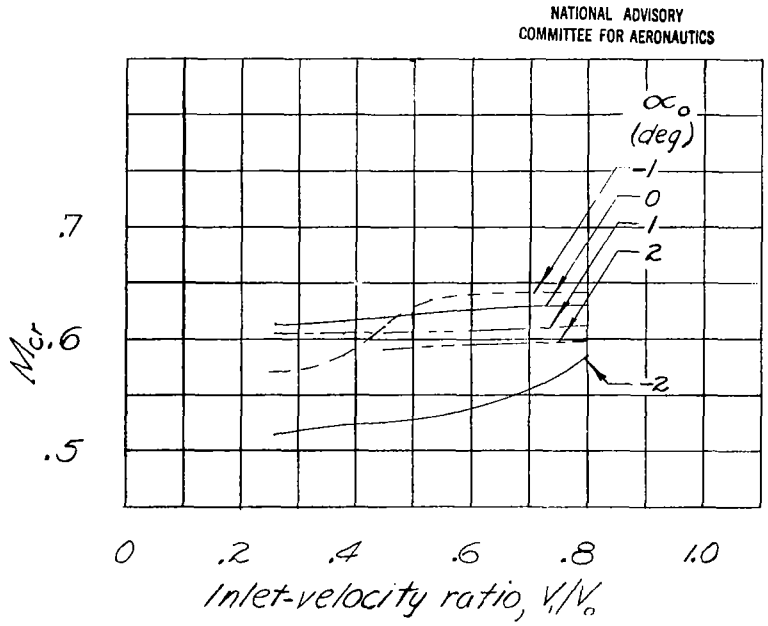

Figure 19.- Variation of critical Mach number with inlet-velocity ratio for inlet section of medium-camber wing.

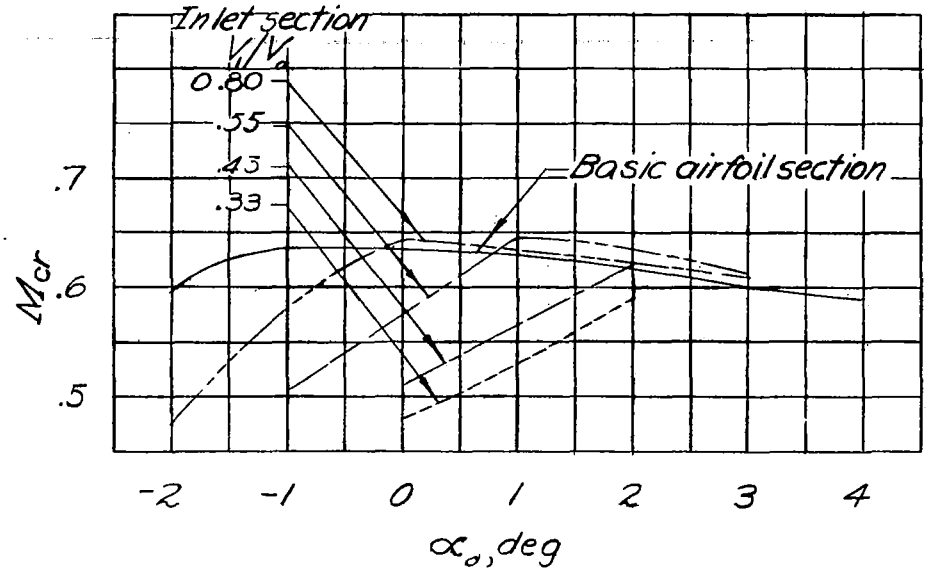

Figure 20.- Variation of critical Mach number with angle of attack for high-camber wing.

NATIONAL ADVISORY
COMMITTEE FOR AERONAUTICS

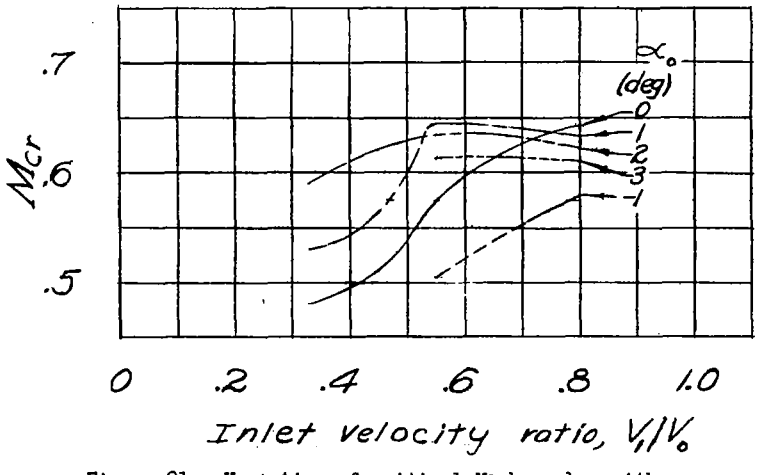

Figure 21.- Variation of critical Mach number with inlet-velocity ratio for inlet section of high-camber wing.

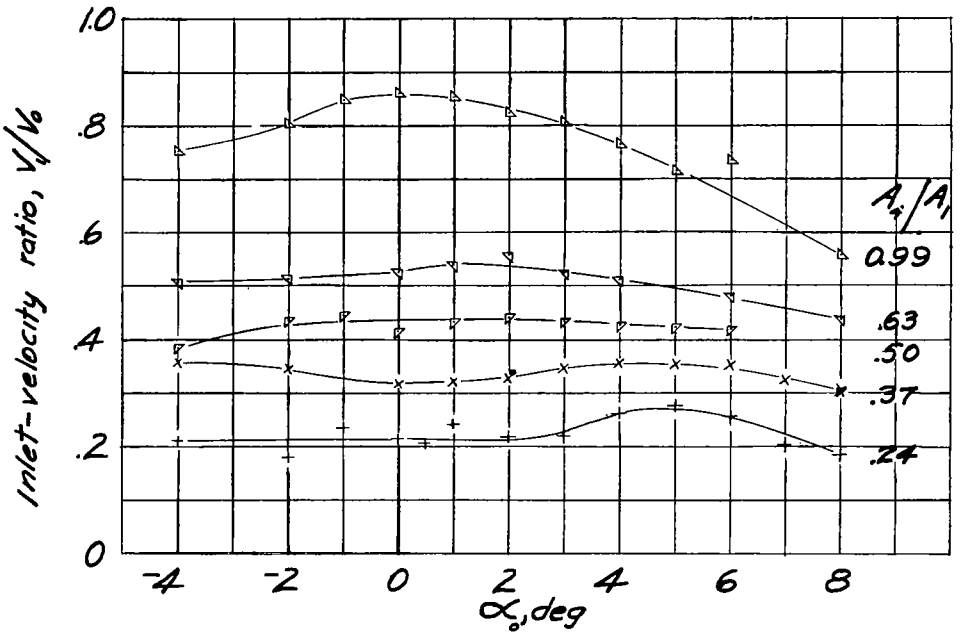

Figure 22.- Variation of inlet-velocity ratio with angle of attack for various exit areas for inlet section of symmetrical wing. $M_o = 0.20$.

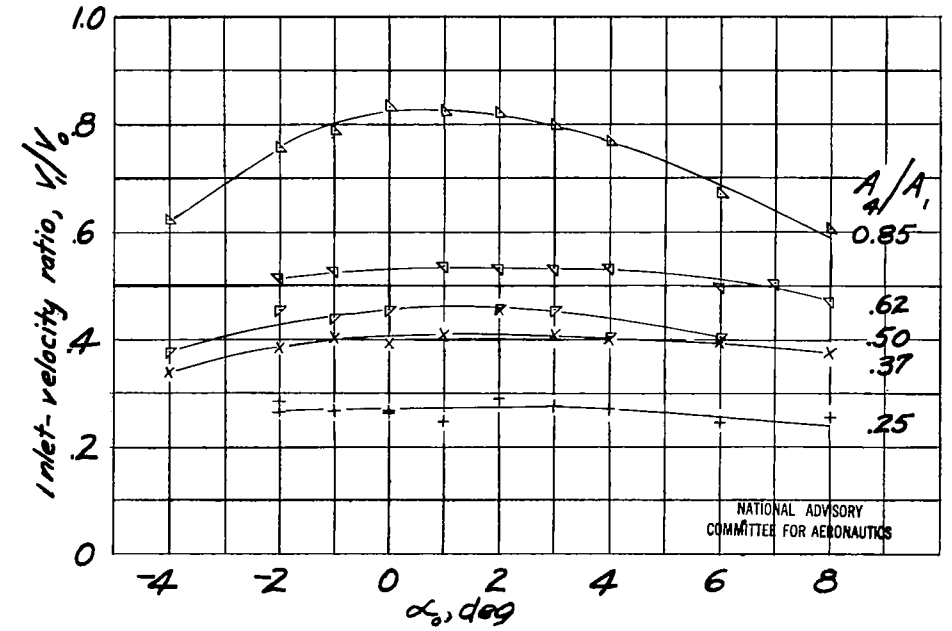

Figure 23.- Variation of inlet-velocity ratio with angle of attack for various exit areas for inlet section of medium-camber wing. $M_o = 0.20$.

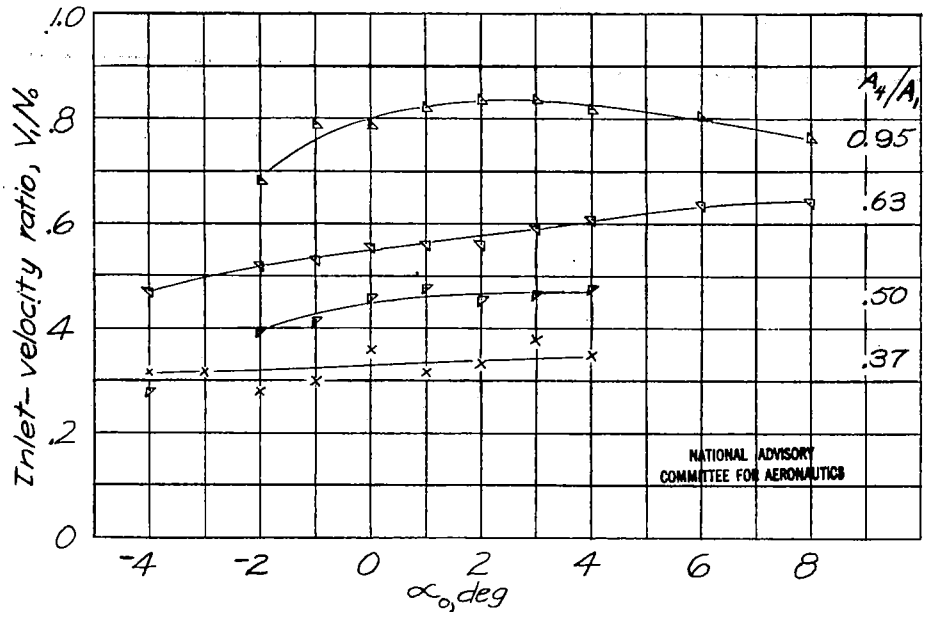

Figure 24.- Variation of inlet-velocity ratio with angle of attack for various exit areas for inlet section of high-camber wing. M_0 = 0.20.

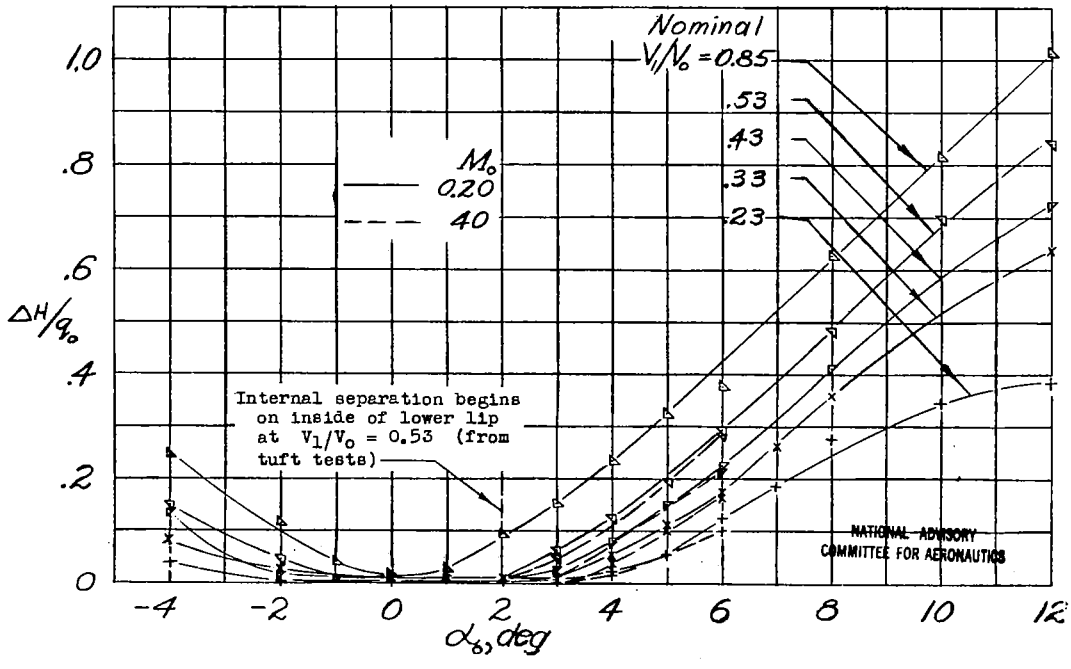

Figure 25.- Variation of internal loss with angle of attack for various inlet-velocity ratios for inlet section of symmetrical wing.

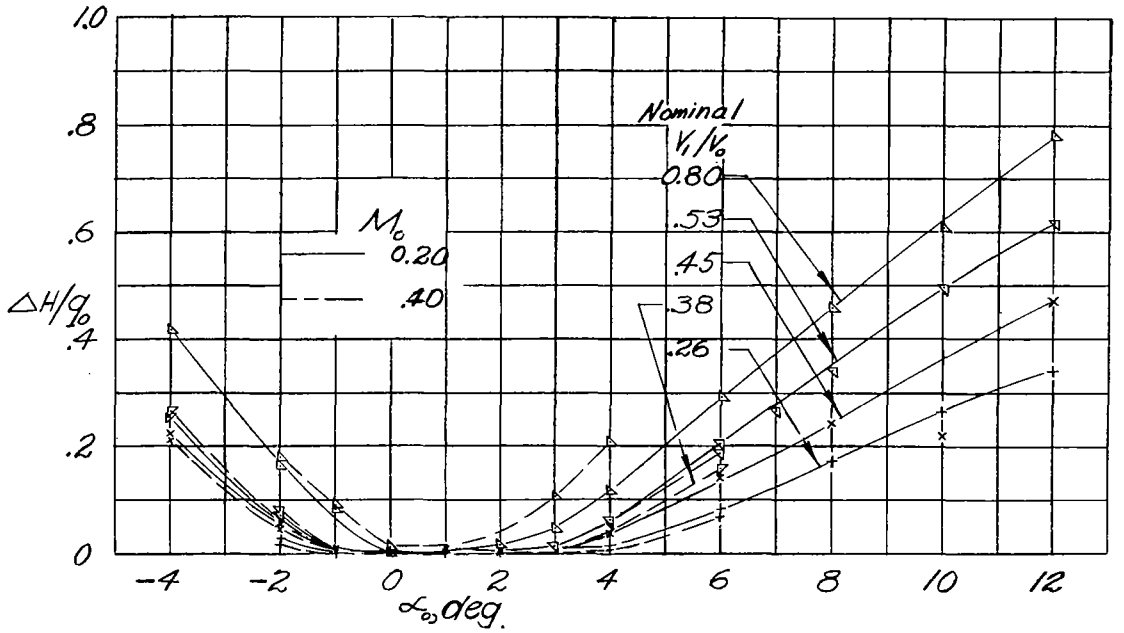

Figure 26.- Variation of internal loss with angle of attack for various inlet-velocity ratios for inlet section of medium-camber wing.

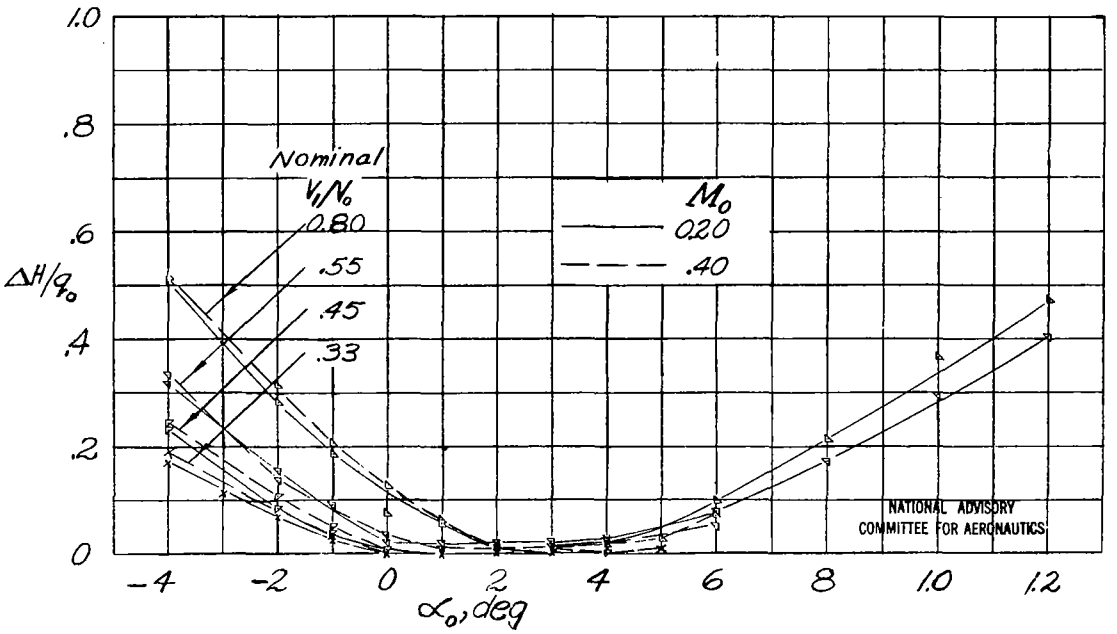

Figure 27.- Variation of internal loss with angle of attack for various inlet-velocity ratios for inlet section of high-camber wing.

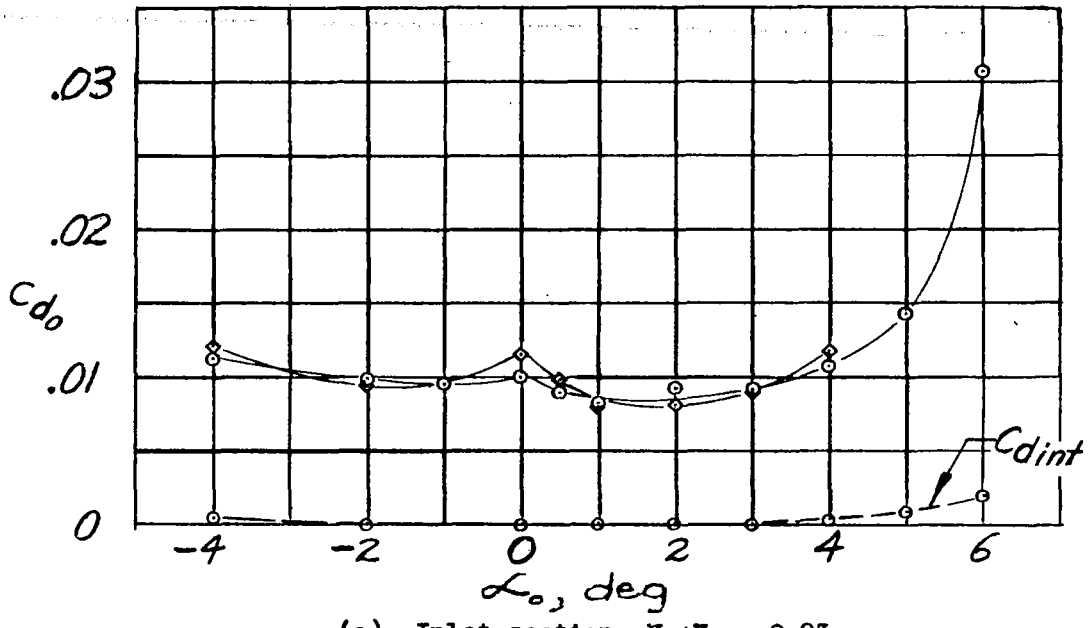

(a) Inlet section, $V_1/V_o = 0.23$.

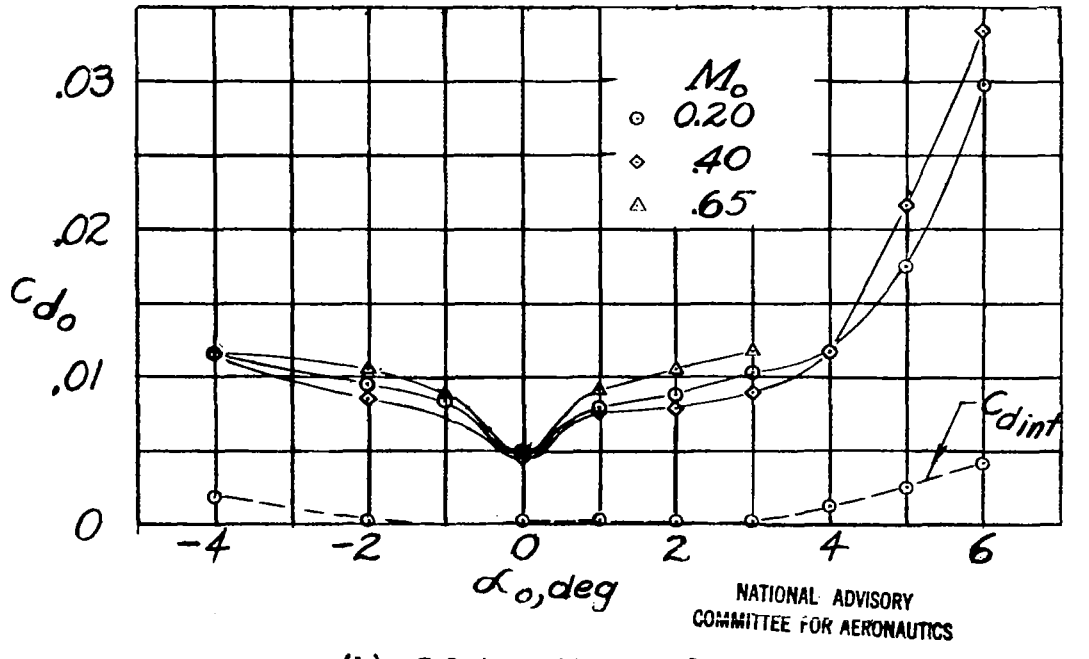

(b) Inlet section, $V_1/V_o = 0.33$.

Figure 28.- Variation of profile drag with angle of attack for symmetrical wing.

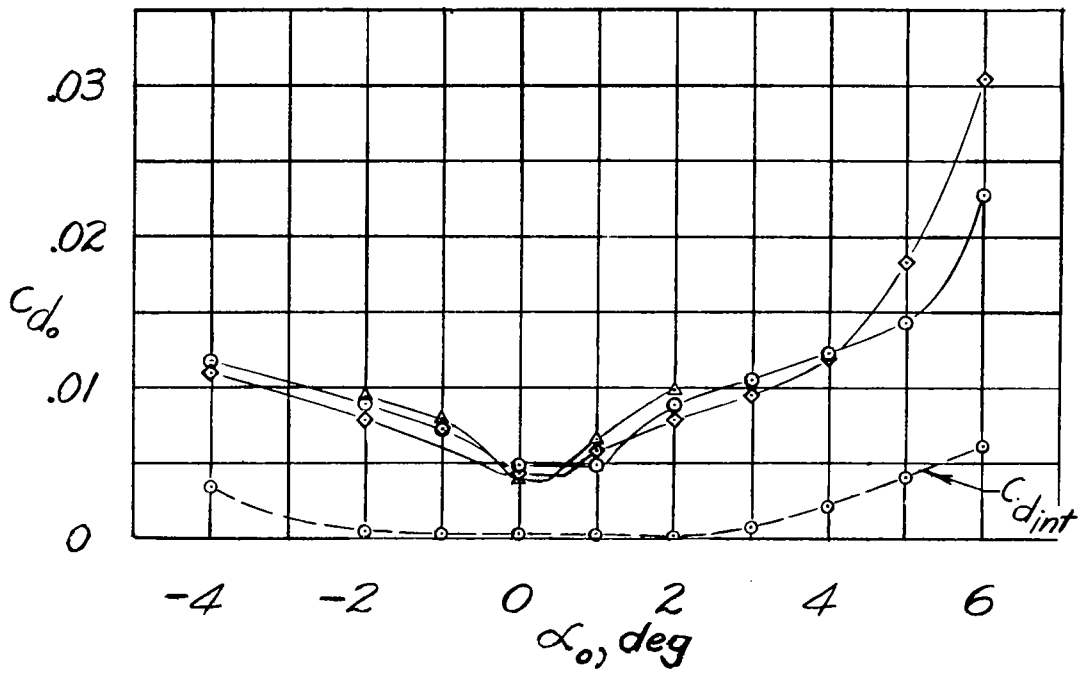

(c) Inlet section, $V_1/V_0 = 0.43$.

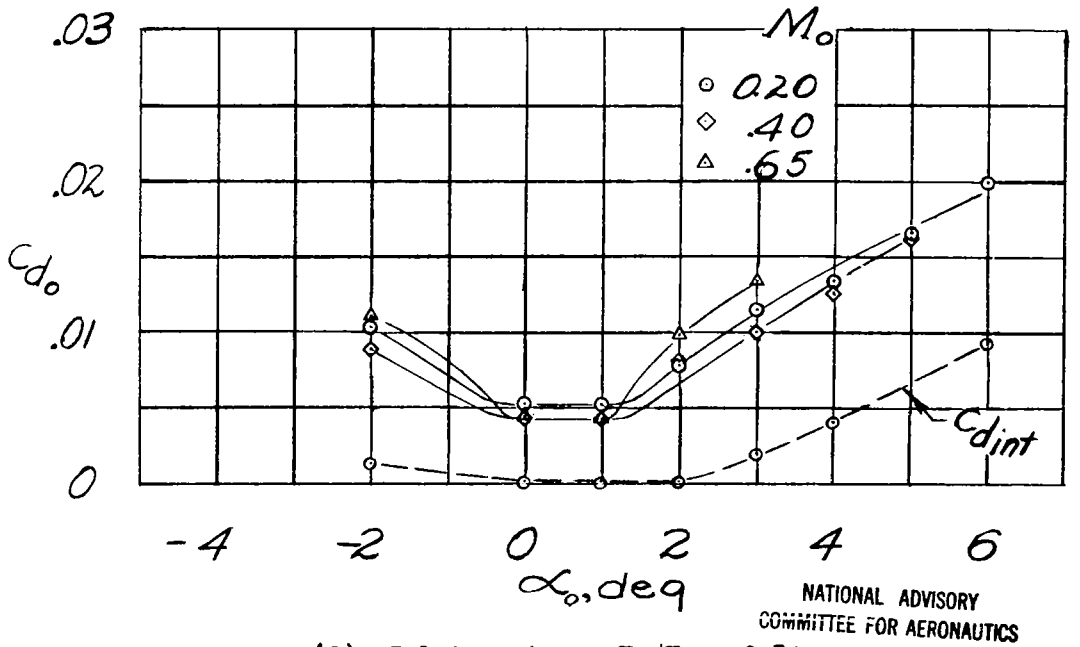

(d) Inlet section, $V_1/V_0 = 0.53$.

Figure 28.- Continued.

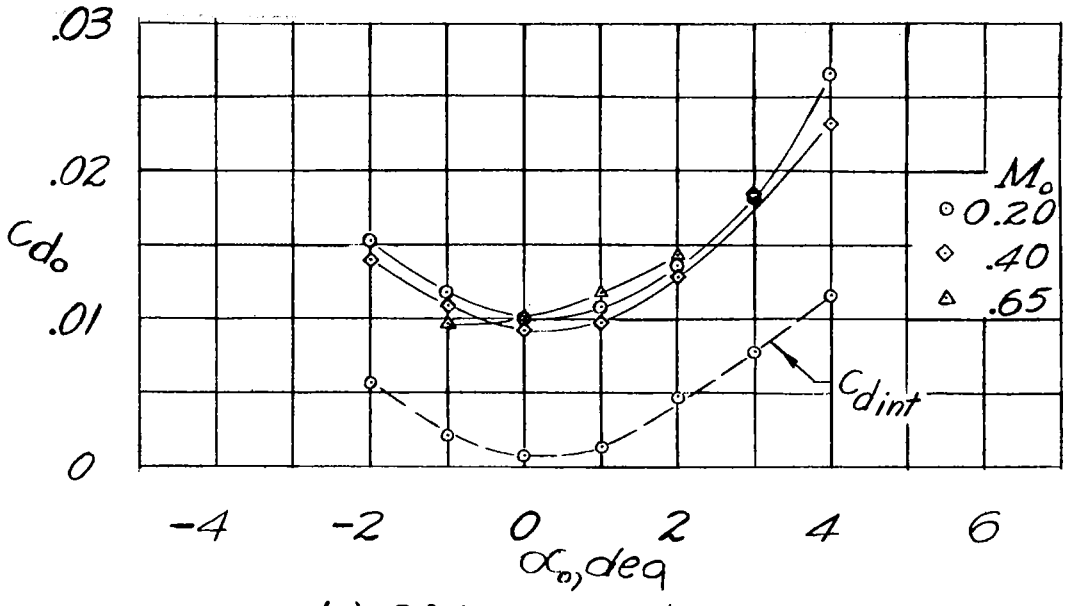

(e) Inlet section, $V_1/V_o = 0.85$.

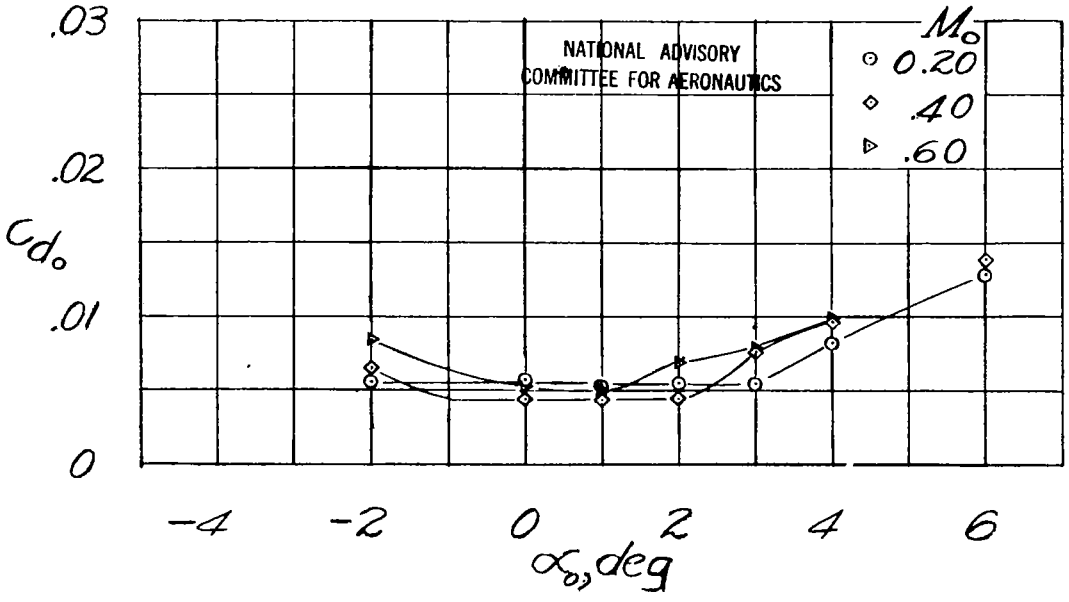

(f) Basic airfoil section.

Figure 28.- Concluded.

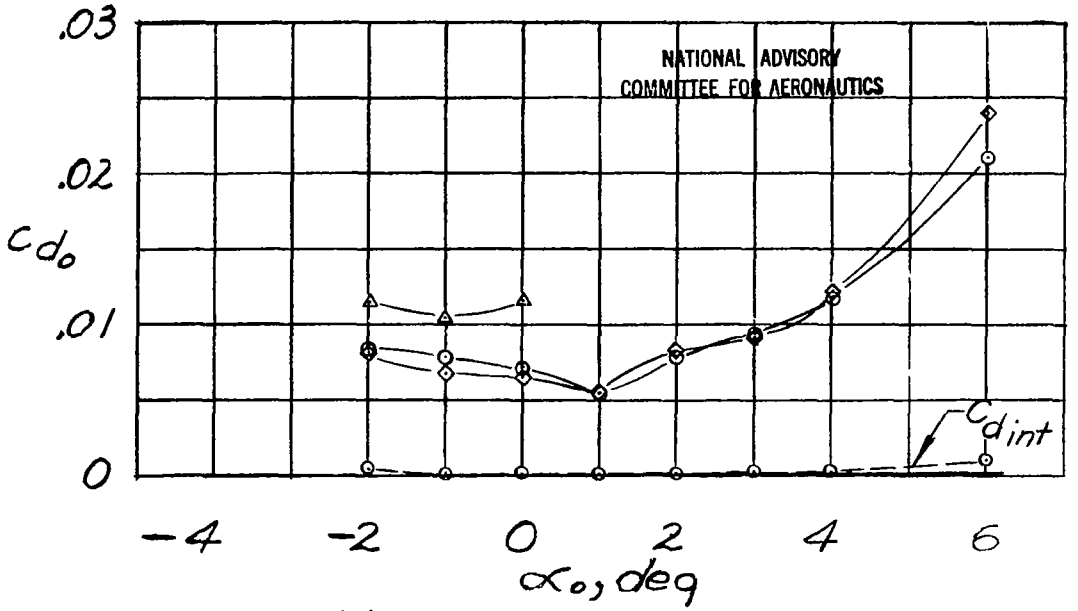

(a) Inlet section, $V_1/V_o = 0.26$.

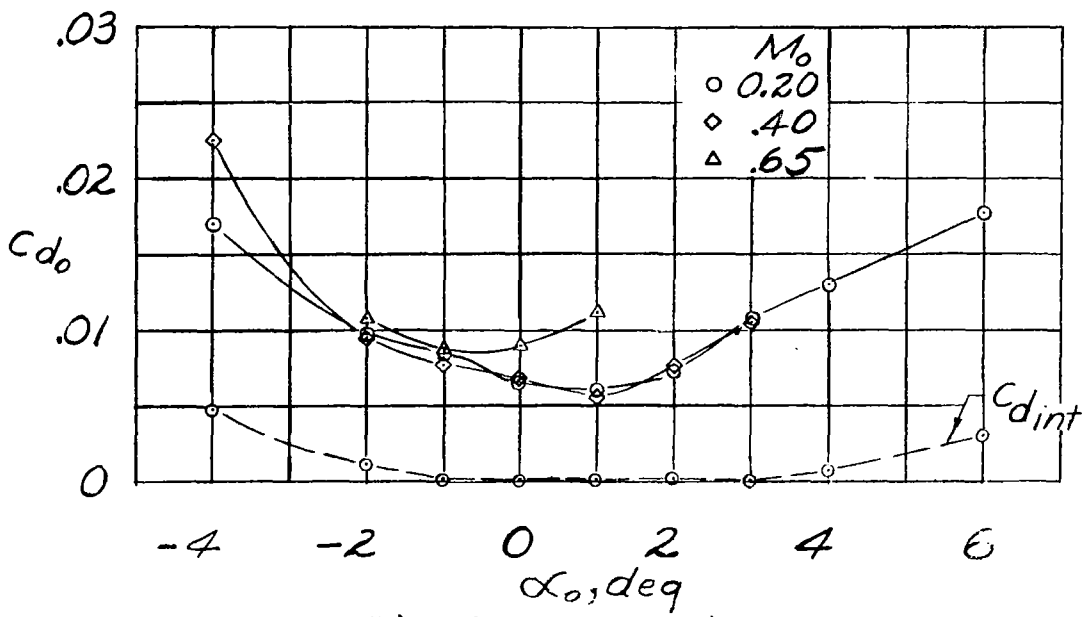

(b) Inlet section, $V_1/V_o = 0.38$.

Figure 29.- Variation of profile drag with angle of attack for medium-camber wing.

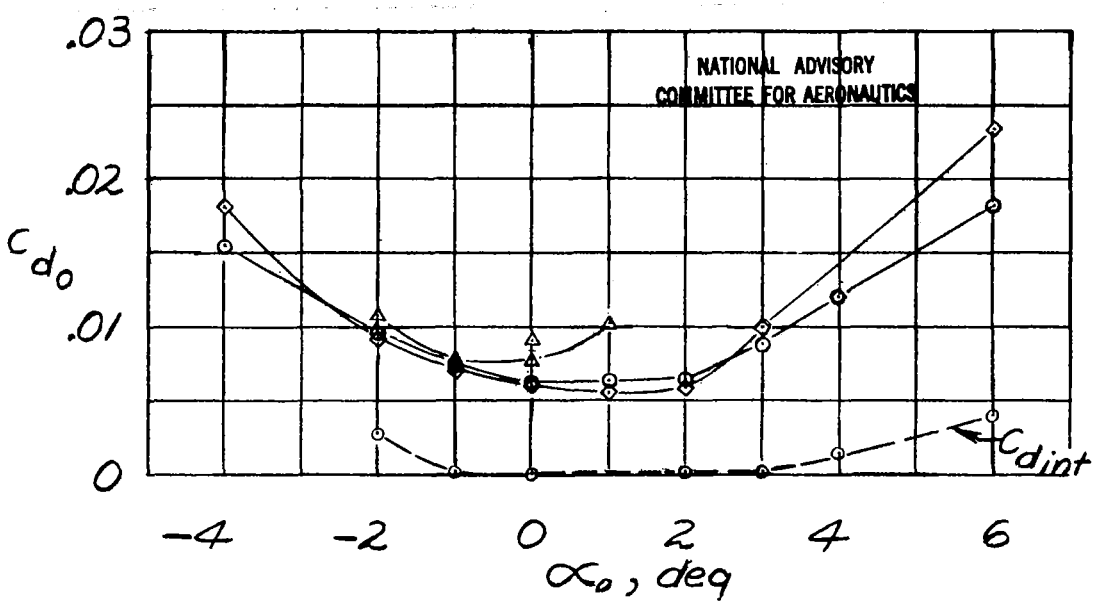

(c) Inlet section, $V_1/V_o = 0.45$.

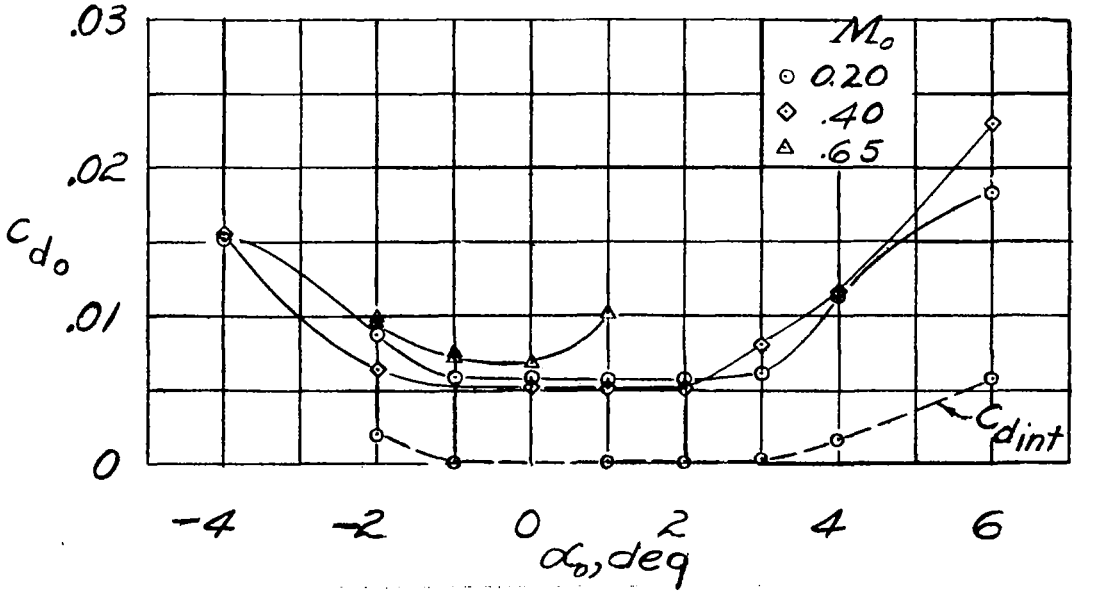

(d) Inlet section, $V_1/V_o = 0.53$.

Figure 29.- Continued.

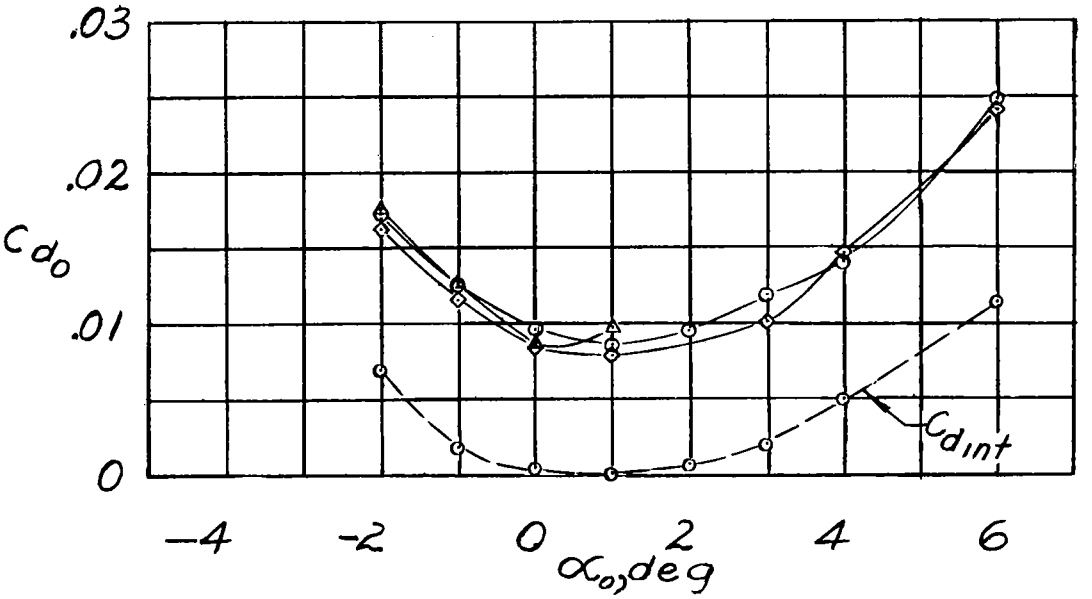

(e) Inlet section, $V_1/V_o = 0.80$.

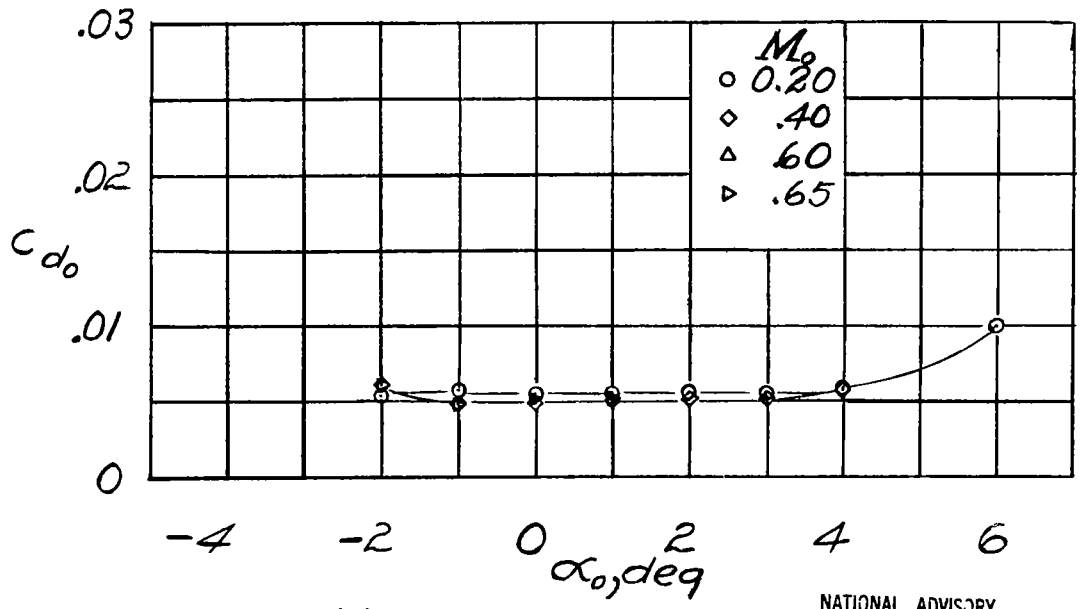

(f) Basic airfoil section.

NATIONAL ADVISORY COMMITTEE FOR AERONAUTICS

Figure 29.- Concluded.

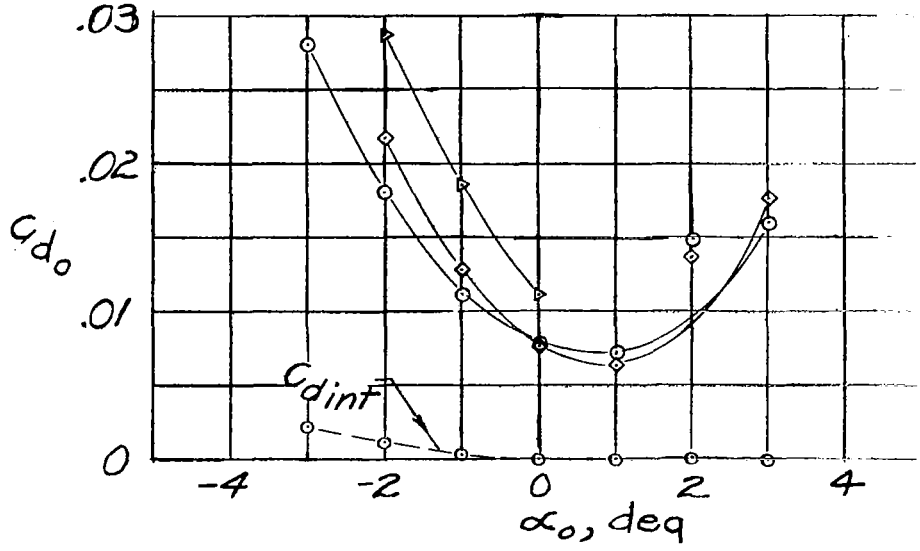

(a) Inlet section, $V_1/V_o = 0.33$.

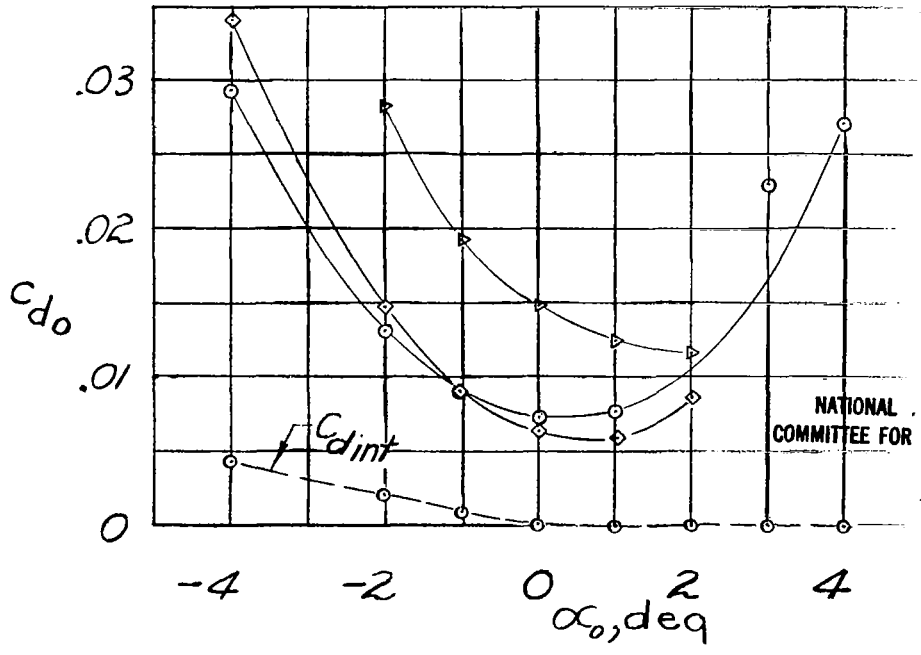

(b) Inlet section, $V_1/V_o = 0.45$.

Figure 30.- Variation of profile drag with angle of a for high-camber wing.

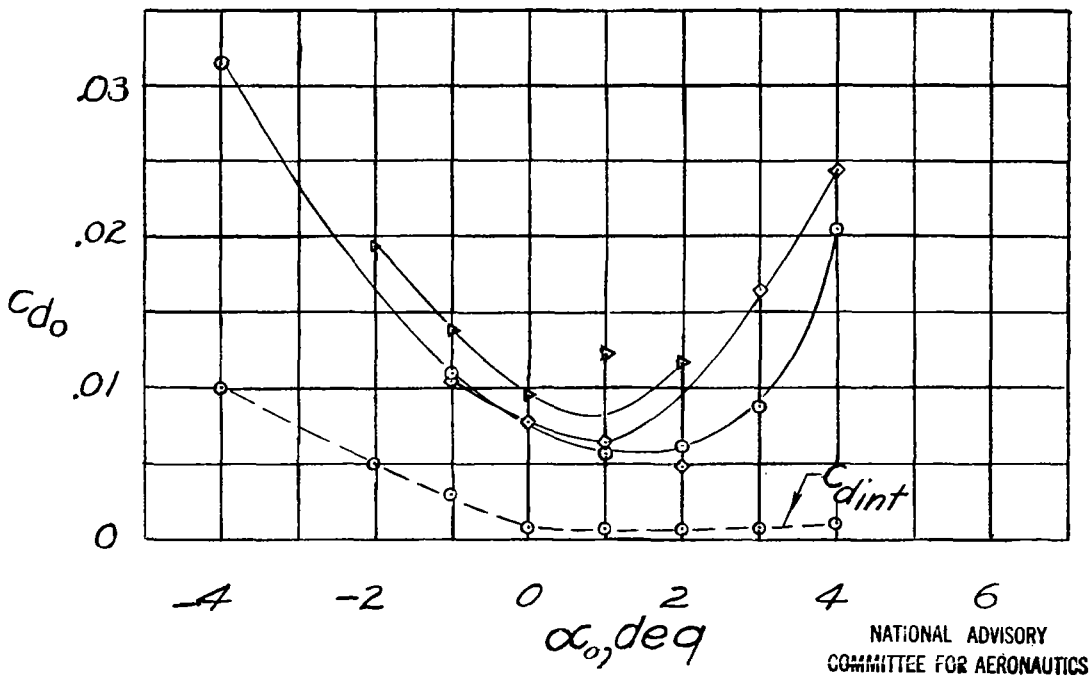

(c) Inlet section, V_1/V_o = 0.55.

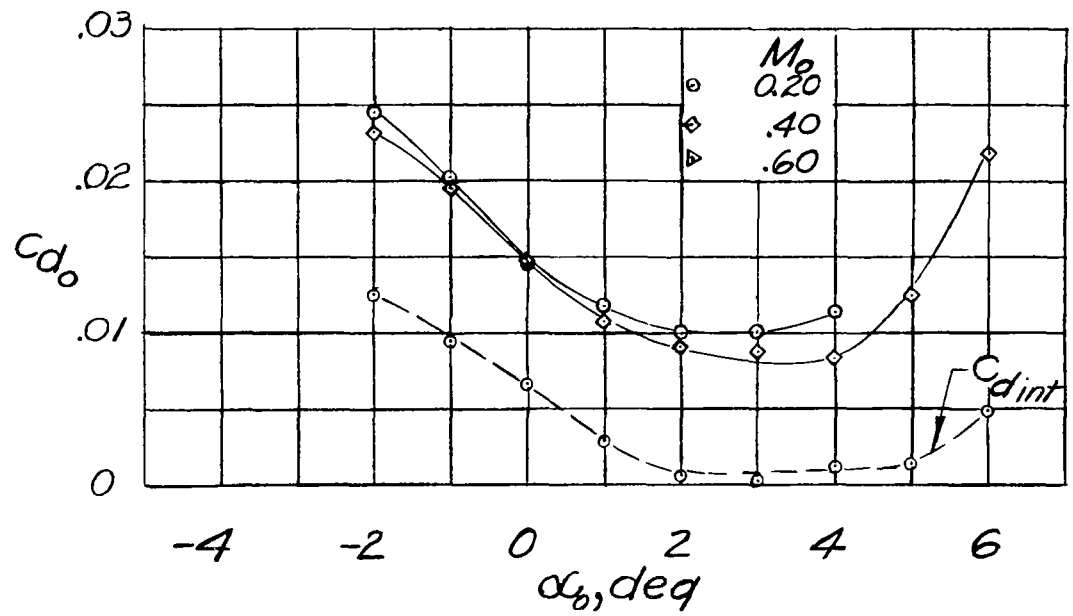

(d) Inlet section, V_1/V_o = 0.80.

Figure 30.- Continued.

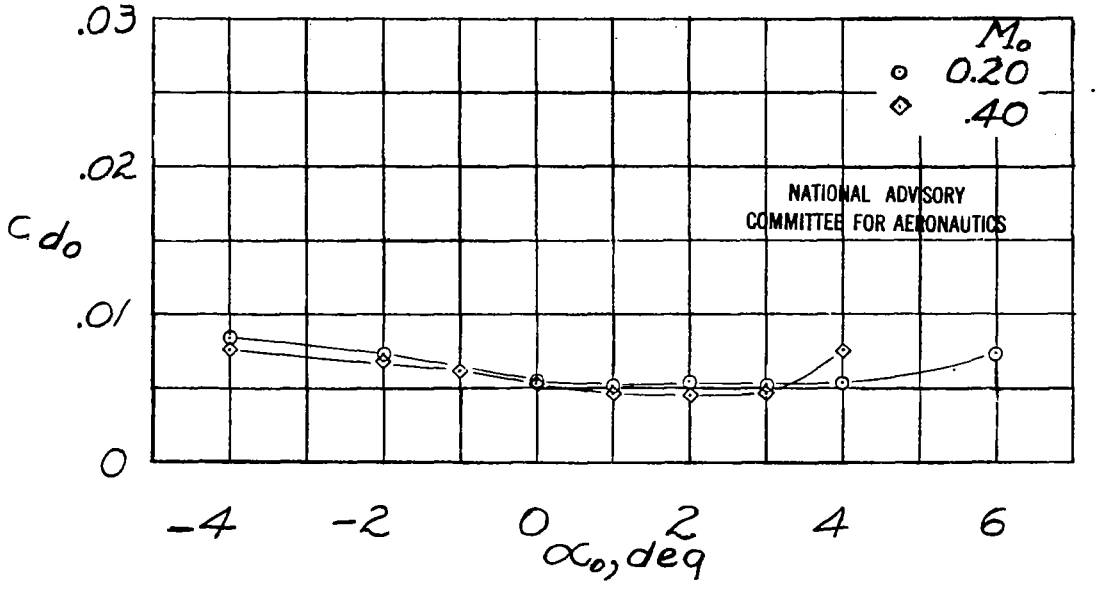

(e) Basic airfoil section.

Figure 30.- Concluded.

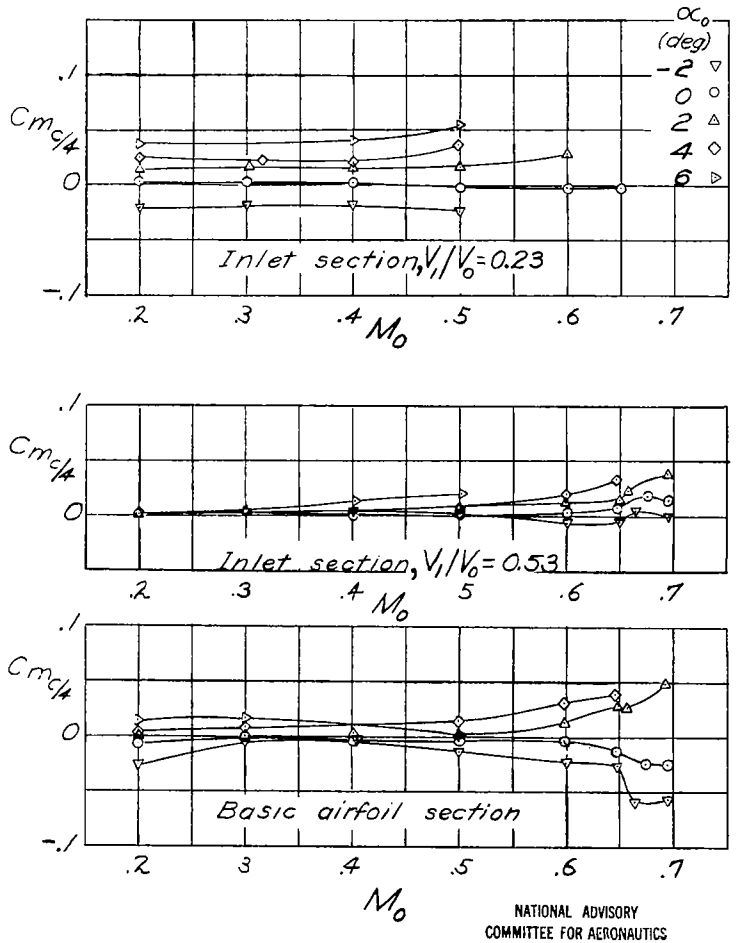

Figure 31.- Variation of section pitching-moment coefficients with Mach number for symmetrical wing.

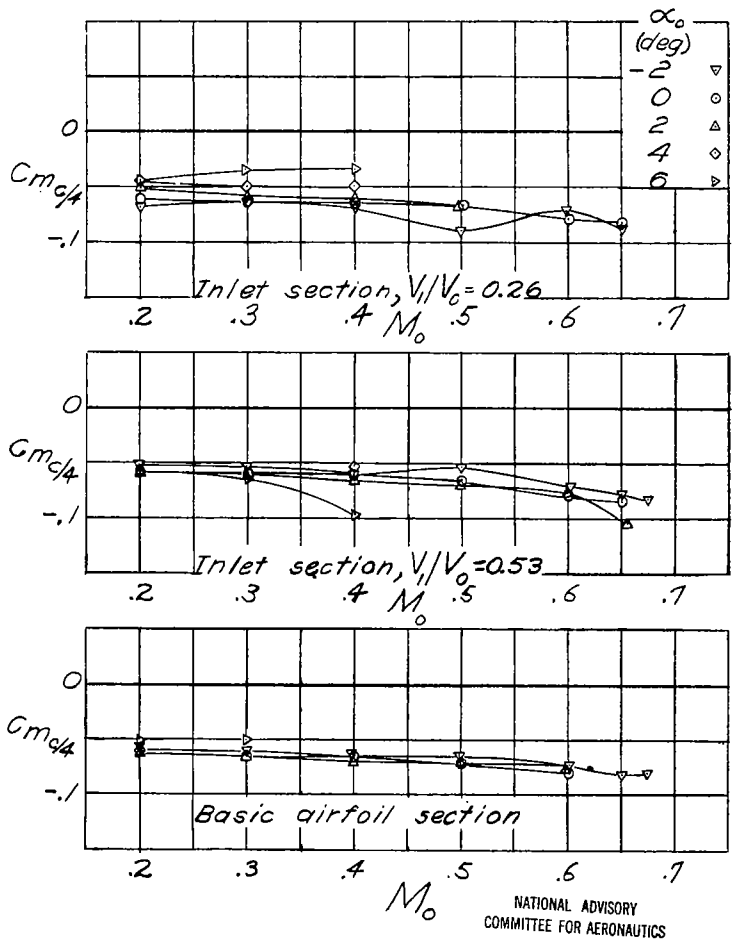

Figure 32.- Variation of section pitching-moment coefficients with Mach number for medium-camber wing.

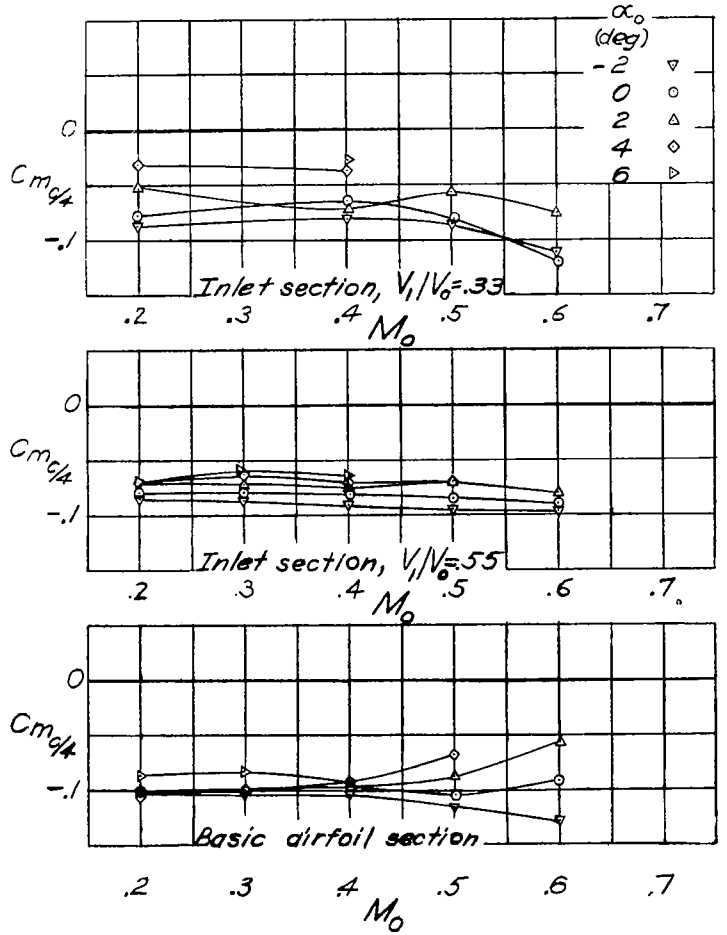

Figure 33.- Variation of section pitching-moment coefficients with Mach number for high-camber wing.

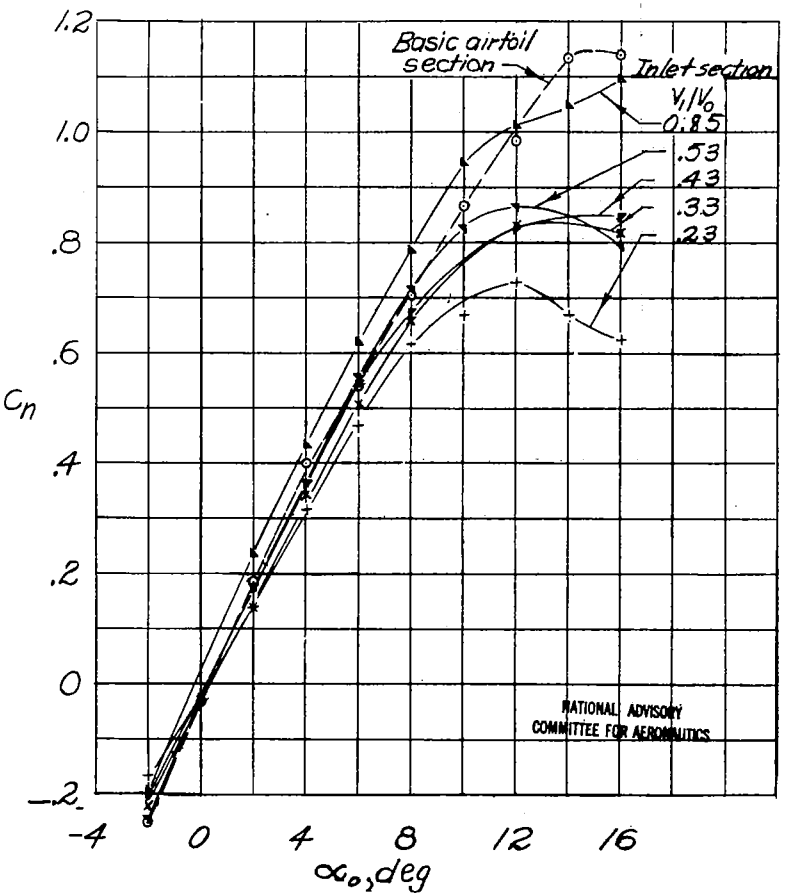

Figure 34.- Section normal-force coefficients for symmetrical wing. M_o = 0.20.

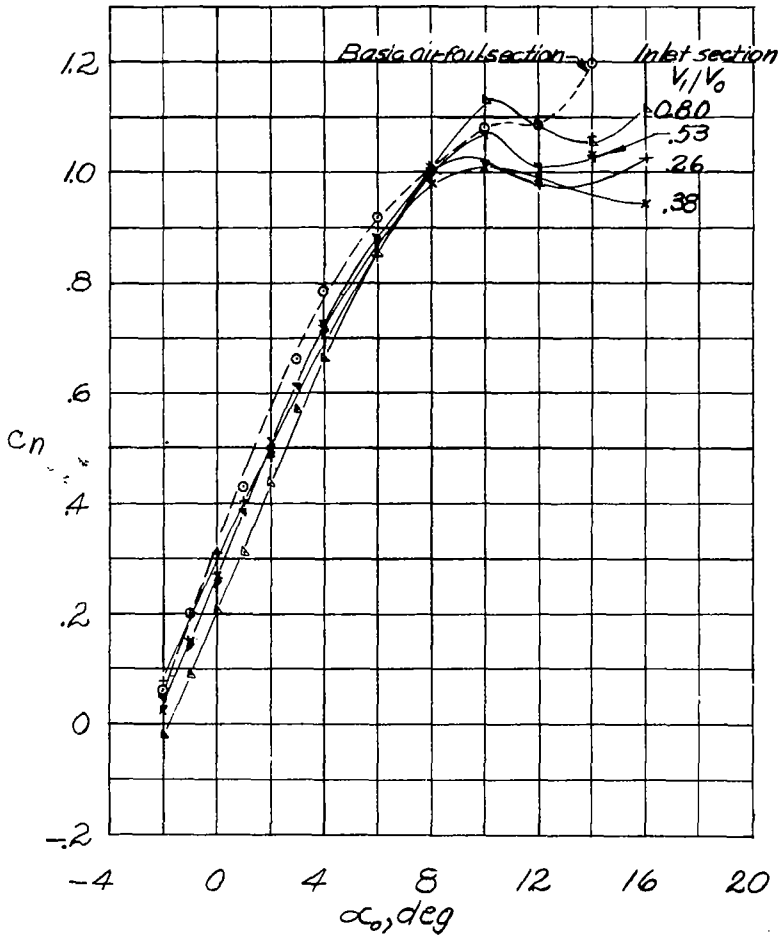

Figure 35.- Section normal-force coefficients for medium-camber wing. M_o = 0.20.

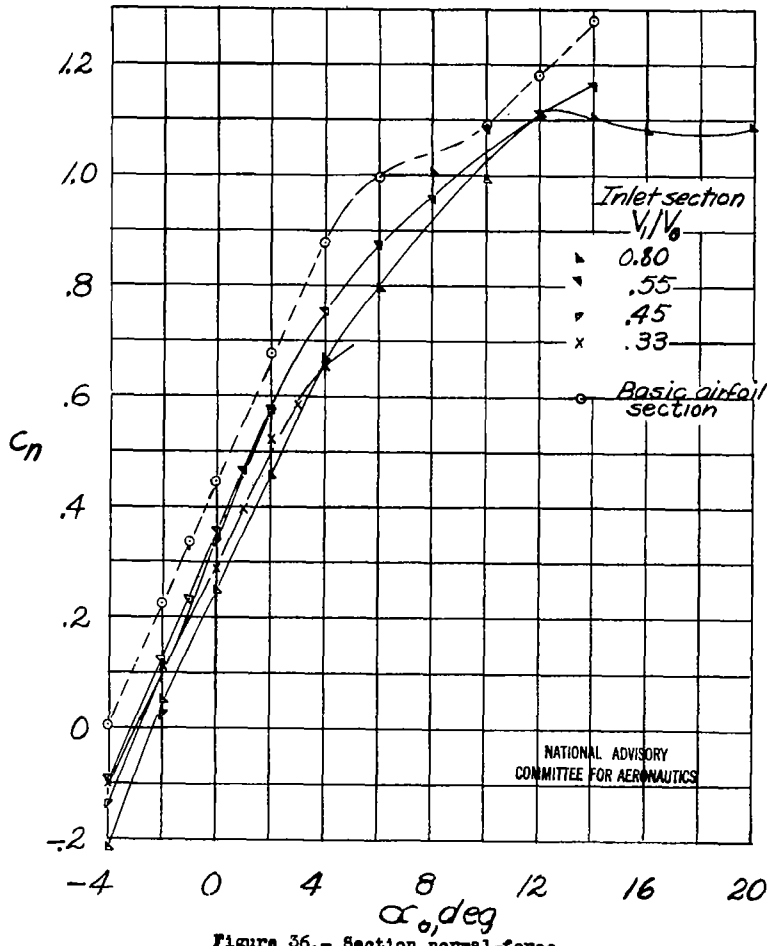

Figure 36.- Section normal-force coefficients for high-camber wing. M_o = 0.20.

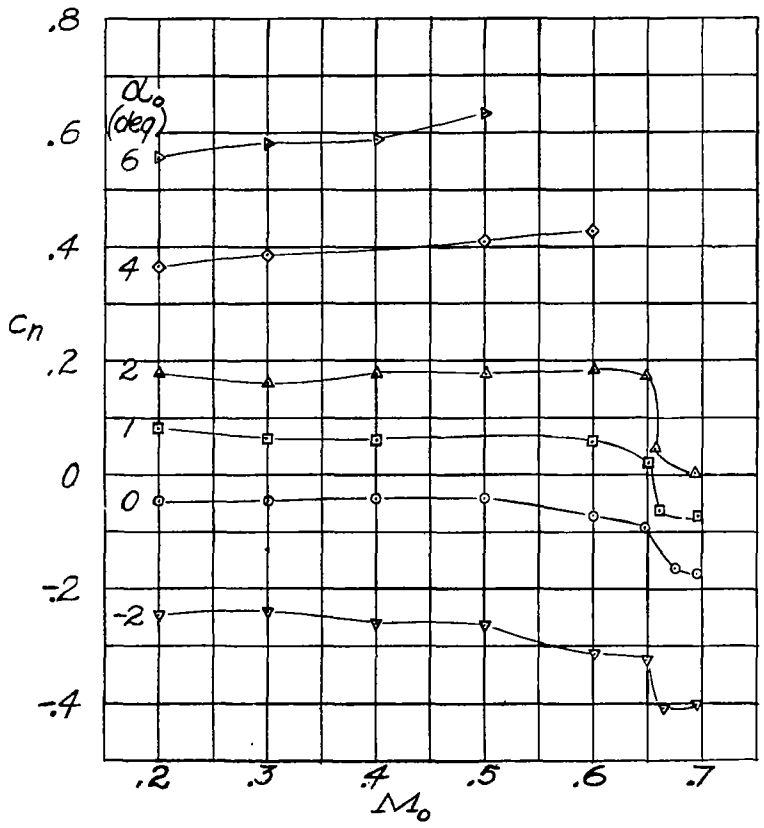

(a) Inlet section, $V_1/V_o = 0.53$.

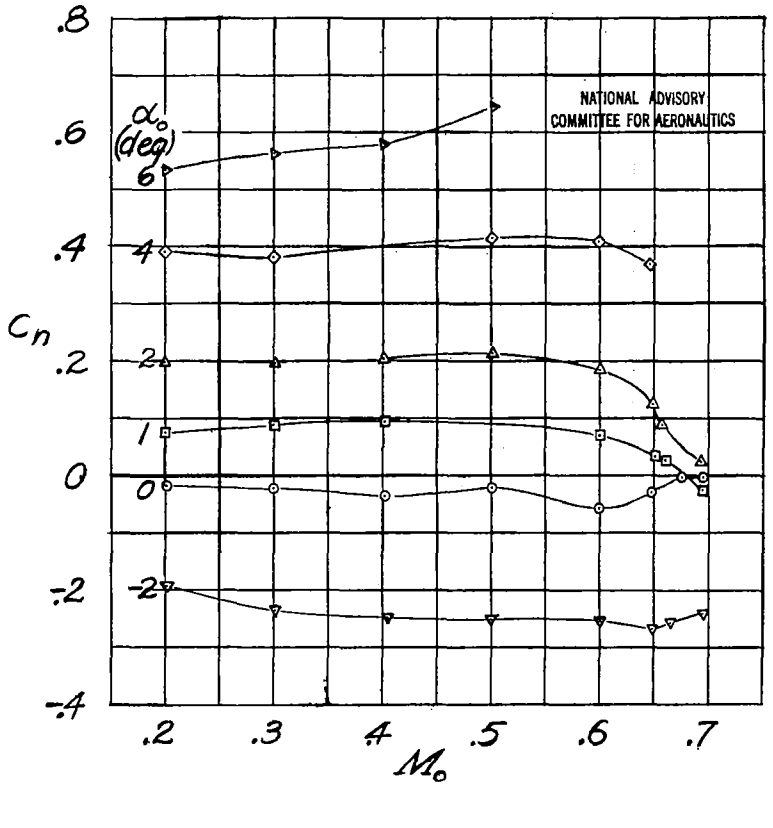

(b) Basic airfoil section.

Figure 37.- Variation of section normal-force coefficients with Mach number for symmetrical wing.

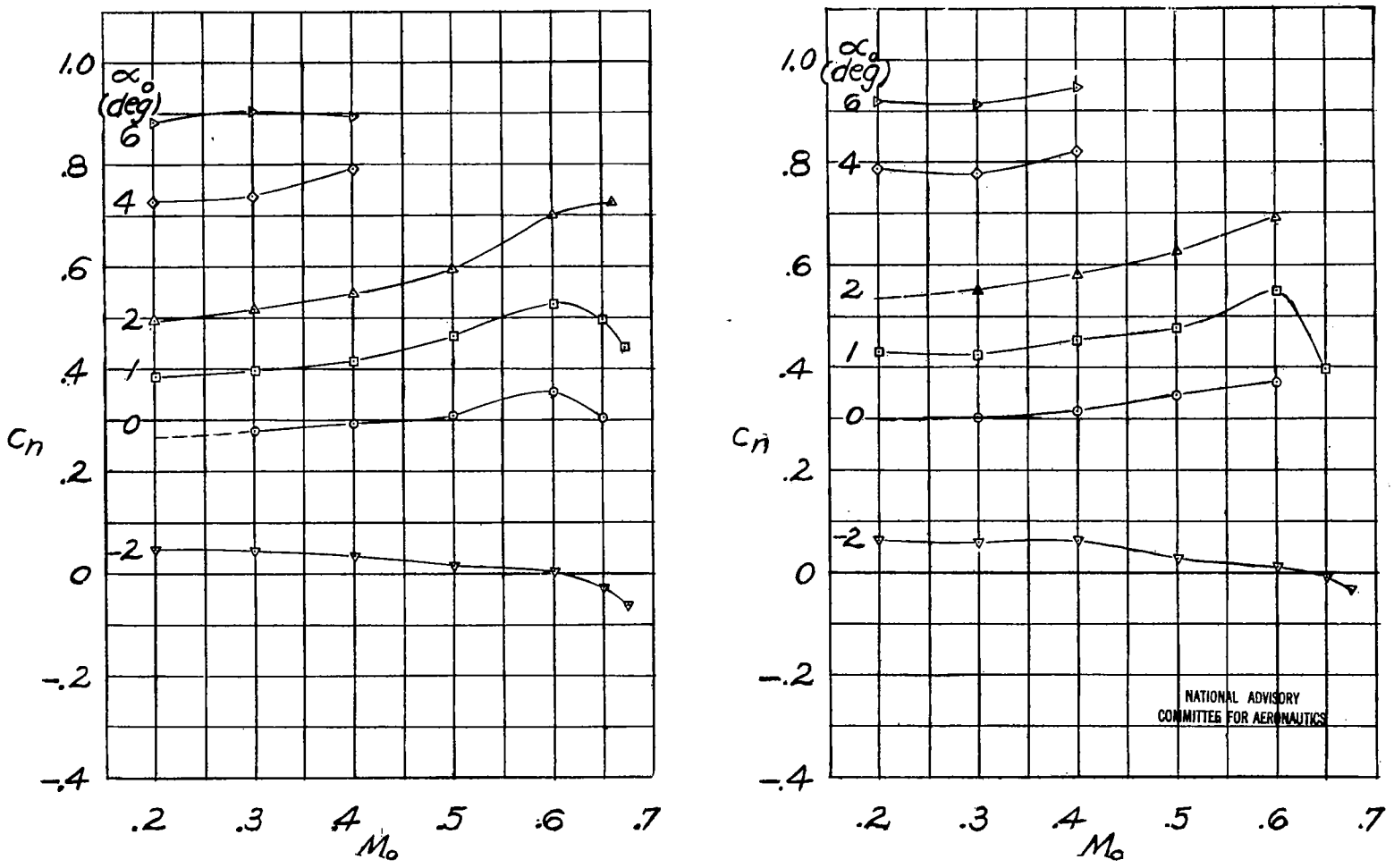

(a) Inlet section, $V_1/V_o = 0.53$.

(b) Basic airfoil section.

Figure 38.- Variation of section normal-force coefficients with Mach number for medium-camber wing.

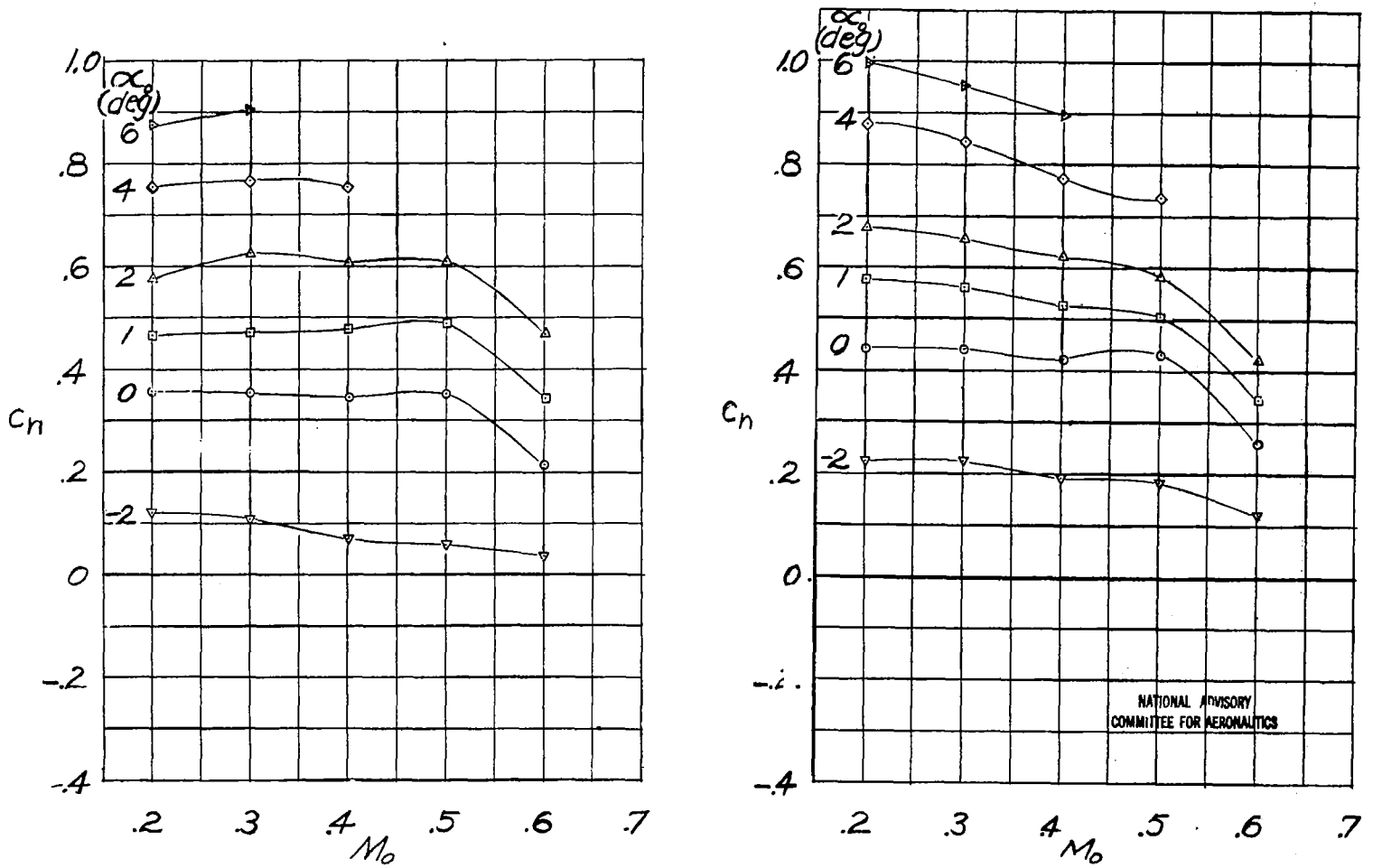

(a) Inlet section, $V_1/V_o = 0.55$.

(b) Basic airfoil section.

Figure 39.- Variation of section normal-force coefficients with Mach number for high-camber wing.

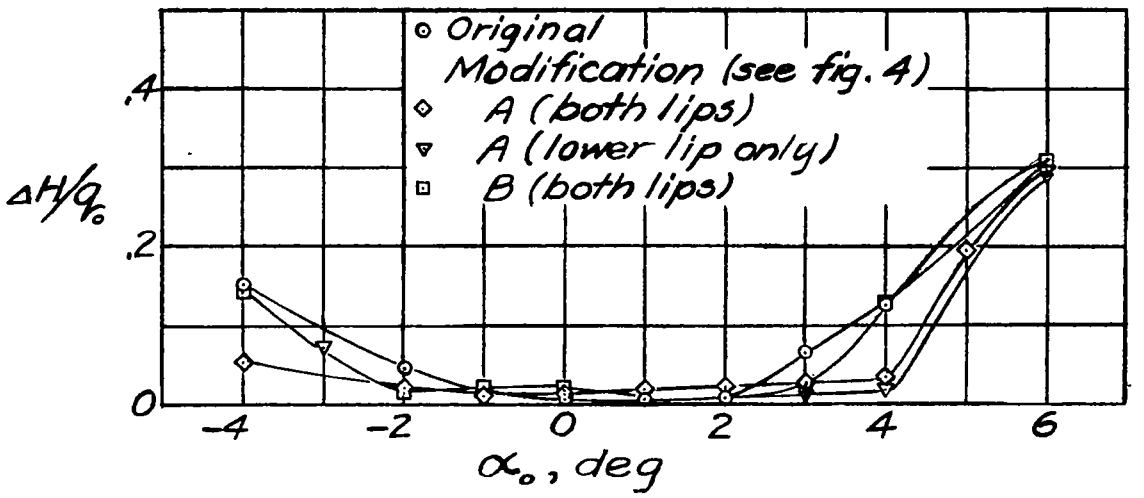

(a) $M_0 = 0.20$.

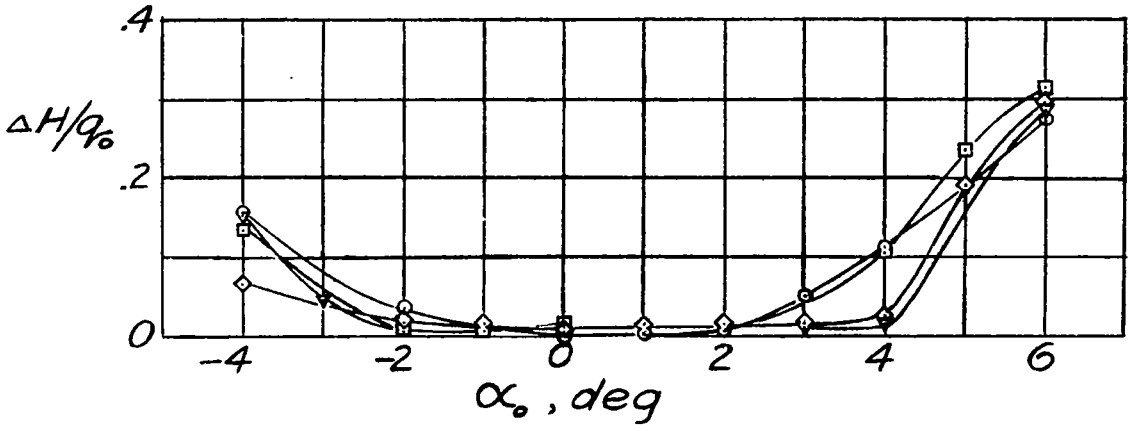

(b) $M_0 = 0.30$.

Figure 40.- Effects of several internal-lip fairings on internal losses for inlet section of symmetrical wing. $V_1/V_0 = 0.53$.